



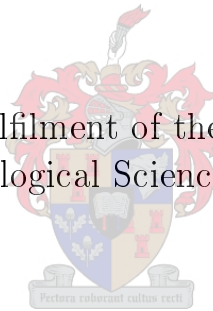
UNIVERSITEIT•STELLENBOSCH•UNIVERSITY  
jou kennisvennoot • your knowledge partner

# Exploring underlying mechanisms driving the onset of stress-induced insulin resistance.

by

Delita Otto

Thesis presented in partial fulfilment of the requirement for the degree of  
Master of Science in Physiological Sciences at Stellenbosch University



Department of Physiological Sciences  
University of Stellenbosch  
Private Bag X1, 7602 Matieland, South Africa

Supervisor: Prof M.F. Essop  
Head of Department of Physiological Sciences  
University of Stellenbosch

March 2012

# Declaration

By submitting this thesis electronically, I declare that the entirety of the work contained therein is my own, original work, that I am the sole author thereof (save to the extent explicitly otherwise stated), that reproduction and publication thereof by Stellenbosch University will not infringe any third party rights and that I have not previously in its entirety or in part submitted it for obtaining any qualification.

Signature: .....

D. Otto

Date: .....

Copyright © 2012 Stellenbosch University  
All rights reserved.

# Abstract

Physical and psychological stressors trigger activation of the hypothalamo-pituitary-adrenocortical (HPA) axis that leads to enhanced secretion of glucocorticoids e.g. cortisol. Moreover, chronic activation of this pathway may elevate oxidative stress that is linked to the onset of insulin resistance and cardiovascular diseases (CVD). Our laboratory previously found that oxidative stress increases flux through metabolic circuits such as the hexosamine biosynthetic pathway (HBP), in effect increasing its modification of target proteins post-transcriptionally with *O*-GlcNAc moieties. This in turn may alter protein function and contribute to the onset of myocardial insulin resistance and impaired contractile function. Since the underlying mechanisms linking chronic stress to cardiometabolic pathophysiology are poorly understood, we hypothesised that cortisol elicits myocardial oxidative stress, HBP activation, and decreased glucose uptake (due to attenuated glucose transport functionality) with detrimental outcomes, i.e. insulin resistance and apoptosis.

To investigate this hypothesis we established an *in vitro* model using HL-1 cardiomyocytes, with which we evaluated the degree of *O*-GlcNAcylation and oxidative stress in response to a range of time-dose treatments with dexamethasone (synthetic glucocorticoid). Glucose transporter 4 (GLUT4) translocation to the sarcolemma was also assessed. In agreement with the literature, results suggest that GLUT4 translocation is significantly decreased subsequent to dexamethasone treatment. Although no significant differences were observed with regards to oxidative stress or *O*-GlcNAcylation, the data show that dexamethasone increased the latter with a maximal effect after two hours exposure to the  $10^{-6}$  M dose.

Although our results were not conclusive, the data suggest a potential novel link between dexamethasone exposure, HBP activation and decreased GLUT4 translocation. Based on our findings we propose that detrimental effects of chronic stress on the heart may be mediated by increased HBP flux. Given that glucocorticoid excess and GLUT4 dysregulation have been associated with insulin resistance (and related metabolic derangements and diseases), these results provide new targets for potential therapeutic agents.

# Uittreksel

Fisiese sowel as psigologiese stressors veroorsaak die aktivering van die hipotalamiese-hipofiseale-bynier (HHB) pad wat lei tot die verhoogde sekresie van glukokortikoïede soos kortisol. Kroniese aktivering van hierdie pad kan ook oksidatiewe stres verhoog wat weer tot insulienweerstandigheid en kardiovaskulêre siektes (KVS) kan lei. Navorsing uit ons laboratorium het voorheen bewys dat oksidatiewe stres 'n toename in vloeï deur metaboliese paaie soos die heksoamine biosintetiese pad (HBP) kan veroorsaak deur die modifisering van teikenproteïene met *O*-GlcNAc motiewe. Dit kan weer proteïen funksie verander en bydra tot die ontstaan van miokardiale insulienweerstandigheid en verswakte kontraktiele funksie. Die onderliggende meganismes wat kroniese stres aan kardiometaboliese patofisiologie verbind word nog nie goed verstaan nie, daarom is ons hipotese dat kortisol miokardiale oksidatiewe stres veroorsaak, die HBP pad aktiveer, en glukose opname verminder (deur die funksionele onderdrukking van glukose transport), wat nadelige uitkomst soos insulienweerstandigheid en apoptose tot gevolg kan hê.

Om hierdie hipotese te ondersoek, is 'n *in vitro* model van HL-1 kardiomyosiete gebruik waarmee die graad van *O*-GlcNAsilering en oksidatiewe stres in reaksie op 'n reeks tyd-konsentrasie behandelings met deksametasoon (sintetiese glukokortikoïed), bepaal is. Glukose transporter 4 (GLUT4) translokasie na die sarkolemma is ook geassesseer. In ooreenstemming met die literatuur, is GLUT4 translokasie insiggewend onderdruk tydens deksametasoon behandeling. Alhoewel geen insiggewende verskille rakende oksidatiewe stres en *O*-GlcNAsilering gevind is nie, het ons data aangedui dat laasgenoemde deur deksametasoon vermeerder het na twee ure van blootstelling aan die  $10^{-6}$  M konsentrasie.

Alhoewel ons resultate geen afdoende bewys lewer nie, stel dit wel voor dat daar 'n potensiële verbinde tussen deksametasoon behandeling en 'n afname in GLUT4 translokasie is. Gebasseer op ons bevindings, stel ons voor dat die nadelige effekte van kroniese stres op die hart bemiddel kan word deur 'n toename in vloeï deur die HBP. Gegewe dat 'n oormaat glukokortikoïede en GLUT4 wanregulering geassosieer is met insulien weerstandigheid (en verbandhoudende metaboliese veranderinge en siektes), verskaf hierdie resultate nuwe teikens vir potensiële terapeutiese ingrepe.

# Acknowledgements

Sincere gratitude goes to the following people who made this experience not only possible, but also pleasurable.

- My husband, Braam, for his love, incredible support, advice and patience.
- My parents, who have always encouraged me to seek enrichment and pursue my goals with perseverance. For all the sacrifices they have made so that I could have the best possible opportunities, I thank them.
- My study leader, Professor Essop, for his guidance, time, and patience throughout, and his kind and gentle way of interacting with people.
- Professor William Claycomb (Department of Biochemistry and Molecular Biology, LSU Health Sciences Centre, New Orleans, USA) for generously donating HL-1 cardiomyocytes.
- Professors Gavin Welsh and Jeremy Tavaré (University of Bristol, Bristol, UK), who kindly donated the HA-GLUT4-GFP construct.
- Dr Craig Kinnear (Department of Medical Biochemistry, University of Stellenbosch) who assisted by amplifying the HA-GLUT4-GFP construct.
- Dirk Lang and Susan Cooper (Imaging Facility, Department of Human Biology, University of Cape Town), for their assistance on the confocal microscope and insightful advice.
- Dr Ben Loos, for always being willing to help, for sharing his expertise and insights into flow cytometry, microscopy and the HA-GLUT4-GFP transfection experiments, and for his assistance with the editing of this document.
- Dr Theo Nell and Prof Anna-Mart Engelbrecht, for further editing assistance.

*ACKNOWLEDGEMENTS*

v

- Dr Annadie Krygsman, for managing the laboratory and her willingness to help.
- Everybody in the Department of Physiological Sciences, for the friendly, cooperative working environment, but especially the members of the CMRG for their friendship and assistance; Burger, Carla, Clare, Jamie, James, Kat, Kirsty, Rinah, Rudo, Uthra, and most importantly, Danzil ‘The Great’.



- For their friendship and comic relief: my brother, Gerhard; the engineers, Braam, Evan, and Renier, who persuaded me to use  $\text{\LaTeX}$  (thanks); and Paul, Carmi, Josh, Lize and Elsje.
- And finally, the National Research Foundation (NRF) for funding.

# Contents

<b>Declaration</b>	<b>i</b>
<b>Abstract</b>	<b>ii</b>
<b>Uittreksel</b>	<b>iii</b>
<b>Acknowledgements</b>	<b>iv</b>
<b>Contents</b>	<b>vi</b>
<b>List of Figures</b>	<b>xi</b>
<b>List of Tables</b>	<b>xiii</b>
<b>Nomenclature</b>	<b>xiv</b>
<b>1 Introduction</b>	<b>1</b>
1.1 The metabolic syndrome . . . . .	2
1.1.1 Definition . . . . .	2
1.1.2 Aetiology . . . . .	4
1.2 Cardiovascular complications . . . . .	4
1.3 Metabolic substrates of the heart . . . . .	5
1.3.1 Glucose metabolism . . . . .	5
1.3.2 Metabolic dysregulation due to excess glucose . . . . .	7
1.3.3 Fatty acid metabolism . . . . .	9
1.3.4 Metabolic dysregulation due to excess fatty acids . . . . .	10
1.4 Insulin resistance . . . . .	11
1.4.1 Fatty acid-induced insulin resistance . . . . .	12

## CONTENTS

vii

1.4.2	Other contributing factors to insulin resistance . . . . .	13
1.5	Stress . . . . .	14
1.5.1	Hypothalamo-pituitary-adrenocortical axis . . . . .	14
1.5.2	Glucocorticoids . . . . .	15
1.5.3	Role of stress in the pathogenesis of the metabolic syndrome . . . . .	16
1.5.4	Glucocorticoid excess and insulin resistance . . . . .	17
1.6	Oxidative stress . . . . .	19
1.6.1	Oxidative stress as a result of psychological stress . . . . .	20
1.6.2	Oxidative stress as an underlying cause of metabolic disorders . . . . .	21
1.7	Damaging pathways activated by hyperglycaemia . . . . .	23
1.7.1	Polyol pathway . . . . .	24
1.7.2	PKC pathway . . . . .	24
1.7.3	AGE formation . . . . .	26
1.7.4	The hexosamine biosynthetic pathway . . . . .	26
1.7.5	Summarising hyperglycaemia-activated pathways . . . . .	30
1.8	Research problem . . . . .	30
1.9	Hypothesis . . . . .	31
1.10	Aims . . . . .	31
<b>2</b>	<b>Materials and Methods</b>	<b>32</b>
2.1	Cell culture . . . . .	32
2.1.1	Establishing the protocol for HL-1 cell culture . . . . .	32
2.1.2	Pharmacological treatments . . . . .	34
2.2	Experimental protocol for analysis after dexamethasone treatment . . . . .	34
2.2.1	Flow cytometry . . . . .	36
2.2.2	Flow cytometric measurement of ROS . . . . .	37
2.2.3	Flow cytometric measurement of <i>O</i> -GlcNAc . . . . .	39
2.3	Measurement of <i>O</i> -GlcNAcylation by Western blotting analysis . . . . .	40
2.3.1	Cell culture, pharmacological treatments, and lysate collection . . . . .	40
2.3.2	Preparing samples for Western blotting . . . . .	41
2.3.3	Gels . . . . .	41
2.3.4	Electrophoresis . . . . .	42
2.3.5	Electrotransfer . . . . .	42
2.3.6	Probing the membrane . . . . .	42
2.3.7	Developing the membrane . . . . .	42

<i>CONTENTS</i>	<b>viii</b>
2.3.8 Densitometry . . . . .	43
2.4 Experimental protocol for the assessment of GLUT4 translocation . . . . .	43
2.4.1 Transfections . . . . .	43
2.4.2 Assessing HA-GLUT4-GFP transfection by immunofluorescence microscopy	46
2.4.3 Assessing HA-GLUT4-GFP transfection by confocal microscopy . . . . .	46
2.5 Statistical analysis . . . . .	47
<b>3 Results</b>	<b>48</b>
3.1 Culturing HL-1 cells . . . . .	48
3.2 Measuring ROS by flow cytometry . . . . .	50
3.3 Measuring the degree of <i>O</i> -GlcNAcylation . . . . .	51
3.3.1 Flow cytometry measurement of <i>O</i> -GlcNAc . . . . .	51
3.3.2 Western blotting measurement of <i>O</i> -GlcNAc . . . . .	52
3.4 Determining the degree of GLUT4 translocation . . . . .	54
3.4.1 Immunofluorescence microscopy . . . . .	54
3.4.2 Confocal microscopy . . . . .	56
<b>4 Discussion</b>	<b>61</b>
4.1 Introduction . . . . .	61
4.2 HL-1 cells . . . . .	62
4.3 Dexamethasone displays minimal effect on ROS . . . . .	63
4.4 Effect of dexamethasone on degree of <i>O</i> -GlcNAcylation . . . . .	64
4.4.1 Flow cytometry . . . . .	64
4.4.2 Western blotting . . . . .	64
4.5 GLUT4 translocation significantly reduced by dexamethasone . . . . .	65
4.5.1 Immunofluorescence microscopy . . . . .	65
4.5.2 Confocal microscopy . . . . .	66
4.6 Conclusion . . . . .	66
4.7 Future recommendations . . . . .	68
<b>Bibliography</b>	<b>69</b>
<b>Appendices</b>	<b>80</b>
<b>A Cell Culture: Growth and care of HL-1 cardiomyocytes</b>	<b>81</b>
A.1 Supplemented Claycomb Medium . . . . .	81

## CONTENTS

ix

A.1.1	Norepinephrine . . . . .	81
A.1.2	L-Glutamine . . . . .	83
A.2	Wash Medium . . . . .	83
A.3	Freezing Medium . . . . .	83
A.4	Pre-coating flasks: Gelatin/Fibronectin . . . . .	83
A.4.1	Preparing Gelatin/Fibronectin . . . . .	83
A.4.2	Coating flasks . . . . .	84
A.5	Culturing cells . . . . .	84
A.6	Passaging . . . . .	84
A.6.1	Soybean Trypsin Inhibitor . . . . .	86
A.7	Freezing cells . . . . .	86
A.8	Thawing cells . . . . .	87
<b>B</b>	<b>Staining protocol</b>	<b>89</b>
B.1	Staining protocol prior to flow cytometry and microscopy . . . . .	89
<b>C</b>	<b>Experimental protocol for analysis after dexamethasone treatment</b>	<b>91</b>
C.1	Flow Cytometry . . . . .	91
<b>D</b>	<b>Western blotting</b>	<b>92</b>
D.1	Cell harvesting . . . . .	92
D.1.1	Modified RIPA buffer . . . . .	92
D.2	Preparing lysates . . . . .	93
D.3	Protein quantification: The Bradford method . . . . .	94
D.3.1	Bradford Reagent . . . . .	95
D.4	Sample preparation for SDS-PAGE . . . . .	95
D.5	SDS-PAGE . . . . .	96
D.5.1	Running buffer . . . . .	97
D.6	Electrotransfer . . . . .	98
D.6.1	Transfer buffer . . . . .	98
D.7	Probing the membrane . . . . .	99
D.7.1	TBS . . . . .	99
D.7.2	TBS-T . . . . .	100
D.7.3	Detection of <i>O</i> -GlcNAc . . . . .	100
D.7.4	Detection of $\beta$ -actin . . . . .	100

<i>CONTENTS</i>	<b>x</b>
D.8 Developing the membrane . . . . .	101
D.9 Stripping membranes to reprobe . . . . .	101
<b>E HA-GLUT4-GFP Transfection</b>	<b>103</b>
E.1 Transfection Protocol . . . . .	103

# List of Figures

1.1	Glucometabolic insulin resistance development . . . . .	8
1.2	Glucometabolic insulin resistance development may protect against lipotoxicity . . . . .	9
1.3	Glucose fatty acid cycle . . . . .	11
1.4	The HPA negative feedback loop . . . . .	14
1.5	Superoxide production by the mitochondrial electron transport chain . . . . .	19
1.6	Alternate hyperglycaemia-activated pathways . . . . .	25
1.7	PUGNAc and OGA . . . . .	28
2.1	HL-1 cells when confluent . . . . .	33
2.2	Growth of HL-1 cells . . . . .	35
2.3	Overview of experimental methods . . . . .	36
2.4	Treatment of cells prior to flow cytometry for ROS analysis . . . . .	38
2.5	Treatment of cells prior to flow cytometry for <i>O</i> -GlcNAc analysis . . . . .	40
2.6	Overview of treatment protocol prior to Western blotting . . . . .	41
2.7	The HA-GLUT4-GFP model . . . . .	44
2.8	Overview of HA-GLUT4-GFP transfection protocol . . . . .	45
3.1	Flow cytometry results for ROS analysed . . . . .	50
3.2	Flow cytometry results for <i>O</i> -GlcNAc analysed . . . . .	51
3.3	Flow cytometry graphs for <i>O</i> -GlcNAc . . . . .	52
3.4	Western blot of <i>O</i> -GlcNAc and analysed results . . . . .	53
3.5	Fluorescence images of HA-GLUT4-GFP transfected control cells . . . . .	54
3.6	HA and GFP fluorescence images of insulin-stimulated cells . . . . .	55
3.7	HA and GFP fluorescence images of insulin-stimulated, dexamethasone-treated cells . . . . .	55
3.8	HA:GFP ratios for fluorescence microscopy images . . . . .	56
3.9	An HA-GLUT4-GFP transfected cell displaying baseline behaviour . . . . .	57
3.10	An HA-GLUT4-GFP transfected cell stimulated with insulin . . . . .	58

*LIST OF FIGURES*

xii

3.11 An HA-GLUT4-GFP transfected cell treated with dexamethasone and insulin-stimulated	59
3.12 Z-stack of an HA-GLUT4-GFP transfected cell . . . . .	60
4.1 Image of salt crystals . . . . .	63

# List of Tables

1.1	Criteria for diagnosis of the metabolic syndrome. Diagnosis of the metabolic syndrome requires detection of three (or more) risk factors within an individual. . . . .	3
1.2	Population- and country-specific thresholds of waist circumference. . . . .	3
A.1	Formulation of Claycomb Medium . . . . .	82
A.2	Supplemented Claycomb medium . . . . .	82
D.1	Modified RIPA buffer . . . . .	94
D.2	Concentrations for standard curve. . . . .	95
D.3	Constituents of polyacrylamide gels . . . . .	96

# Nomenclature

## Abbreviations:

A	Amperes
ACC	Acetyl CoA carboxylase
ACTH	Adrenocorticotrophic hormone
ADP	Adenosine diphosphate
AGE	Advanced glycation end product
AHA	American Heart Association
AMP	Adenosine monophosphate
AMPK	AMP-activated protein kinase
ANOVA	Analysis of variance
ATP	Adenosine triphosphate
AU	Arbitrary units
BP	Band pass
BSA	Bovine serum albumin
CoA	Coenzyme A
CPT-1	Carnitine palmitoyl transferase-1
CRH	Corticotropin-releasing hormone
CVD	Cardiovascular disease
DAG	Diacylglycerol
DAPI	4'-6'diamidino-2-phenylindole
DCF	Dichlorofluorescein
DHAP	Dihydroxyacetone phosphate
DMEM	Dulbecco's Modified Eagle's medium

*NOMENCLATURE*

xv

DMSO	Dimethyl sulphoxide
DNA	Deoxyribonucleic acid
EDTA	Ethylenediaminetetraacetic acid
ETC	Electron transport chain
Fab region	Fragment antigen-binding region
Fc region	Fragment crystallisable region
FA	Fatty acid
FABP	Fatty acid binding protein
FACS	Fatty acyl CoA synthase
FAD	Flavin adenine dinucleotide (oxidised)
FADH <sub>2</sub>	Flavin adenine dinucleotide (reduced)
FAT	Fatty acid translocase
FFA	Free fatty acid
FITC	Fluorescein isothiocyanate
GAPDH	Glyceraldehyde-3-phosphate dehydrogenase
G/F	Gelatin/Fibronectin
GFAT	Glutamine:fructose-6-phosphate amidotransferase
GFP	Green fluorescent protein
GlcN	Glucosamine
GLUT	Glucose transporter
GR	Glucocorticoid receptor
GSH	Glutathione (reduced)
GSSG	Glutathione (oxidised)
GSV	Glucose transporter storage vesicles
H <sub>2</sub> DCFDA	Dihydrodichlorofluorescein diacetate
HA	Haemagglutinin
HBP	Hexosamine biosynthetic pathway
HDL	High-density lipoprotein
HF	Heart Failure
HK	Hexokinase

## NOMENCLATURE

xvi

HPA	Hypothalamic-pituitary-adrenocortical
HSP	Heat-shock protein
IL	Interleukin
IDF	International Diabetes Federation
IR	Insulin receptor
IRS	Insulin receptor substrate
JNK	c-Jun NH <sub>2</sub> -terminal kinase
LP	Long pass
LDH	Lactate dehydrogenase
LDL	Low density lipoproteins
MAPK	Mitogen-activated protein kinase
mOGT	Mitochondrial OGT
MPO	Myeloperoxidase
MR	Mineralocorticoid receptor
mRNA	Messenger ribonucleic acid
NHLBI	National Heart, Lung, and Blood Institute
NAD <sup>+</sup>	Nicotinamide adenine dinucleotide (oxidised)
NADH	Nicotinamide adenine dinucleotide (reduced)
NADP <sup>+</sup>	Nicotinamide adenine dinucleotide phosphatase (oxidised)
NADPH	Nicotinamide adenine dinucleotide phosphatase (reduced)
NAG	N-acetylglucosamine
NCEP	National Cholesterol Education Program
NEFA	Non-esterified fatty acids
NF $\kappa$ -B	Nuclear factor $\kappa$ -B
NLO	Non-linear optical
NOS	Nitric oxide synthase
OGA	<i>O</i> -GlcNAcase
<i>O</i> -GlcNAc	<i>O</i> -linked $\beta$ -N-acetylglucosamine
<i>O</i> -GlcNAcase	<i>O</i> -linked $\beta$ -N-acetylglucosaminidase
OGT	Uridine diphospho-N-acetylglucosamine:polypeptide $\beta$ -N-acetylglucosaminyl-transferase or <i>O</i> -GlcNAc transferase

## NOMENCLATURE

xvii

p	Probability
P	Phosphate
PAGE	Polyacrylamide gel electrophoresis
PARP	Poly(ADP-ribose) polymerase
PBS	Phosphate-buffered solution
PDH	Pyruvate dehydrogenase
PDK	PDH kinase
PDK-1	Phosphoinositide-dependent kinase-1
PE-TxRed	R-phycoerythrin-conjugated Texas Red
PFK	Phosphofructokinase
PGI	Phosphoglycerate isomerase
PGK	Phosphoglycerate kinase
PI3K	phosphoinositide 3-kinase, or PI 3-kinase
PK	Pyruvate kinase
PKB	Protein kinase B, also known as Akt
PKC	Protein kinase C
PMSF	Phenylmethanesulfonyl fluoride
PUGNAc	O-(2-acetamido-2-deoxy-D-glucopyranosylidene)amino-N-phenylcarbamate
PVDF	Polyvinylidene flouride
RAGE	AGE receptor
RIPA	Radioimmunoprecipitation assay
ROS	Reactive oxygen species
RNS	Reactive nitrogen species
SDH	Sorbitol dehydrogenase
SDS	Sodium dodecyl sulphate
SDS-PAGE	SDS-polyacrylamide gel electrophoresis
SEM	Standard error of the mean
SERCA2a	Sarcoendoplasmic reticulum Ca <sup>2+</sup> -ATPase
SOD	Superoxide dismutase
T2DM	Type 2 Diabetes Mellitus

## NOMENCLATURE

xviii

TBS	Tris-buffered saline
TBS-T	TBS-Tween
TEMED	N,N,N'N'-tetramethylene diamine
TG	Triacylglycerol
TIM	Triose phosphate isomerase
TxRed	Texas red
TNF- $\alpha$	Tumor necrosis factor- $\alpha$
UCP	Uncoupling protein
UDP	Uridine diphosphate
UDP-GlcNAc	Uridine diphospho- $\beta$ -N-acetylglucosamine
UN	United Nations
V	Volts
W	Watt
WHO	World Health Organisation
<i>(aq)</i>	Aqueous
$\alpha$ -OHCA	$\alpha$ -cyano 4-hydroxyl cinnamic acid
$\beta$ -actin	Beta-actin
11 $\beta$ -HSD	11 $\beta$ -hydroxysteroid dehydrogenase
Ca <sup>2+</sup>	Calcium ion
CO <sub>2</sub>	Carbon dioxide
H <sup>+</sup>	Hydrogen ions
HCO <sub>3</sub> <sup>-</sup>	Bicarbonate
H <sub>2</sub> CO <sub>3</sub>	Carbonic acid
H <sub>2</sub> O	Water
K <sup>+</sup>	Potassium ion
Na <sup>+</sup>	Sodium ion
NaCl	Sodium chloride
NaHCO <sub>3</sub>	Sodium bicarbonate

*NOMENCLATURE***xix**

NaOH	Sodium hydroxide
H <sub>2</sub> O <sub>2</sub>	Hydrogen peroxide
O <sub>2</sub> ·	Superoxide
·OH	Hydroxyl
NO·	Nitroxyl
RO·	Alkoxy
ROO·	Peroxy
ROOH	Hydroperoxide

# Chapter 1

## Introduction

The world is getting fat. The McKinsey Quarterly of October 2010 [1], and a plethora of frightening statistics robustly support this notion. Moreover, according to the World Health Organisation (WHO) [2], *obesity* has more than doubled globally since 1980. The International Diabetes Federation (IDF) estimates that 366 million people have *diabetes* in 2011 and that it will escalate to 552 million people by 2030 [3], with type 2 diabetes mellitus (T2DM) accounting for more than 85% - 95% of the total prevalence [4]. To underline the severity of the current situation, earlier this year the United Nations (UN) at their sixty-sixth general assembly, included diabetes and heart diseases (frequently associated with overweight and obesity) as socio-economic and development challenges of ‘epidemic proportions’ [5].

Africa has not remained unscathed by this metabolic ‘epidemic’. The IDF projects a doubling in the number of people with diabetes in Africa between 2011 and 2030, i.e. from 14.7 to 28 million [6]. Ziraba et al. [7] compiled research from a number of studies throughout the continent, spanning at least a decade, and found that the prevalence of urban overweight/obesity was on the rise ( $\sim 35\%$ ). The increase was highest among the poor (+50%) and non-educated groups, although the affluent sections of the population (+7%) were also affected. This is a paradoxical finding, considering that many people in developing countries remain significantly malnourished [1]. Interestingly, developing countries undergoing socioeconomic and demographic transition often display a nutrition paradox in which so-called ‘dual-burden households’ have both underweight and overweight family members [8]. Furthermore, where T2DM, a disease with many complications, was once considered to be a disease of wealthy nations, it is now a global affliction [9], with 80% of affected individuals living in low- and middle-income countries [3].

So-called 'Western' eating and lifestyle habits are trending globally e.g. sedentary lifestyles married to energy rich diets - much too high in processed carbohydrates and lipids - are becoming the norm. This results in an energy imbalance in the body, and consequently leads to an excess of fuel substrate supply which may be 'toxic' to our cells. In most people, fuel substrate excess invariably leads to metabolic dysregulation and a host of damaging, intracellular alterations with severe functional consequences. This thesis will focus on some myocardial metabolic derangements and the mechanisms that underlie their pathophysiology in the context of T2DM.

## 1.1 The metabolic syndrome

A cluster of risk factors have been identified as key warning signs for diseases involving metabolic dysregulation. These risk factors are more frequently observed in concert than in isolation [10], and constitute what is known as the metabolic syndrome. There is often great overlap of risk factors among metabolic diseases. Therefore, it is likely that a person suffering from diabetes, obesity or cardiovascular disease (CVD) may also be diagnosed with the metabolic syndrome. Thus, the metabolic syndrome has become an inclusive concept (an umbrella term) for metabolic disorders. The ability to identify risk factors in patients provides a valuable tool to assess individual risk profiles and susceptibility to metabolic diseases. It also pinpoints risk areas which allows for its early detection, and provides an opportunity to promote prevention of cardiometabolic diseases by appropriate lifestyle changes.

### 1.1.1 Definition

The two main causes of the metabolic syndrome, and its rapidly increasing spread across the world, are high caloric diet and physical inactivity. Since it was first described by Reaven in 1988 [11], various definitions have been formulated for the characterisation of the metabolic syndrome by organisations such as the IDF, and the WHO. In 2009, a number of associations<sup>1</sup> met in an attempt to unify the criteria to be considered for diagnosis of the metabolic syndrome [12]. The physiological parameters agreed on were released in a joint statement<sup>2</sup> [refer Table 1.1].

---

<sup>1</sup>International Diabetes Federation Task Force on Epidemiology and Prevention; National Heart, Lung, and Blood Institute (NHLBI); American Heart Association (AHA); World Health Federation; International Atherosclerosis Society; and International Association for the Study of Obesity.

<sup>2</sup>Furthermore, the revised National Cholesterol Education Program (NCEP) definition (2004) also includes patients being treated for dyslipidaemia, hyperglycaemia, or systemic hypertension.

Risk factors	Parameters
Elevated waist circumference	Population- and country-specific
Elevated serum triglycerides	$\leq 1.7$ mmol/l
Reduced high-density lipoprotein (HDL) cholesterol	$< 1$ mmol/l (males) $< 1.3$ mmol/l (females)
Elevated blood pressure	$\geq 130$ mm Hg (systolic) and/or $\geq 85$ mm Hg (diastolic)
Elevated fasting glucose	$\geq 5.6$ mmol/l

**Table 1.1:** Criteria for diagnosis of the metabolic syndrome. Diagnosis of the metabolic syndrome requires detection of three (or more) risk factors within an individual.

Elevated waist circumference, elevated serum triglycerides, reduced high-density lipoprotein (HDL) cholesterol, elevated blood pressure, and elevated fasting glucose are major indicators of the manifestation of the metabolic syndrome. The parameter values provided in Table 1.1 (right column) indicate values that extend beyond the normal range. Detection of three (or more) of the aforementioned risk factors within an individual constitutes diagnosis of the metabolic syndrome. However, discussions between the American Heart Association (AHA) and National Heart, Lung, and Blood Institute (NHLBI), and the IDF recently concluded in the agreement that visceral adiposity should not be the main prerequisite for diagnosis [12]. Moreover, elevated waist circumference now has population- and country-specific parameters [refer Table 1.2].

Population	Organisation	Men	Women
European	IDF	$\geq 94$ cm	$\geq 80$ cm
Caucasian	WHO	$\geq 94$ cm or 102 cm	$\geq 80$ cm or 88 cm
United States	AHA/ATPIII	$\geq 102$ cm	$\geq 88$ cm
Asian	IDF/WHO	$\geq 90$ cm	$\geq 80$ cm
China	Cooperative task force	$\geq 85$ cm	$\geq 80$ cm
Sub-Saharan Africa	IDF	$\geq 94$ cm	$\geq 80$ cm
Ethnic Central & South American	IDF	$\geq 90$ cm	$\geq 80$ cm

**Table 1.2:** Population- and country-specific thresholds of waist circumference.

AHA/NHLBI guidelines for metabolic syndrome recognise that risk for CVD and diabetes is increased beyond waist circumference measurements of 94 cm in men, and 80 cm in women, and suggest that individuals or populations with increased insulin resistance consider these as optional cut-off points.

The risk factors of the syndrome are varied but all point to metabolic dysregulation. Therefore, it is understandable that the metabolic syndrome results in an alteration of glucose homeostasis and glucose intolerance, which is an indicator of insulin insensitivity<sup>3</sup> [13]. To compensate, an increase in insulin blood levels can occur, but since sensitivity to insulin has decreased, glucose levels in the blood stream are often increased and may give rise to a diabetic state [13].

### 1.1.2 Aetiology

Aside from lack of physical activity and a high caloric diet, there is evidence to indicate that psychosocial, neuroendocrine, immunogenic, and oxidative stress are key factors in the development of metabolic syndrome, CVD, and T2DM [14]. Identifying causes (whether systemic or environmental) provides clues to pinpointing molecular mechanisms underlying the pathophysiology of the syndrome. The mechanisms are not yet fully understood, however, a number of theories have been proposed, frequently based on insulin resistance [15]. [*Insulin resistance* and its possible underlying mechanisms are discussed in Section 1.4].

## 1.2 Cardiovascular complications

The metabolic syndrome, which has also been referred to as ‘Reaven’s Syndrome X’ [15], has become a major health concern as a result of its strong link to T2DM and CVD [16]. CVD has been described as the major cause of morbidity and mortality associated with diabetes [17]. According to Mottillo et al. [16] metabolic syndrome is associated with a 2-fold increase in risk for CVD, CVD mortality, myocardial infarction, and stroke; and a 1.5-fold increase in risk for all-cause mortality. The metabolic syndrome is further associated with the development of atherosclerosis [10] and heart failure [18]. Moreover, independent factors such as ageing and genetic susceptibility may accelerate and/or exaggerate disease risks or complications, and the mechanisms that mediate the tissue-damaging effects, which are yet to be discussed [19].

Other complications that may arise due to the metabolic syndrome or some of the associated risk factors include triglyceride accumulation. Moreover, it may also arise due to hyperlipidaemia, or obesity, and when it occurs within cardiomyocytes, may be associated with cell death (as a result of toxic lipid intermediates), and impaired contractile function [20]. It is

---

<sup>3</sup>Insulin insensitivity can be considered as the reduced capacity of insulin to promote glucose uptake in cells.

also relatively common in non-ischaemic heart failure, e.g. failing hearts display attenuated fatty acid (FA) oxidation, and if myocardial insulin resistance is present concomitantly, glucose oxidation may be impaired too, resulting in ‘energy starvation’ of the heart [20].

## 1.3 Metabolic substrates of the heart

For nearly a century, it has been known that there is competition between substrates for mitochondrial respiration in animal tissues. The most important interaction, quantitatively, lies in the glucose fatty acid cycle [refer Section 1.3.4.1], also known as the Randle cycle - described in 1963 by Randle et al. [21] as a reciprocal metabolic relationship, rather than a dependent one [22].

The heart, like the body, is an omnivore in terms of its fuel substrate selection, i.e. FAs, glucose, lactate, and ketone bodies. However, under normal physiologic conditions the heart utilises FAs as its primary energy substrate<sup>4</sup> and since cardiomyocytes have limited capacity for triglyceride storage, the uptake and oxidation of FAs is tightly regulated [24]. On this metabolic tightrope, the heart can adapt to the prevailing milieu, and convert the chemical energy contained in myriad oxidisable substrates to meet the energy demands of contraction [25].

Substrate metabolism is kept in a delicate balance. Substrate uptake, CO<sub>2</sub> production and O<sub>2</sub> consumption are matched, almost precisely, with ATP turnover [25]. At the same time, provision of free FAs promote oxidation and storage of FAs, it inhibits glucose oxidation (Randle cycle), and if glycogen reserves are low, glucose storage may be promoted. On the other hand, availability of glucose promotes glucose oxidation, storage of both glucose and lipids, and inhibits FA oxidation (reverse Randle cycle) [22].

### 1.3.1 Glucose metabolism

Before glucose metabolism can take place, glucose needs to enter the cell, and for this to happen efficiently, glucose transporters need to be stimulated to migrate to the cell membrane. Insulin stimulation and the insulin signaling pathway are a vital part of the process. When insulin binds to the extracellular insulin receptor a phosphorylation cascade is triggered. This signalling pathway functions to mediate glucose transporter 4 (GLUT4) translocation to the cell

---

<sup>4</sup>FAs contribute approximately 70% of the ATP required for normal heart function [23].

membrane so that glucose transport into the cell can be facilitated.

Under normal circumstances, insulin binds to the  $\alpha$  subunit of the insulin receptor (IR) and activates the tyrosine kinase in the  $\beta$  subunit within the cell. The activated tyrosine kinase phosphorylates the insulin receptor substrate (IRS) proteins.<sup>5</sup> Then, the phosphotyrosine residues on IRS become targets for regulation by the p85 subunit of phosphoinositide 3-kinase (PI3K) which in turn catalyzes phosphatidylinositol 4,5 diphosphate into phosphatidylinositol 3,4,5 triphosphate. Downstream, phosphatidylinositol-dependent kinase and Akt (a serine/threonine kinase also known as protein kinase B, PKB) have a pleckstrin homology domain that facilitate the migration of GLUT4 to the membrane [26]. This PI3K-Akt<sup>6</sup> activation is crucial for insulin-stimulated GLUT4 translocation to the sarcolemma [illustrated in steps 1 - 4 of Figure 1.1], and thus for allowing glucose into the cell.

Once in the cell, glucose becomes phosphorylated to glucose-6-phosphate and can either be stored as glycogen or proceed through the glycolytic pathway to form pyruvate. Pyruvate dehydrogenase irreversibly catalyses the decarboxylation of pyruvate into acetyl CoA. Acetyl CoA enters mitochondria to undergo glycolytic oxidation via the citric acid cycle, producing CO<sub>2</sub> and H<sub>2</sub>O.

### 1.3.1.1 Glucose transporters in metabolism

GLUT1 and GLUT4 are the two major glucose transporter isoforms responsible for basal and insulin-stimulated glucose uptake. These have been identified in rodent cardiomyocytes and specifically, in HL-1 mouse cardiomyocytes [28]. The two primary sites of insulin-dependent glucose disposal, and GLUT4 synthesis, are muscle and adipose tissue. In isolated rat cardiomyocytes GLUT1 accounts for approximately 30% of total glucose carriers (as opposed to  $\sim 5 - 10\%$  in adipocytes and skeletal muscle), and GLUT4 for about 70% [29]. As the name implies, GLUT4 proceeds to transport glucose, increasing its flux into the cell by a net 10- to 40-fold [27]. Upon extracellular insulin stimulation, GLUT4 is redistributed from intracellular storage vesicles to the cell membrane. GLUT4 is present in two vesicle populations in cardiomyocytes: pool 1 contains GLUT4 and little or no GLUT1; whilst pool 2, aside from GLUT4, contains

---

<sup>5</sup>When insulin signalling becomes dysregulated, serine (instead of tyrosine) on the IRS is phosphorylated. IRS-1 has more than 70 potential serine phosphorylation sites, and their phosphorylation generally affect IRS signalling negatively [26].

<sup>6</sup>Substantial evidence exists in support of Akt being involved in insulin-stimulated GLUT4 translocation to the cell membrane, promoting glucose transport. PI3K is an intermediate in this insulin signalling pathway but Akt is the furthest-known downstream target [27].

a substantial GLUT1 and secretory carrier membrane proteins (SCAMPs) component [29]. Becker et al. [30] elaborate on hypothetical models of distribution and trafficking of glucose transporters. The models differ with regard to component composition of the intracellular pools, and the differential effects of insulin stimulation on them.

Interestingly, contraction also stimulates GLUT4 translocation but by a different mechanism, independent of insulin stimulation [31]. This is observed in skeletal muscle, but is more prevalent in cardiac muscle where contraction occurs continuously. GLUT4 translocation may also be stimulated by AMP-activated protein kinase (AMPK), an enzyme (activated by exercise) involved in cellular energy homeostasis. AMPK inhibits anabolic and promotes catabolic processes by influencing various mechanisms (including increased delivery and metabolism of both glucose and fatty acids) [32].

### 1.3.2 Metabolic dysregulation due to excess glucose

When a surplus glucose is present in the cell, and it cannot be stored as glycogen, glucose metabolism produces an overabundance of acetyl CoA (a precursor to the lipogenic pathway) in mitochondria. Excess unoxidised acetyl CoA is shuttled out of mitochondria back to the cytosol where it is carboxylated by acetyl CoA carboxylase (ACC) to malonyl CoA - the primary intermediate of FA synthesis. In this way, insulin can also stimulate lipogenesis. Malonyl CoA in abundance inhibits carnitine palmitoyl transferase-1 (CPT-1), the rate-limiting enzyme which facilitates movement of FAs into the mitochondrion. In other words, increased malonyl CoA exerts an inhibitory effect on FA oxidation, and this is referred to as the McGarry effect [33], [34]. Within the pre- or full-blown diabetic milieu (high FA supply), blunted FA oxidation leads to an accumulation of FA CoA and/or its derivatives, triglycerides and/or ceramide, which interferes with the phosphorylation of Akt.<sup>7</sup>

Unger [34] implicates increased insulin-stimulated lipogenesis as a cause of glucometabolic insulin resistance [see Figure 1.1], and then continues to explain how this form of insulin resistance may protect against severe lipotoxicity [Figure 1.2]. Here it is important to note the role of the glucose transporter, GLUT4. By limiting the entry of glucose into the cell, malonyl CoA production is reduced with two beneficial effects. Firstly, it lowers FA acid synthesis; and secondly, it removes the inhibition of CPT-1, thereby allowing FA oxidation to proceed.

---

<sup>7</sup>Notably, the presence of the sphingomyelin derivative ceramide has been shown to induce a 60% reduction in insulin-stimulated Akt activity (and thus attenuated GLUT4 translocation and glucose uptake) [27].

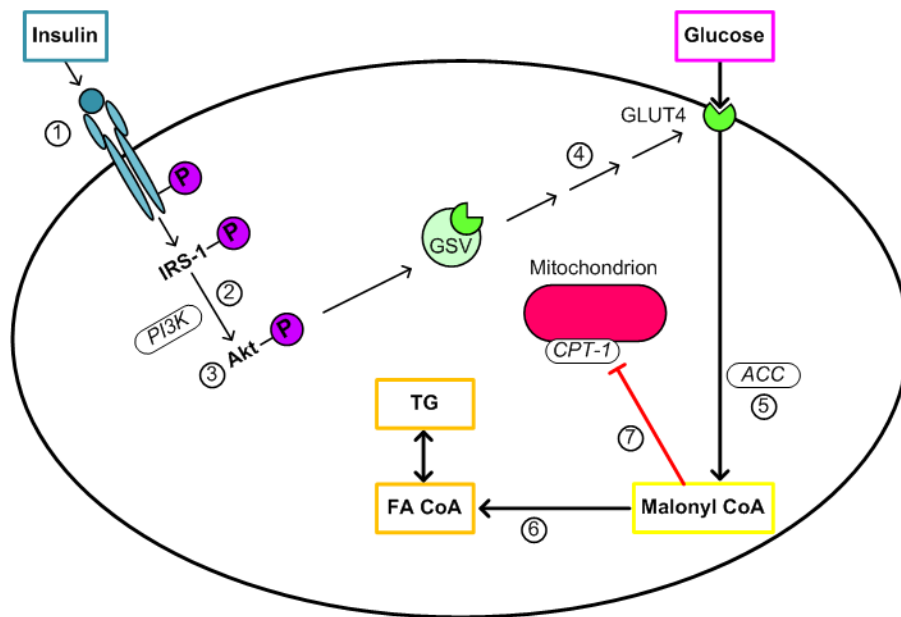


**Figure 1.1:** Increased insulin-stimulated lipogenesis contributes to the development of glucometabolic insulin resistance (adapted from Unger [34]). Insulin action is initiated when it binds to its receptor (1). A tyrosine phosphorylation cascade results in which insulin receptor substrate (IRS-1)-associated phosphoinositide 3-kinase (PI3K) activity (2) and the phosphorylation of Akt (3) are essential for GLUT4 translocation (4) from glucose transporter storage vesicles (GSVs) in the cytoplasm to the sarcolemma. Once at the membrane, it transports glucose into the cell. Excess glucose that cannot be metabolised oxidatively or stored as glycogen enters the lipogenic pathway as acetyl CoA (5). Acetyl CoA carboxylase (ACC) catalyses the formation of malonyl CoA, the first step in the synthesis of long-chain fatty acids (FA CoA) (6), triacylglycerols (TGs) and their lipotoxic derivatives e.g. ceramides (not shown). Increased malonyl CoA inhibits carnitine palmitoyl transferase 1 (CPT-1), an enzyme which mediates the transport of long-chain fatty acids (FAs) into the mitochondrial matrix. CPT-1 inhibition blocks FA oxidation (McGarry effect). As a result, intracellular Fa CoA and/or derivatives thereof accumulate, which interferes with the phosphorylation of Akt (3).

Collectively these effects limit accumulation of intracellular lipids, ultimately reversing their inhibitory effect on GLUT4 translocation. This theory makes sense from a homeostatic perspective. However, it also demonstrates how natural defences become detrimental if chronically activated e.g. chronic hyperglycaemia will defeat the purpose of this mechanism. Under these conditions intracellular homeostasis will not be achieved, but instead a greater insensitivity to insulin.

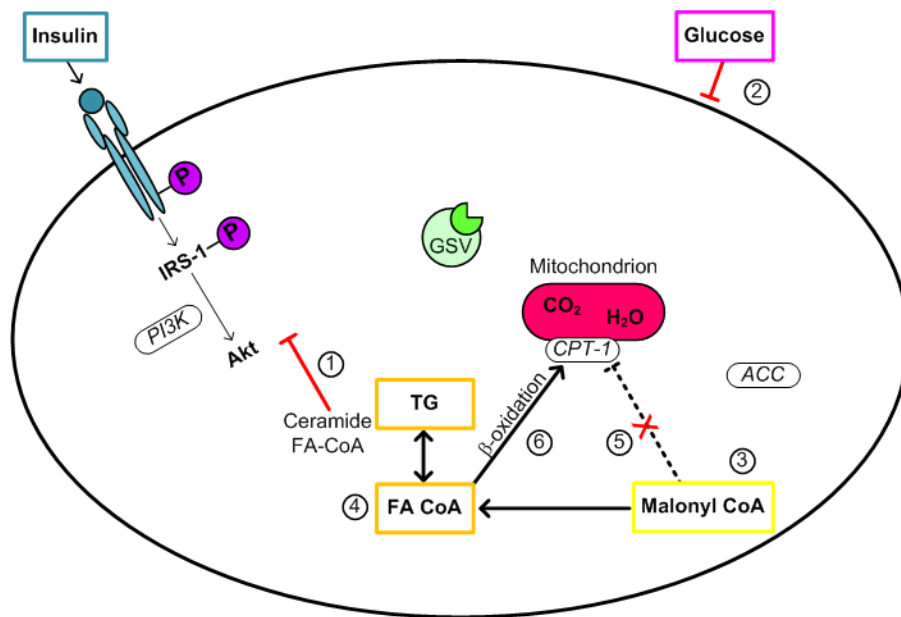


**Figure 1.2:** Glucometabolic insulin resistance may protect against severe lipotoxicity. Accumulated FAs or lipid derivatives such as ceramide (1) blunt GLUT4 translocation and thereby glucose transport into the cell (2). Malonyl CoA formation is reduced (3), and so too FA-CoA synthesis (4) removing the CPT-1 inhibition (5). Consequently, FA oxidation by mitochondria increases, producing CO<sub>2</sub> and H<sub>2</sub>O (6). In this way, the accumulation of intracellular lipids (including ceramide) will be lessened. Adapted from Unger [34].

### 1.3.3 Fatty acid metabolism

The greater the availability of free fatty acids (FFAs), the higher its uptake into cells. Myocardial FA uptake occurs via passive diffusion or by protein-mediated transport across the sarcolemma, facilitated by proteins such as fatty acid translocase (FAT) and plasma membrane fatty acid binding protein (FABP). FFAs, which are usually transported in non-esterified form, bind to the FABP where it can immediately be esterified to fatty acyl CoA by fatty acyl CoA synthase (FACS). Depending on their composition and the energy demands of the cell, fatty acyl CoAs, may be shunted into one of three pathways:  $\beta$ -oxidation, glycerolipid formation, or sphingolipid formation [35].  $\beta$ -oxidation of acyl CoAs takes place in the mitochondrion<sup>8</sup> where energy equivalents can be donated to the electron transport chain (ETC) for ATP synthesis.

<sup>8</sup>CPT-1 regulates the entry of long-chain fatty acyl CoAs into mitochondria but short-chain acyl CoAs can bypass the CPT shuttle system (consisting of CPT-1 and CPT-2 in the outer and inner mitochondrial membranes, respectively). Thus, it is unlikely that short-chain acyl CoAs contribute to the formation of other lipid metabolites [35].

### 1.3.4 Metabolic dysregulation due to excess fatty acids

FAs, particularly non-esterified fatty acids, known to play a role in the metabolic syndrome, are released from adipose tissue into the bloodstream after lipolysis. The release of FAs increases with greater adipose mass. Consequently, greater release of FAs will continue despite elevated insulin levels present in (overweight) diabetic individuals [36] which would normally suppress lipolysis [37]. In the fasting state, FAs are the primary, nutrient energy source, but within the obese context FA availability exceeds myocardial metabolic demand leading to dysregulation. Grundy [36] suggests that metabolic fuel excess initiates defence mechanisms, but that such processes may contribute to increased metabolic risk factors.

#### 1.3.4.1 Glucose Fatty Acid Cycle

The glucose fatty acid cycle [Figure 1.3], also known as the Randle cycle, after Philip Randle [21] was put forward as a mechanism of FA-induced insulin resistance. It posits that an increase in FA oxidation results in augmentation of the acetyl CoA/CoA and NADH/NAD<sup>+</sup> ratios within the mitochondrion. Increased acetyl CoA and NADH would inactivate pyruvate dehydrogenase (PDH). As a result, citrate concentrations would rise, leading to inhibition of phosphofructokinase (PFK). This, in turn, results in accumulation of glucose-6-phosphate causing an inhibition of hexokinase (HK) activity and decreased glycolytic flux. With glycolysis thus attenuated, intracellular glucose concentrations increase and glucose uptake diminishes [38].

Various researchers challenged the glucose fatty acid cycle hypothesis [39]. For example, Shulman [38] cited two reasons for disagreeing with the Randle hypothesis. Firstly, that decreased intramuscular glucose-6-phosphate concentrations may be observed under conditions of fat-induced insulin resistance. Secondly, the interference that FAs seem to exert (in a very early step) on insulin-stimulated GLUT4 transporter and/or hexokinase activity.

Here, Shulman [38] argues that increasing intracellular FA metabolites (e.g. diacylglycerol, FA CoAs, or ceramides) trigger a serine/threonine kinase cascade, which leads to phosphorylation of serine/threonine sites on IRS. Furthermore, Shulman suggests that the phosphorylation cascade may be initiated by PKC $\theta$ , and that phosphorylation of the serine residues (rather than threonine) lead to impaired PI3K activation. In turn, this results in reduced activation of glucose transport and other downstream processes.

In summary, the theories discussed make it clear that both glucose and FA excess have pathogenic

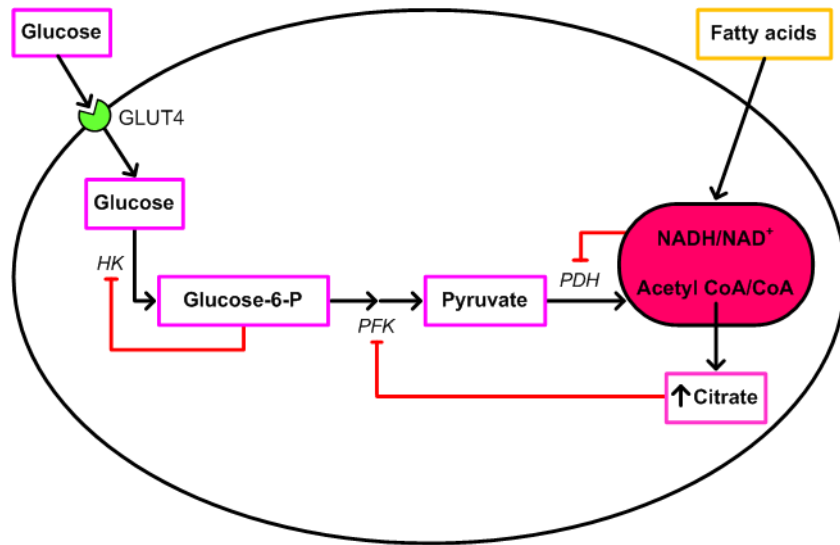


**Figure 1.3:** Schematic representation of the glucose fatty acid cycle, also known as the Randle cycle. Randle et al. [21] suggested that greater FA oxidation would increase acetyl CoA and NADH resulting in the inactivation of PDH. As a result, citrate concentrations would rise, leading to inhibition of PFK, and thus, accumulation of glucose-6-phosphate. Upstream, HK activity would be inhibited leading to decreased glycolytic flux. Consequently, intracellular glucose concentrations would increase, thereby reducing glucose uptake. Figure adapted from Shulman [38].

effects, compounded in unison. Taegtmeyer & Stanley [25] used the term ‘cardiac lipotoxicity’<sup>9</sup> coined by Roger Unger, and extended the concept to include the adverse effects of glucose and resulting toxic metabolites, and called it ‘cardiac glucolipotoxicity’. This serves to emphasise the point that fuel excess is toxic to (myocardial) cells, and if left unchecked can lead to metabolic dysregulation. Dysregulation of both glucose and fatty acid metabolism repeatedly point to insulin resistance.

## 1.4 Insulin resistance

A number of theories have been proposed to describe the mechanisms of defective insulin signalling. Some of these mechanisms were discussed in Sections 1.3.2 [*Metabolic dysregulation due to excess glucose*] and 1.3.4 [*Metabolic dysregulation due to excess fatty acids*] since the onset of insulin resistance usually coincides with dysregulation of metabolism due to glucose and/or FA excess.

<sup>9</sup>Taegtmeyer et al. [25] assert that lipid-lowering interventions or weight loss may rescue the deleterious sequence of events in which lipotoxicity leads to cell death, contractile dysfunction and heart failure.

### 1.4.1 Fatty acid-induced insulin resistance

The most prominent theories surrounding the aetiology of insulin resistance are based on dysregulation of fatty acid metabolism. This is probably because excess glucose metabolites (such as acetyl CoA) also enter the lipogenic pathway contributing to an accumulation of intracellular FAs.

#### 1.4.1.1 Decreased GLUT4 translocation

In the context of toxic fuel excess, the lipid theory for the development of myocardial insulin resistance has increasingly been put forward to explain the pathogenesis of the disease. For example, Sharma et al. [20] emphasise that increased fatty acid delivery (due to obesity and diabetes), as well as impaired FA oxidation (as in heart failure) can have severe intramyocardial triglyceride accumulation as a consequence. This accumulation of long chain FAs is a key factor in the lipid theory.

Unger [34] describes lipid overload and its contribution to the metabolic syndrome, however, holds that the underlying mechanism leading to the metabolic syndrome is in fact a loss of leptin<sup>10</sup> action, which contrasts the popularly held belief that it is an insulin-resistance syndrome.<sup>11</sup> Unger [34] also highlights that there is extensive evidence linking glucocorticoids to obesity [elaborated on in Section 1.5]. It has also been illustrated that high local levels of the steroid hormone may cause leptin resistance [41]).

#### 1.4.1.2 Decreased expression of insulin receptor

Another FA-induced mechanism postulated to play a role in promoting loss of insulin sensitivity is the inhibition of insulin receptor (IR) gene expression. It has been shown that palmitate (FA), inhibits IR expression which results in reduced IR protein in insulin target cells [42]. Furthermore, this reduction in IR expression was found to be due to phosphoinositide-dependent kinase-1 (PDK-1)-independent phosphorylation of PKC $\epsilon$ . Phospho-PKC $\epsilon$  is translocated to the nucleus, but exactly how it downregulates the IR gene remains unclear. Bhattacharya et al. [42] also review recent reports that have implicated various PKC isoforms in insulin signalling

---

<sup>10</sup>Leptin is a key regulator of energy intake and expenditure. It is a hormone which acts, under normal physiological conditions, as an appetite suppressant.

<sup>11</sup>The protective role of leptin and adiponectin against lipotoxicity has gained support from other researchers as shown in a review by Lewis, Carpentier, Adeli & Giacca [40].

regulation, and note that expression levels and activity of a few PKC isoforms are also associated with insulin resistance.

## 1.4.2 Other contributing factors to insulin resistance

There are also other factors that have been implicated in the pathophysiology of insulin resistance, including glucocorticoids [refer Section 1.5.4], oxidative stress [elaborated on in Section 1.6], and the hexosamine biosynthetic pathway (HBP) [Section 1.7.4]. The HBP is a major focus of this research project.

### 1.4.2.1 The hexosamine biosynthetic pathway

The HBP is an overflow pathway of glycolysis. Depending on the cell type, two to five per cent of glucose that enters cells will flux through the HBP. The pathway, involved primarily in nutrient sensing, will thus be upregulated by high intracellular glucose levels. Insight into the HBP shows how glucose shifts to hold a regulatory role in cellular processes. Thus, the role of glucose is expanded beyond its traditional role(s) in energy metabolism [43].

The HBP is known to be responsible for post-translational glycosylation of target proteins [44]. This *O*-linked  $\beta$ -N-acetylglucosamine (*O*-GlcNAc) intracellular modification, occurs on threonine or serine residues of nucleocytoplasmic proteins. Interestingly, *O*-GlcNAc and *O*-phosphate have been mapped to the same serine or threonine residue on a subset of proteins, and display extensive crosstalk [45]. It is also known to compete for phosphorylation sites.

*O*-GlcNAcylation is a highly dynamic process, with rapid cycling in response to cellular signals [46]. Being responsive to many stimuli and conditions suggests that it holds importance in many regulatory pathways. *O*-GlcNAcylation acts as a cellular regulator of growth and proliferation, but mainly holds status as a nutrient- and stress-sensor [47].

Since the focus of this research is on the involvement of stress in the aetiology of insulin resistance and the metabolic syndrome, the HBP as stress and nutrient sensor is a pertinent pathway to investigate in the context of metabolic dysregulation. The following section will review stress and its role in the pathogenesis of the metabolic syndrome.

## 1.5 Stress

Stress is another side effect of the modern, westernised lifestyle which takes a bigger toll on health than realised. Although the stress phenomenon is recognised as a ‘survival mechanism’, chronic activation of stress responses are known to have adverse effects. Rosmond [10] provides a historic perspective and quotes the writings of Claude Bernard from 1878: ‘All the vital mechanisms, varied as they are, have only one object, that of preserving constant conditions of life in the internal environment’. About 50 years later the term ‘homeostasis’ was coined by Walter B. Cannon, who defined it as the ‘the coordinated physiological process which maintains most of the steady states in the organisms’. What is most relevant to this study is that Cannon then (borrowing the terms ‘stress’ and ‘strain’ from physics) proceeded to describe failure to maintain homeostasis. He explained that a ‘critical stress’ level is one that produces a ‘breaking strain’, thereby disrupting homeostasis and the ability to maintain it [10]. By 1956, Hans Selye had expanded the axiom of homeostasis to include the responses mediated by the hypothalamo-pituitary-adrenocortical (HPA) axis.

### 1.5.1 Hypothalamo-pituitary-adrenocortical axis

In short, the HPA is a negative-feedback system which involves the hypothalamus and the anterior pituitary and its main purpose is to regulate cortisol secretion from the adrenal cortex. As stresses occur or are perceived, the hypothalamus is stimulated to secrete corticotropin-releasing hormone (CRH) [refer Figure 1.4]. CRH in turn stimulates adrenocorticotropic hormone (ACTH) secretion from the anterior pituitary, which stimulates the adrenal cortex to secrete cortisol. To complete the feedback loop, cortisol exhibits an inhibitory effect on CRH and ACTH secretion from the hypothalamus and anterior pituitary, respectively [48].

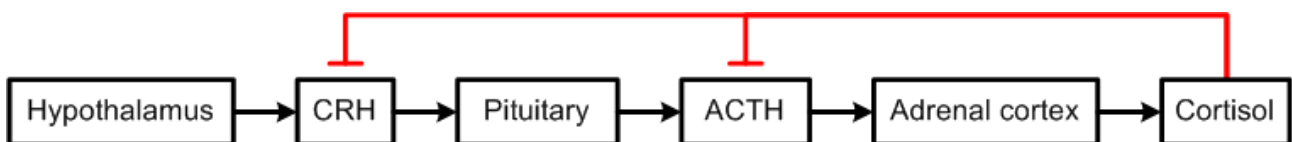


**Figure 1.4:** The HPA negative feedback loop in which excess cortisol secretion inhibits the release of CRH and ACTH from the hypothalamus and anterior pituitary, respectively, thereby limiting further secretion of cortisol.

A key regulator of the HPA is the hippocampus, which contains both glucocorticoid and mineralocorticoid receptors, and has a primarily inhibitory effect on basal secretion of cor-

ticosteroids [49]. Under conditions of elevated glucocorticoid levels, the (rat and primate) hippocampus may suffer damage which becomes exaggerated with increasing age. Therefore, it is conceivable that protracted stresses may disrupt negative feedback by the persistent down-regulation of corticosteroid receptors [49]. The receptor loss and neuronal damage caused by increased corticosteroids further exacerbate the feed-forward cascade. These data indicate that excessive stress in itself may detrimentally affect regulation of stress responses. The defective regulation of complex neuroendocrine networks may be a crucial component in development of metabolic disorders [37].

### 1.5.2 Glucocorticoids

Glucocorticoids, a class of steroid hormones, are key players in regulating salt and water metabolism, blood pressure, immune function and metabolism. Glucocorticoids have a myriad of effects on human behaviour such as sleep patterns, mood and the reception of sensory input, while also playing a substantial role in maintaining brain activities, including prefrontal cortical cognitive function (specifically for working memory). Immunologic, cardiovascular, homeostatic, and metabolic function, are some of the essential physiological functions cortisol is involved in which have ensured it the status of most important glucocorticoid [50], [51]. Deemed most important during times of stress, glucocorticoids will provide longer-term signals capable of overriding acute responses to illness and ‘reset’ metabolism in favour of providing substrates for oxidative metabolism [15].

Glucocorticoids are produced in the adrenal cortex under control of the HPA, and contribute to the HPA feedback system. Cortisone is the inactive metabolite in humans that is converted to the active form, cortisol, in a reversible reaction catalysed by 11 $\beta$ -hydroxysteroid dehydrogenase (11 $\beta$ HSD) types 1 and 2, respectively. In rodents, corticosterone is the active metabolite.

These steroid hormones diffuse readily through cell membranes. There are two types of glucocorticoid receptors both of which reside in the cytoplasm in an inactivated state; type I, mineralocorticoid receptors (MR), and type II, glucocorticoid receptors (GR). Glucocorticoids bind to, and activate the receptors that then migrate to the nucleus where they exert either direct or indirect influences on nuclear transcription. Activated glucocorticoid-receptor complexes can bind directly to DNA and thus enhance or inhibit gene expression of responsive genes (known as glucocorticoid response elements) by interacting with their promoter regions. Glucocorticoids can also affect protein expression indirectly by interacting with transcription factors

(and not binding directly to DNA). It appears that this indirect mechanism is responsible for most of the anti-inflammatory effects of glucocorticoids [52].

### 1.5.3 Role of stress in the pathogenesis of the metabolic syndrome

Miller et al. [53] highlight that many theories prominently feature the idea that ‘chronic stress fosters disease by activating the HPA axis’. In agreement with this statement, Girod & Brotman [52] argue that the short-term benefit of the physiologic stress response can be detrimental in the long term. Rosmond [10] cites Claude Bernard who recognised in 1878, that all living processes exist in a dynamic state of internal physiologic equilibrium (‘milieu intérieur’). Bernard ascribed this to the organic liquid by which all of the tissue elements are surrounded.

Stress elicits reactions at the central nervous, neurohormonal, cellular and molecular levels that aim to restore equilibrium [14]. These defence mechanisms can, however, have detrimental effects on the regulation of nutrient metabolism, the cardiovascular system, and brain function, if they are overactive or prolonged. Therefore, Abraham et al. [14] suggest that stress can be seen as a threat to the organism’s homeostasis. It is also suggested that insulin resistance (or, the attenuated effect of insulin in target tissues) may be a common pathway linking stress and the development of metabolic syndrome and T2DM [14].

Toussaint et al. [54] highlight a number of key issues regarding stresses and their cellular responses. For example, stresses vary in degree and thus generate different degrees of damage, which may be responsible for accelerated ageing. Cells in turn exert protective efforts in an attempt to eliminate damages, which induce defence and repair systems. However, with ageing, damages accumulate and result first in decreases (in the constitutive level or inducibility) of defences, followed by dysregulation of defence system networks. Secondly, with ageing, a decrease in energy metabolism is induced, and specifically its inductibility by stress. This is undesirable since energy metabolism is a necessity for efficient cell response and survival under stress conditions. With insulin resistance and glucose intolerance, energy metabolism needs will most likely not be met timely, despite the supply of accumulated FAs, because the more rapid stress-stimulated glucose metabolism is now blunted. Interestingly, an *in vivo* study demonstrates that FA oxidation in the heart is increased four to eight hours after a dexamethasone<sup>12</sup>

---

<sup>12</sup>Dexamethasone is a potent synthetic glucocorticoid which mimics the action of cortisol and is therefore frequently used in studies which investigate the effects of stress, glucocorticoids or cortisol in a given system. Similar to cortisol, dexamethasone acts as an immunosuppressant and anti-inflammatory agent.

injection [23].

Radahmadi [55] reports that stress (with mainly psychological component) exacerbated diabetes mellitus in streptozotocin-treated<sup>13</sup> rats, and also raised glucose levels significantly in non-diabetic controls.

Abraham et al. [14] propose that stress (even psychosocial factors) can lead to metabolic perturbation and increase cardiovascular risk via activation of neuroendocrine responses. In the long run, these neuroendocrine responses may be of significance in the development of insulin resistance and T2DM. For example, high glucocorticoid levels promote storage of lipid in visceral rather than subcutaneous tissue, and the proinflammatory cytokines secreted by adipocytes are considered to increase oxidants and cell injury.

#### 1.5.4 Glucocorticoid excess and insulin resistance

Cortisol excess is characterised by such phenomena as hypertension, central obesity and glucose intolerance. These effects of cortisol depend in part on opposing the actions of insulin. Thus, an induced state of insulin resistance will contribute to the aforementioned phenomena. The cardiovascular consequences of cortisol excess are described as ‘protean’ [57] and include elevation of blood pressure, truncal obesity, hyperinsulinaemia, hyperglycaemia, insulin resistance, and dyslipidaemia. Various studies into glucocorticoid effects on GLUT4 translocation have been conducted, some of which will be discussed below.

Within the prenatal setting, GLUT1 (the major glucose transporter in the foetal rat heart) is suppressed at birth whilst GLUT4 takes over as major glucose transporter in the adult. Similar to thyroid hormones (in control of this GLUT1-GLUT4 switching in the perinatal period), cortisol is involved in development. In addition, cortisol may affect GLUT1 expression [58]. Upon analysis of cortisol-treated foetal sheep hearts, mRNA levels of GLUT1 were found to be reduced, and Lumbers et al. [58] deduced that cortisol may play a role in neonatal GLUT1 suppression. mRNA levels of GR and MR were, however, not affected by cortisol treatment.

Under normal physiological conditions dexamethasone is reported to increase AMPK activ-

---

<sup>13</sup>Streptozotocin is a drug that displays selective toxicity to pancreatic, insulin-producing beta cells. The toxicity is mediated by reactive oxygen species (ROS) [56], and induces diabetes mellitus. In this case a single intraperitoneal injection was administered and success determined by positively testing for glucose in urine samples.

ity which leads to augmented FA oxidation [59], and promotes glucose uptake and glycogen synthesis [32]. A rat model was employed to investigate effects of glucocorticoid excess on the sensitivity of glucose transport and metabolism to insulin in skeletal muscle, and results indicated that glucocorticoid excess causes insulin resistance directly by inhibiting insulin-induced GLUT4 translocation to the sarcolemma [60]. However, total GLUT4 content was not decreased by dexamethasone treatment (confirmed by Sakoda et al. [61]), although the capacity for insulin to recruit the transporters to the membrane was diminished. Based on these results, Dimitriadis et al. [60] argue that although glucocorticoids may increase lipolysis (suggesting that increased oxidation of non-esterified FAs may be the cause of insulin resistance) it may not be the main mechanism underlying glucocorticoid-induced insulin resistance.

A review by Qi & Rodrigues [23] reports some of the effects that dexamethasone treatment exerted on insulin signalling, including significantly inhibited total mRNA and tyrosine phosphorylation of IRS-1, citing Sakoda et al. [61], among others. Giorgino et al. [62] reported a similar finding when insulin signalling factors upstream from GLUT4 were investigated. Here, glucocorticoid-treated skeletal muscle exhibited decreased tyrosine phosphorylation of IRs, due to a reduction in the pool of receptors undergoing tyrosine phosphorylation. A decline in the IRS-1 content and reduced serine and/or threonine phosphorylation of IRS-1 was also observed.

Sakoda et al. [61], however, report that even after IRS-1 and PI3K were normalised via IRS-1 overexpression, there was no significant improvement of insulin-induced glucose uptake impaired by dexamethasone. This finding led others [23] to speculate that glucocorticoids may decrease glucose uptake by their inhibition of glucose transport rather than insulin signalling transduction. In support, a recent study found that dexamethasone may inhibit the activation of GLUT4 in the cell membrane (of adipocytes) through p38 mitogen-activated protein kinase (MAPK) signalling [63]. This may correlate with a study that found that cell membrane association of GLUT4 is decreased in the hippocampi of corticosterone-treated (type 1 and type 2) diabetes rats [64].

Taken together, these data emphasise the capacity of glucocorticoids to influence the onset of insulin resistance and related cardiometabolic diseases. Another major player in the aetiology of these diseases is oxidative stress, which can also be induced by glucocorticoids [52]. However, oxidative stress is frequently associated with inflammation and may thus be indirectly downregulated by the potent anti-inflammatory effects of glucocorticoids [52].

## 1.6 Oxidative stress

Reactive oxygen species (ROS) occur as a result of normal metabolism and exposure to xenobiotic compounds [65]. ROS describes short-lived, diffusible entities such as hydroxyl ( $\cdot\text{OH}$ ), alkoxyl ( $\text{RO}\cdot$ ) and peroxy ( $\text{ROO}\cdot$ ) radicals, as well as (medium lifetime) superoxide ( $\text{O}_2\cdot^-$ ) and nitroxyl ( $\text{NO}\cdot$ ) radicals functions [66]. ROS also includes non-radicals e.g. hydrogen peroxide ( $\text{H}_2\text{O}_2$ ) and hydroperoxides ( $\text{ROOH}$ ). Sites of ROS generation within the heart include cardiac myocytes, endothelial cells and neutrophils [67]. Under normal conditions, ROS may provide beneficial functions [66]. However, this is another defence mechanism that can be detrimental to cells if homeostasis is exceedingly perturbed. When the production of reactive oxygen species overwhelms the intrinsic anti-oxidant defences, oxidative stress can cause indiscriminate damage including loss of function and even cell death [68].

In the mitochondrial ETC, there are four protein complexes (I, II, III, and IV) situated within the inner mitochondrial membrane [refer Figure 1.5]. During mitochondrial metabolism electron donors are generated. The flow of electrons from these electron donors through the ETC to the final electron acceptors constitutes oxidative phosphorylation. For example, if glucose is

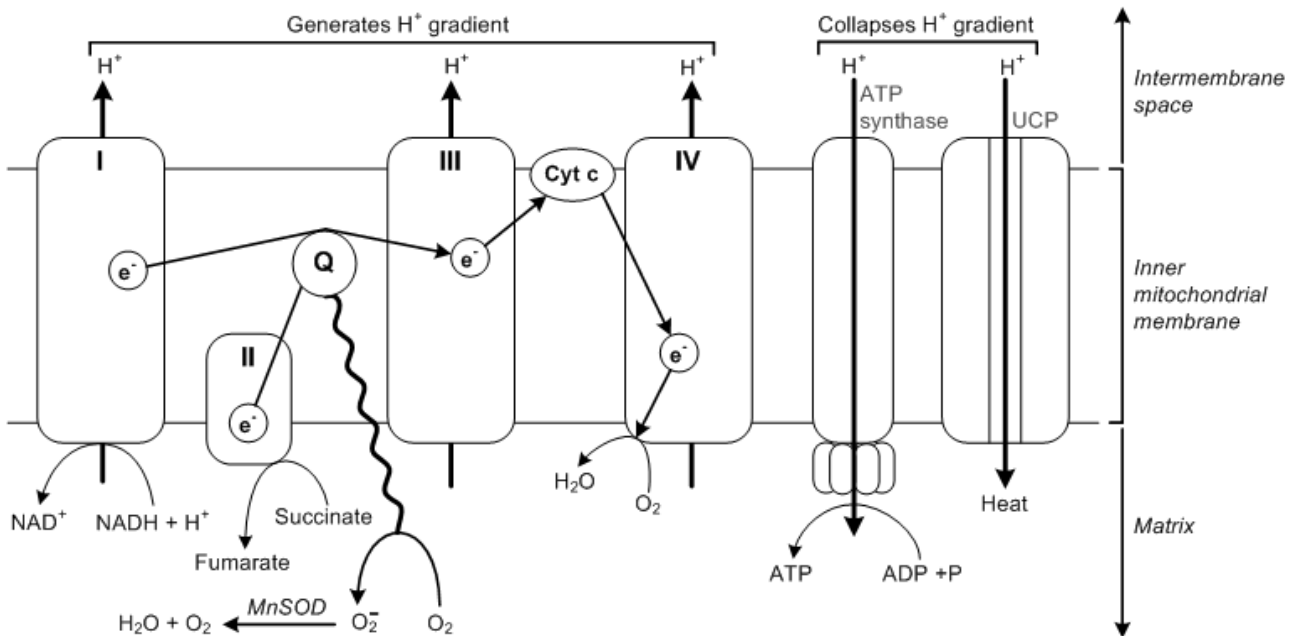


**Figure 1.5:** Superoxide production by the mitochondrial electron transport chain. Figure adapted from Brownlee [19].

metabolised via the citric acid cycle, it generates NADH and FADH<sub>2</sub> as electron donors. The main electron donor, NADH, releases electrons to complex I (also known as NADH dehydrogenase or NADH-coenzyme Q oxidoreductase). FADH<sub>2</sub> donates electrons to complex II (which is also known as succinate dehydrogenase or succinate-Q oxidoreductase). The electrons from both complexes move to complex III via the intermediate coenzyme Q, and are then transferred to cytochrome C and complex IV. Finally, the electrons are passed to molecular oxygen which they reduce to water [19].

The electron transport system is organised such that ATP can be precisely regulated. The following scenario is based on normal cells. Some of the energy the electrons release is used to pump protons across the membrane into the intermembrane space by complexes I, III and IV. A voltage gradient results. ATP synthase utilises the energy from the voltage difference across the mitochondrial membrane for ATP synthesis. To keep the rate of ATP generation constant, the voltage gradient can also be reduced by uncoupling proteins (UCPs) producing heat.

However, in the high-glucose milieu of diabetes, greater glucose oxidation will yield more electron donors (NADH and FADH<sub>2</sub>) for entry into the ETC. Consequently, the voltage gradient across the mitochondrial membrane will increase until a critical threshold is reached, at which point electron transfer inside complex III is blocked [19]. Electrons will then accumulate at coenzyme Q which will donate one electron at a time to molecular oxygen, generating superoxide. Superoxide can be degraded by the mitochondrial isoform of superoxide dismutase (SOD) to hydrogen peroxide (H<sub>2</sub>O<sub>2</sub>), and this followed by enzymatic conversion to H<sub>2</sub>O and O<sub>2</sub>. However, if homeostasis is perturbed and superfluous superoxide is produced, it may have detrimental consequences.

According to Taegtmeyer et al. [25], the consequences of excess fuel if left unchecked are a metabolic ‘disaster’ zone in the heart. The build-up of ROS, and metabolic substrates (chiefly, glucose and long-chain FAs) are proposed to cause the greatest damage. Many intracellular signalling cascades aimed at maintaining homeostasis (with the direct environment) involve ROS as an important second messenger.

### 1.6.1 Oxidative stress as a result of psychological stress

Psychosocial and socioeconomic factors interact with biological mechanisms including cognitive, neuroendocrine, metabolic and molecular responses [37]. There is mounting evidence that

psychological stress can lead to oxidant production and oxidative damage to cellular macromolecules, such as proteins, lipids and DNA [49]. When stress is perceived or experienced there is a change in glucocorticoid regulatory activity of the HPA axis. Chronic tissue exposure to glucocorticoids may lead to metabolic and vascular changes that could accelerate vascular ageing [52]. Furthermore, stress stimulates metabolic pathways that yield ATP to meet increased energy demands. If these stress-mediated pathways are overstimulated, concomitant increasing ROS production could activate molecular mechanisms leading to cytotoxicity [49].

### 1.6.2 Oxidative stress as an underlying cause of metabolic disorders

Oxidative stress is caused by an imbalance between ROS production and the cell's anti-oxidant capacity to neutralise reactive intermediates and/or repair the resulting damage [65], [69]. Conditions of higher substrate influx such as hyperglycaemia and hyperlipidaemia may bring about such an imbalance - or 'substrate stress' as referred to by Baynes & Thorpe [70] - since the mitochondrion, which is largely responsible for molecular metabolism, is a critical site of ROS production.

It is proposed that the pathogenic effect of high glucose is significantly mediated via increased production of ROS and reactive nitrogen species (RNS) [71]. This is suspected to happen in concert with effects of high FAs. Oxidative stress, resulting from ROS accumulation, is implicated in atherosclerosis, microvascular complications of diabetes, and  $\beta$ -cell failure in T2DM [37].

According to Sugamura & Keaney [72] there is considerable data portraying ROS and oxidative stress as key features of cardiovascular diseases including atherosclerosis, hypertension, and congestive heart failure. By contrast, others [65] note that 1) there is an association between superfluous oxidants and the multifactorial pathogenesis of insulin resistance, and 2) there are numerous possible sites of ROS production (ROS being implicated in the relationship between oxidative stress and aetiology of insulin resistance) yet there is surprisingly limited evidence to support this notion.

One of the mechanisms by which oxidative stress may be a causative factor in the development of insulin resistance involves impaired insuling signalling [18] and GLUT4 translocation. Karnieli & Armoni [73] cite evidence that protracted ROS exposure affects glucose transporter transcription, i.e. increased GLUT1 levels and a concomitant reduction in GLUT4 gene ex-

pression.

With regards to dysregulated glucose metabolism, hyperglycaemia has repeatedly been identified as a cause of superoxide production [69], [74], [75]. In addition, hyperglycaemia-induced ROS and -RNS are considered to damage macromolecules directly (by oxidising DNA, proteins and lipids), and indirectly induce tissue damage (by activating cellular, stress-sensitive pathways) [71]. Activation of these pathways (including nuclear factor  $\kappa$ -B (NF $\kappa$ -B), p38 MAPK, NH<sub>2</sub>-terminal Jun kinases/stress-activated kinases and hexosamines, inter alia) is associated with the pathogenesis of insulin resistance.

Oxidative stress has also been identified as a key factor in hyperglycaemia-induced apoptosis in mouse myocardium and rat cardiomyocytes [76]. Since the focus of this research includes hexosamine production via the HBP, the findings of a similar study by Rajamani & Essop [77] are more relevant. The findings include identification of a novel pathway in which oxidative stress (and the HBP) may play a crucial role in diabetes-related onset of heart disease via increased myocardial apoptosis. They found that hyperglycaemia induces intensified oxidative stress in H9c2 cardiomyoblasts, along with increased HBP activation and *O*-GlcNAcylation of the anti-apoptotic protein, BAD. Furthermore, Du et al. [78] found that overproduction of hyperglycaemia-induced mitochondrial superoxide increases hexosamine synthesis as well as *O*-linked glycosylation of Sp1. Sp1 glycosylation activates gene expression that plays a role in the pathogenesis of diabetic complications. These data provide various mechanisms by which oxidative stress, and the resulting hexosamine glycosylation, are involved in the development of metabolic disorders.

Another factor known to increase oxidative stress is lipid overload. Lipid overload occurs when FA uptake exceeds oxidising capacity and is known to result in elevated triglycerides, accumulation of lipid metabolites (specifically, ceramides), endoplasmic stress, and lipid mediated alterations in membrane function. Excess lipid is lipotoxic in that it results in programmed cell death, contractile dysfunction and heart failure [25]. Furthermore, superoxide production is increased by high glucose concentrations while high fat levels elevate both superoxide and peroxynitrite production [69].

Henriksen et al. [65] suggest that an important goal of future clinical investigations should involve the development and implementation of anti-oxidant interventions. The latter should

have improved oral bioavailability and target the critical sites of oxidant overproduction, such as (skeletal) muscle mitochondria. This suggestion is made in light of increasing evidence in obesity-associated rat models of oxidative stress and insulin resistance that antioxidant treatments mediate improved glucose tolerance and insulin sensitivity, as well as ameliorate functionality of the glucose transport system in skeletal muscle. Sugamura et al. [72] warn, however, that it is oversimplistic to expect specific (beneficial) results on cardiovascular disease when employing a general anti-oxidant strategy, and then reviews the most important sources of ROS that have been associated with CVD pathology. They include the mitochondrial respiratory chain, nicotinamide adenine dinucleotide phosphate (NADPH) oxidases, xanthine oxidase, lipoxygenase, uncoupled nitric oxide synthase (NOS), and myeloperoxidase (MPO). Others [65] highlight mitochondrial hydrogen peroxide and NADPH oxidases as relevant to the aetiology of insulin resistance. Notably, inhibition of xanthine oxidase has recently been reported to reduce hyperglycaemia-induced oxidative stress, and ameliorate mitochondrial alterations in diabetic mice [79].

In order to further understand the molecular relationship between oxidative stress, glucocorticoids and stress, insulin resistance as well as the metabolic syndrome, and how these factors contribute to the pathophysiology of the aforementioned diseases, greater insight is required into damaging hyperglycaemia-activated pathways, specifically the HBP.

## 1.7 Damaging pathways activated by hyperglycaemia

One of the risk factors of the metabolic syndrome is elevated blood glucose levels, a symptom which is exacerbated by insulin resistance i.e. decreased glucose uptake. In a hyperglycaemic setting such as diabetes, cells are bathed in glucose. In an attempt to maintain constant glucose levels and homeostasis, cells reduce their glucose uptake. Certain cell types are, however, more proficient at this than others, leaving some cells subsets more vulnerable to hyperglycaemia-induced 'tissue' damage [19]. Retinal capillary endothelial cells, mesangial cells in the renal glomerulus, as well as neurons and Schwann cells are among the vulnerable cell types, which explains the retinopathy, nephropathy and neuropathy complications widely associated with diabetes.

Glycolysis typically consumes the majority of glucose entering the cell, but there are pathways or mechanisms that branch off, diverting (excess) glucose flux. Increased hyperglycaemia-induced

superoxide causes glycolytic intermediates to be shunted into the major pathways of hyperglycaemic damage [80]. The four major implicated molecular mechanisms include increased polyol pathway flux, increased activation of the protein kinase C (PKC) pathway, increased formation of advanced glycation end products (AGEs), as well as increased flux through the HBP [81] [refer Figure 1.6].

### 1.7.1 Polyol pathway

Although many theories have been proposed to explain the harmful effects of hyperglycaemia, one of the oldest theories involves the polyol pathway [82], described for the first time in peripheral nerve in 1966 [83]. One of the key aldo-keto reductase enzymes of this pathway, aldose reductase, is found in tissues such as retina, lens, glomerulus, nerve, and vascular cells.<sup>14</sup> These reductase enzymes, with NADPH, can reduce a large variety of carbonyl compounds to their sugar alcohols (polyols) [74]. Similarly, aldose reductase normally functions to reduce toxic aldehydes in the cell to inactive alcohols, but it also reduces excess glucose to sorbitol which undergoes oxidation to fructose [19] by the enzyme, sorbitol dehydrogenase (SDH). Apart from being the cofactor in the aldose reductase reaction, NADPH is also the essential cofactor for the production of reduced glutathione (GSH), an important intracellular anti-oxidant. Thus, in the context of hyperglycaemia the process of reducing high intracellular glucose depletes NADPH, decreasing the production of GSH, leaving the cell more vulnerable to oxidative stress [19].

Elevated flux of the polyol pathway has been associated with decreased myoinositol uptake, attenuated sodium/potassium adenosine triphosphatase ( $\text{Na}^+/\text{K}^+$  ATPase) activity, and increased production of vasodilatory prostaglandins in many of the target tissues of hyperglycaemia-induced damage [82].

### 1.7.2 PKC pathway

There are at least 11 isoforms of PKC and they are widely distributed in mammalian tissues. Diacylglycerol (DAG) is an essential activating cofactor of the classic isoforms of PKC- $\beta$ , - $\delta$ , and - $\alpha$  [74]. The activity of the classic isoforms are dependent on both  $\text{Ca}^{2+}$  ions and phosphatidylserine, while DAG enhances it.

---

<sup>14</sup>The retina, glomeruli and neuronal tissue are sites where the hyperglycaemia-induced microvascular complications of diabetes are clearly visible [82].

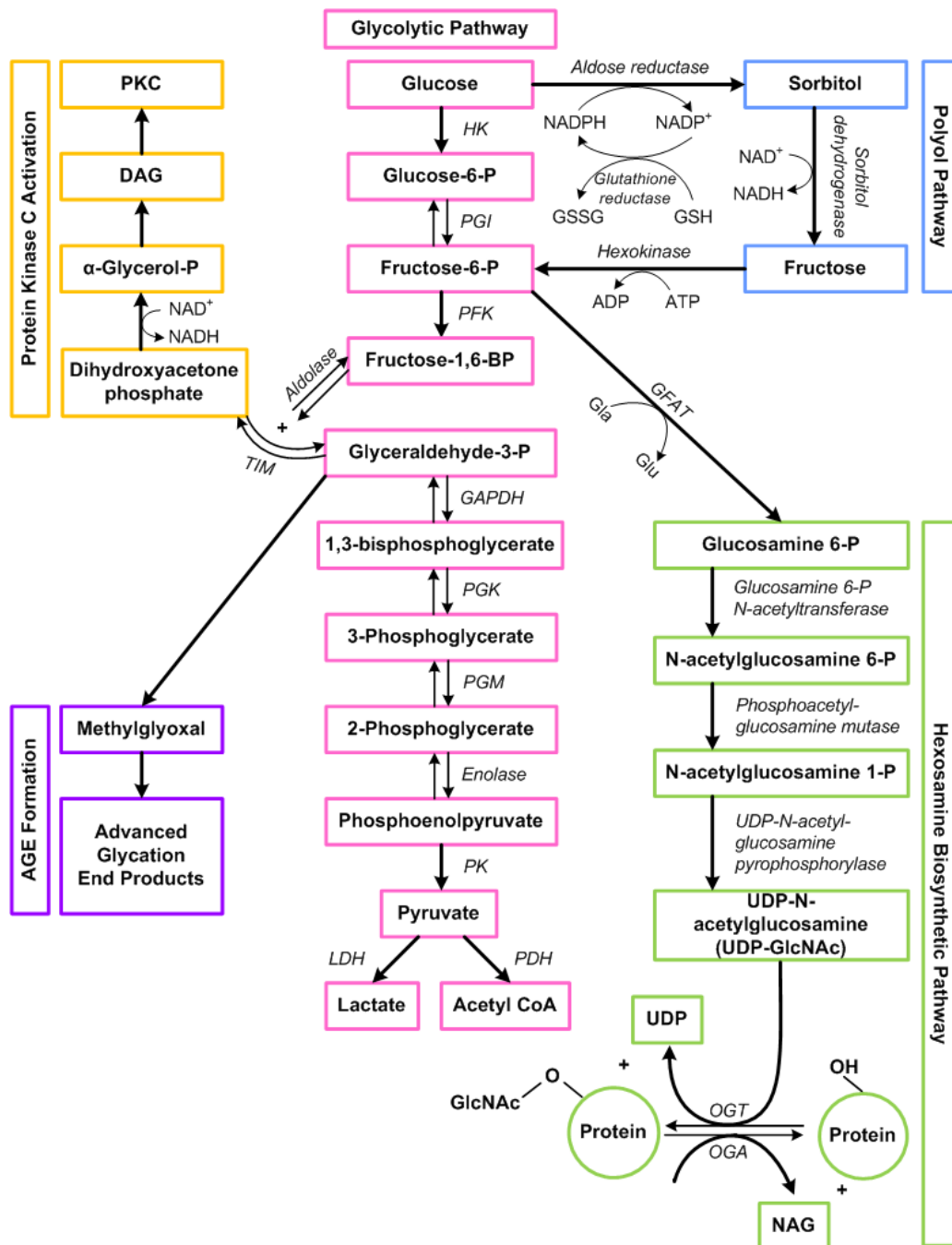


**Figure 1.6:** Hyperglycaemia-activated pathways include AGE formation, PKC activation, the polyol and hexosamine biosynthetic pathways (adapted from Rolo & Palmeira [81]). These are known to be damaging during hyperglycaemia. AGE, advanced glycation end product; BP, bisphosphate; DAG, diacylglycerol; GAPDH, glyceraldehyde-3-phosphate dehydrogenase; GFAT, glutamine:fructose-6-phosphate amidotransferase; GSH, glutathione (reduced); GSSG, glutathione (oxidised); HK, hexokinase; LDH, lactate dehydrogenase; NAD<sup>+</sup>, nicotinamide adenine dinucleotide (oxidised); NADH, nicotinamide adenine dinucleotide (reduced); NADP<sup>+</sup>, nicotinamide adenine dinucleotide phosphate (oxidised); NADPH, nicotinamide adenine dinucleotide phosphate (reduced); NAG, N-acetylglucosamine; P, phosphate; PDH, pyruvate dehydrogenase; PFK, phosphofructokinase; PGI, phosphoglycerate isomerase; PGK, phosphoglycerate kinase; PK, pyruvate kinase; PKC, protein kinase C; TIM, triose phosphate isomerase; UDP, Uridine diphosphate.

Intracellular hyperglycaemia enhances *de novo* synthesis of DAG. This is achieved by the reduction of glycolytic intermediate dihydroxyacetone phosphate (DHAP) to glycerol-3-phosphate and stepwise acylation [75]. Prolonged and superfluous activation of several PKC isoforms may also lead to ROS-mediated means of tissue damage. Furthermore, since increased ROS inhibits activity of the glycolytic enzyme glyceraldehyde-3-phosphate dehydrogenase (GAPDH) [84], intracellular levels of the DAG precursor, triose phosphate, are elevated which would ultimately increase PKC activation. Moreover, hyperglycaemia-mediated PKC isoforms ( $\beta$  and  $\delta$ ) may also result in a variety of effects on gene expression [19].

### 1.7.3 AGE formation

Glucose and other glycating compounds - derived from both glucose and increased fatty acid oxidation - react non-enzymatically to form AGEs [74]. AGEs can arise by intracellular auto-oxidation of glucose to glyoxal, decomposition of the Amadori product (glucose-derived 1-amino-1-deoxyfructose lysine adducts) to 3-deoxyglucosone, and fragmentation of glyceraldehyde-3-phosphate and dihydroxyacetone phosphate to methylglyoxal. When these reactive intracellular dicarbonyls (glyoxal, methylglyoxal and 3-deoxyglucosone) react with amino groups of intracellular and extracellular proteins, AGEs form [75].

Sugimoto et al. [85] proposed that oxidative stress mediates hyperglycaemia-induced cell injury, via signalling pathways involving an interaction between exogenous AGEs and their receptors (RAGEs). Subsequently, Coughlan et al. [86] confirmed that AGE-RAGE interactions disrupt the mitochondrial respiratory chain under normoglycemic conditions. Under hyperglycaemic conditions, RAGE-induced cytosolic ROS promoted significant generation of mitochondrial superoxide (at the level of complex I). There is also a difference between acute hyperglycaemia, and chronic diabetes which exhibits significantly elevated levels of superoxide production in renal mitochondria [87]. AGEs are also known to increase NF $\kappa$ -B activity, the production of vasoactive factors and cytokines such as interleukin-1 (IL-1), and -6 (IL-6), and tumour necrosis factor- $\alpha$  (TNF- $\alpha$ ) [88].

### 1.7.4 The hexosamine biosynthetic pathway

The HBP was first described by Torres & Hart in 1984 [89], and its key role in regulating the insulin-responsive glucose transport system was acknowledged as early as 1991 [90]. It has been shown that one of the most rapid cellular responses from a variety of unrelated sources is an

increase in *O*-GlcNAcylation on many proteins [91].

In this pathway, fructose-6-phosphate is diverted from glycolysis as substrate to the rate-limiting enzyme of the HBP; glutamine:fructose-6-phosphate amidotransferase (GFAT) [74]. GFAT converts fructose-6-phosphate to glucosamine 6-phosphate. The fate of glucose entering this pathway is conversion to uridine diphospho- $\beta$ -N-acetylglucosamine (UDP-GlcNAc) which is used by *O*-GlcNAc transferase (OGT)<sup>15</sup> in the biosynthesis of *O*-GlcNAc-modified proteins. In the reverse reaction, *O*-GlcNAcase (OGA) catalyses the removal of GlcNAc moieties from modified proteins.<sup>16</sup> Pharmacological inhibition of OGA, specifically by PUGNAc, is regarded an invaluable tool for examining cellular functions of *O*-GlcNAc [93]. Figure 1.7 shows structures of PUGNAc interacting with its OGA binding site.

Excess glucose flux into the HBP has been linked to the onset of insulin resistance and vascular complications of diabetes [94]. Furthermore, dysregulation of *O*-GlcNAcylation has been associated with various chronic disease processes apart from diabetes and diabetic complications [95], including ageing, neurodegeneration, cancer, and AIDS [45]. Another widely recognised causal link between diabetes and diabetic complications is hyperglycaemia that results from uncontrolled glucose regulation. Brownlee's laboratory postulates that hyperglycaemia which results in upstream accumulation of glycolytic metabolites, such as fructose-6-phosphate, may augment flux through the HBP [96]. Rajamani & Essop [77] have shown in H9c2 rat cardiomyoblasts that hyperglycaemia-induced activation of the HBP results in cell death and thus tissue damage .

#### 1.7.4.1 Involvement of HBP in insulin resistance and diabetes

Flux of fructose-6-phosphate into the HBP is increased by hyperglycaemia and insulin resistance-induced excess fatty acid oxidation, thereby contributing to the pathogenesis of diabetic complications [19], [78]. The requirement for glucosamine in the pathophysiology of insulin resistance in adipocytes [90] strongly implicates the HBP in the aetiology of the disease. This is compounded by the finding that GFAT inhibitors improved insulin-stimulated glucose uptake. Furthermore, UDP-GlcNAc levels were considerably increased in rats administered lipid emulsion

---

<sup>15</sup>Aside from sensitivity to the availability of UDP-GlcNAc, OGT is also sensitive to insulin. Upon insulin stimulation OGT associates to cell membrane phosphoinositides, and the IR directly tyrosine phosphorylates the enzyme, thereby activating it [92].

<sup>16</sup>OGT and OGA are highly conserved enzymes [44] and animals usually only have one gene encoding OGT [92].

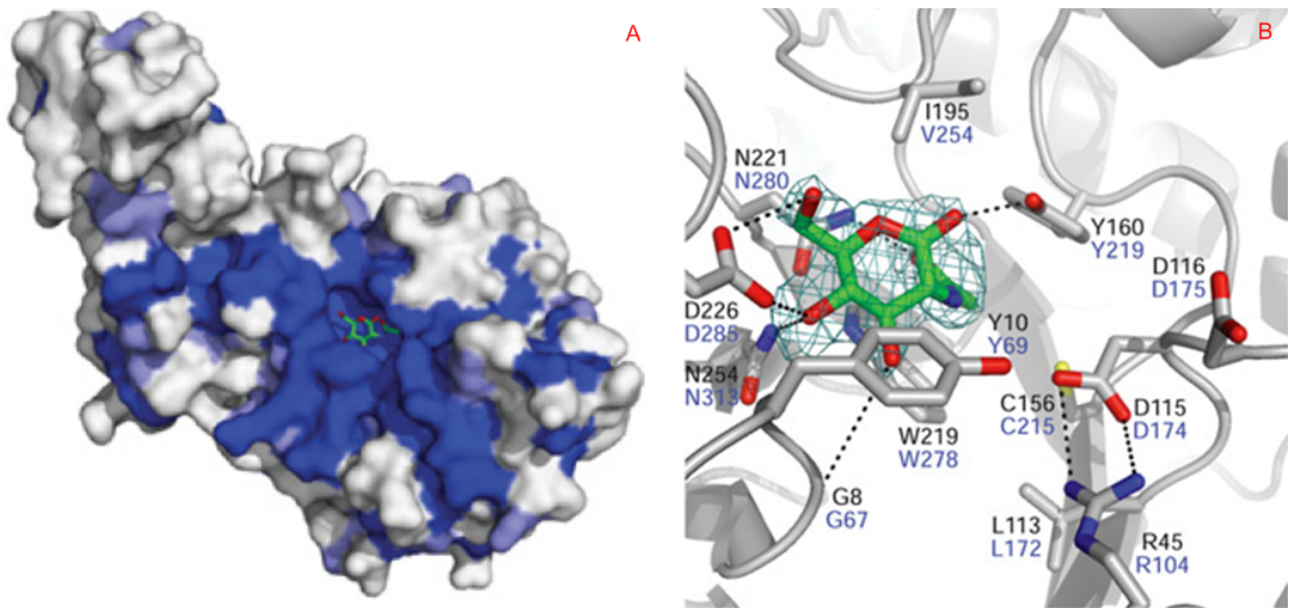


**Figure 1.7:** Schimpl et al. [93] presented these structural diagrams of *Oceanicola granulosa* OGA (*OgOGA*) and PUGNAc. [A] The light blue on this surface view of *OgOGA* represents sequence conservation among metazoan OGAs, whilst the dark blue represents the same amongst metazoan OGAs+*OgOGA*. PUGNAc is shown (in green) with additional ordered loops from the apo-structure. [B] The active site of the *OgOGA*-PUGNAc represented in a stick model. The ligands are shown as sticks with carbons in green, and hydrogen bonds drawn as broken, black lines. Hydrogen bonds to/from the protein backbone amides are depicted as originating from the  $C\alpha$ . Residues of the *OgOGA* active site are labelled in black, with the equivalent hOGA residues in blue.

infusions, prior to the onset of insulin resistance. Insulin resistance onset was also promoted in adipocytes by competitive inhibition of OGA, the enzyme responsible for *O*-GlcNAc removal [97].

Oxidative stress increases flux through metabolic circuits such as the HBP [69]. The HBP modifies numerous target proteins, including IRS, Akt and GLUT4 [98] but when modification becomes dysregulated adverse consequences result. Chronic HBP activation increases AMPK activity (in adipocytes) [99] which increases FA oxidation, possibly leading to greater oxidative stress.

Interestingly, OGT is highly concentrated in mitochondria, which Love et al. [100] ascribe to mitochondrial OGT (mOGT) being the smallest (103 kDa) of the three known isoforms. They also found that it localises to the inner mitochondrial membrane. A recent study showed that increased *O*-linked glycosylation of mitochondrial proteins, including key proteins

of the ETC, is involved in diabetes-associated mitochondrial dysfunction in cardiomyocytes [101]. In addition to impaired activity of complexes I, III, and IV of the ETC, high *O*-GlcNAc levels are also associated with lower mitochondrial  $\text{Ca}^{2+}$  and cellular ATP content.  $\text{Ca}^{2+}$  flux into cardiomyocytes is diminished due to hyper-*O*-GlcNAcylation of the nuclear transcription factor Sp1 and the resulting decrease in sarcoendoplasmic reticulum  $\text{Ca}^{2+}$ -ATPase (SERCA2a) gene expression [101]. Furthermore,  $\text{Ca}^{2+}$  plays an important regulatory role in cellular events, including GLUT4 gene expression. High cytosolic  $\text{Ca}^{2+}$  increases GLUT4 expression via the activation of  $\text{Ca}^{2+}$ /calmodulin-dependent protein kinase (CaMK) [73]. The adverse effects of the HBP-induced  $\text{Ca}^{2+}$  reduction are multiple; including possible disruption of mitochondrial membrane potential, and diminished GLUT4 content.

Chronically activated HBP flux is associated with impaired GLUT4 translocation [102], and thus with insulin resistance aetiology. Upstream of GLUT4 translocation, upregulation of the HBP reportedly leads to impaired IRS-PI3K-Akt signalling [103]. In a model of GFAT over-expression, mice developed insulin resistance and muscle glucose disposal rates decreased which was linked to reduced levels of GLUT4 [104].

Collectively, these studies portray chronically elevated HBP flux as having far-reaching adverse effects on regulatory factors in the onset of insulin intolerance. Dysregulation of transcription factors, glucose transporter signalling, as well as mitochondrial respiratory processes and the resulting oxidative stress are highlighted as key targets of the HBP in the context of insulin resistance development.

#### 1.7.4.2 Acute versus chronic HBP activation

It has been suggested that short-term increases in *O*-GlcNAc modification of proteins may be important for cellular survival [91], and that acute increases in *O*-GlcNAcylation is cardioprotective [95]. For example Liu et al. [105] showed that specifically increasing *O*-GlcNAcylation during reperfusion is sufficient for cardioprotection. In doing so glucosamine and *O*-(2-acetamido-2-deoxy-D-glucopyranosylidene)amino-N-phenylcarbamate (PUGNAc, a non-specific inhibitor of *O*-GlcNAc removal) were identified as potentially useful cardioprotective agents.

In contrast to the school of thought that *O*-GlcNAc is a protective agent, it has also been shown that chronic activation of the HBP negatively affects cardiac function in diabetic models [106], and contributes directly to cardiomyopathy [92]. A similar paradox exists between the

roles of *O*-GlcNAc in diabetes and neurodegeneration where, in contrast to diabetes, higher *O*-GlcNAcylation appears to prevent disease and lower *O*-GlcNAcylation in the brain contributes to neuronal cell death [92]. In other words, this same pathway can have different, even opposing, functional outcomes, depending on the conditions of or surrounding its activation. This paradox demands further investigation since *O*-GlcNAc has a multitude of target proteins, and complex interplay exists between 1) the cellular processes that it regulates and 2) crosstalk with phosphorylation [107]. This has been described more eloquently by Hart et al. [92] using the analogy of an electrical circuit; ‘...if phosphorylation events represent ‘microswitches’, which turn on or off protein activity, *O*-GlcNAcylation could be thought of as a ‘rheostat’ tuning the pathways and processes to accommodate nutrient status and cellular stress.’

### 1.7.5 Summarising hyperglycaemia-activated pathways

Brownlee [19] puts forth a unifying hypothesis, postulating that the polyol, PKC, AGE and HBP pathways are activated due to impaired GAPDH activity. Hyperglycaemia induces increases of inner mitochondrial membrane potential which results in intensified mitochondrial superoxide production [75], as well as single strand DNA damage which elicits the reparative response of poly(ADP-ribose) polymerase (PARP) [108]. GAPDH is inhibited by both hyperglycaemia-induced mitochondrial superoxide and the resulting activation of PARP [19], [84].

Furthermore, it has been shown that specific inhibitors of each of these pathways ameliorate various diabetes abnormalities in cell culture or animal models [74]. Although ROS emerges as a common element, it has not been clarified whether a common cause(s) underlies these processes, or if they are all interconnected.

## 1.8 Research problem

Despite multipronged approaches to increase awareness of metabolic diseases, the incidence of these diseases worldwide remains extremely high. Clearly the words of Bernard (1878), Cannon (1939), Selye (1956), and Taegtmeier & Stanley (2011), who all emphasise (homeostatic) balance as a key factor in health and survival, are not heeded. Although some may be able to reverse detrimental effects of poor lifestyle habits and choices with regards to diet, physical activity, and stress, it may be too late for others. Urgent action is needed to curb the growth of this epidemic. More specifically, elucidation of mechanisms underlying these diseases is required to help rescue patients from otherwise irreparable damage.

Interestingly, it has been shown (at cellular level) that *O*-GlcNAc levels are increased in response to stress [95]. In fact, the earliest detected response to cellular stress in every mammalian cell type examined so far is a rapid and global increase in *O*-GlcNAcylation on many proteins [109]. Stress-induced increases in *O*-GlcNAc return to normal after 24 to 48 hours [91]. Based on this information, the HBP plays a pivotal role in this research problem, and as such, is the major research focus.

## 1.9 Hypothesis

We hypothesise that the synthetic glucocorticoid, dexamethasone, would increase oxidative stress and HBP flux. Through greater *O*-GlcNAcylation of the insulin signalling pathway, GLUT4 translocation would be attenuated, contributing to the onset of myocardial insulin resistance.

## 1.10 Aims

1. Establish the HL-1 cardiac myocyte cell line in our laboratory
2. Establish an *in vitro* model for dexamethasone-treated cardiac cells
3. Assess oxidative stress in response to dexamethasone treatment
4. Evaluate the degree of *O*-GlcNAcylation in response to dexamethasone treatment
5. Determine the extent of GLUT4 translocation upon dexamethasone treatment

# Chapter 2

## Materials and Methods

### 2.1 Cell culture

The initial aim was to assess the effect of the glucocorticoid, dexamethasone (a synthetic cortisol analogue), on HBP flux and explore whether it had any link to cardiometabolic pathophysiology. An immortalised cardiac-derived cell line, namely HL-1 cardiomyocytes, was kindly donated by Professor William C. Claycomb<sup>1</sup> for this purpose. Establishing this cell line was no simple task as the cells are very sensitive to changes in the environment, specifically carbon dioxide (CO<sub>2</sub>) levels. HL-1 cells also have a very unique trait which requires great care, i.e. the ability to contract in culture. In light of this, a large part of this study involved optimisation of cell culturing conditions for HL-1 cells.

#### 2.1.1 Establishing the protocol for HL-1 cell culture

The HL-1 cell line is derived from AT-1 cardiac myocytes, and has been determined to be a homogenous population at passages beyond 30 [110]. These cells bear two important characteristics, namely spontaneous action potentials and contractions they display in culture [111]. HL-1 cells can be serially passaged for more than two hundred times and retain their ability to contract together with the cardiomyocyte phenotype.

The HL-1 cell line, at passage 63, was donated to the Cardio-Metabolic Research Group housed within the Department of Physiological Sciences at Stellenbosch University (the first research group to establish this cell line in South Africa) by Professor Claycomb. A detailed protocol

---

<sup>1</sup>Department of Biochemistry and Molecular Biology, LSU Health Sciences Centre, New Orleans, USA.

for culturing HL-1 cells can be found in Appendix A under *Growth and care of HL-1 cardiomyocytes*. The growth of the cells was tracked from seeding to near-confluency [refer Figure 2.2].

After the cells were first received (at passage 63) live in two T25 flasks, at ambient temperature, they were immediately placed in an incubator with a humidified atmosphere (95% air, 5% CO<sub>2</sub>) at 37°C and allowed time to acclimatise. It was recommended that cells be passaged [refer *Passaging* in Appendix A.6] only once they reached confluency (refer Figure 2.1), soon after their arrival.

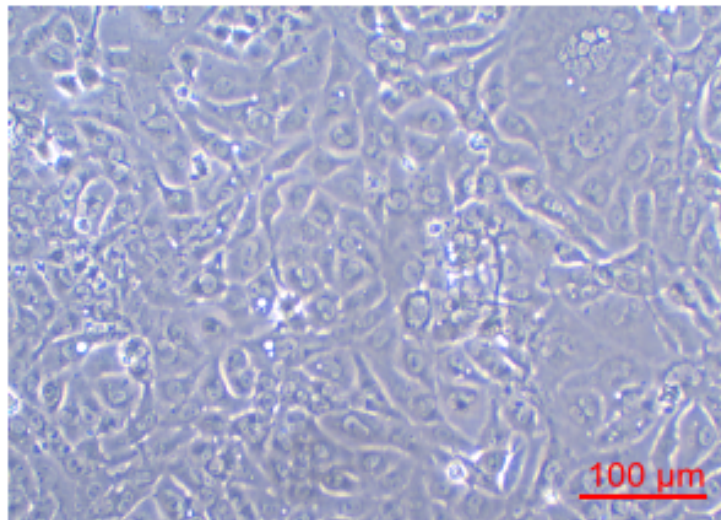


**Figure 2.1:** HL-1 cells when confluent  $\sim$  two days after seeding roughly one million cells in a T25 flask. The image was acquired with an Olympus CKX41 light microscope using a 10 $\times$ /0.25 objective.

One of the T25 flasks would be passaged in coated flasks [Appendix A.4.2] and maintained as a ‘working’ set of cells, while the other would be cultured for the purpose of freezing cells and to ensure a build-up of ‘cell stocks’.

- **‘Working’ set of cells:** The first T25 flask was split 1:2, resulting in two T25 flasks (Greiner, Kremsmünster, Austria).
- **‘Cell stocks’:** The other T25 was split 1:3, into one T75 flask. Once the cells in this flask were confluent, it was split 1:2 into two T75 (Greiner, Kremsmünster, Austria) flasks, and

this process was repeated. When the four T75 flasks reached confluency they were frozen [protocol can be viewed in Appendix A.7 under *Freezing*].

Cells were cultured in T75 culture flasks with Claycomb medium (12103C, Batch 8A0177, Sigma-Aldrich, Steinheim, Germany) supplemented with 10% foetal bovine serum (12103C, Batch 8A0177, SAFC Biosciences, KS), 2 mM L-glutamine (G7513, Sigma-Aldrich, Steinheim, Germany), 0.1 mM norepinephrine [(±)arterenol](A0937, Sigma-Aldrich, Steinheim, Germany) and penicillin-streptomycin (100 U/ml-100 µg/ml), (P4333, Sigma-Aldrich, Steinheim, Germany) as instructed [refer Table A.2]. The cells were grown [Appendix A.5] in a humidified atmosphere (95% air, 5% CO<sub>2</sub> at 37°C). HL-1 cells should be grown to 100% confluency as visible in Figure 2.2<sup>2</sup> before passaging [Appendix A.6].

### 2.1.2 Pharmacological treatments

In an attempt to manipulate or simulate various responses, some pharmacological treatments were administered to the cells. In order to elicit a stress-response, the synthetic analogue for cortisol, dexamethasone (D4902, Sigma-Aldrich, Steinheim, Germany), was used.  $\alpha$ -cyano 4-hydroxyl cinnamic acid (OHCA), (Sigma-Aldrich, Steinheim, Germany), a previously described anti-oxidant, was used at a concentration of 250 µM as described [69]. PUGNAc (CarboGen Labs, Aarau, Switzerland) is a known inhibitor of OGA [refer Figure 1.7], the enzyme responsible for the removal of *O*-GlcNAc moieties from proteins. Preventing the activity of OGA is essential when determining the degree of *O*-GlcNAcylation, which makes PUGNAc (administered at 50 µM) a key treatment for Western blotting analysis. Lastly, insulin was administered to the cells after a period of serum starvation in order to stimulate the translocation of the glucose transporter, GLUT4, from storage vesicles in the cytosol to the sarcolemma. Insulin was administered at 300 nM as was previously done in a similar study [28].

## 2.2 Experimental protocol for analysis after dexamethasone treatment

In order to investigate the effect of cortisol-like glucocorticoids on HBP flux, an *in vitro* model was established. Here, HL-1 cells were treated with various doses of dexamethasone, after which *O*-GlcNAc and ROS levels were measured by flow cytometry [Figure 2.3].

---

<sup>2</sup>Images of the HL-cells growing were captured with a CKX41 light microscope (Olympus Corporation, Tokyo, Japan) using a 10×/0.25 objective.

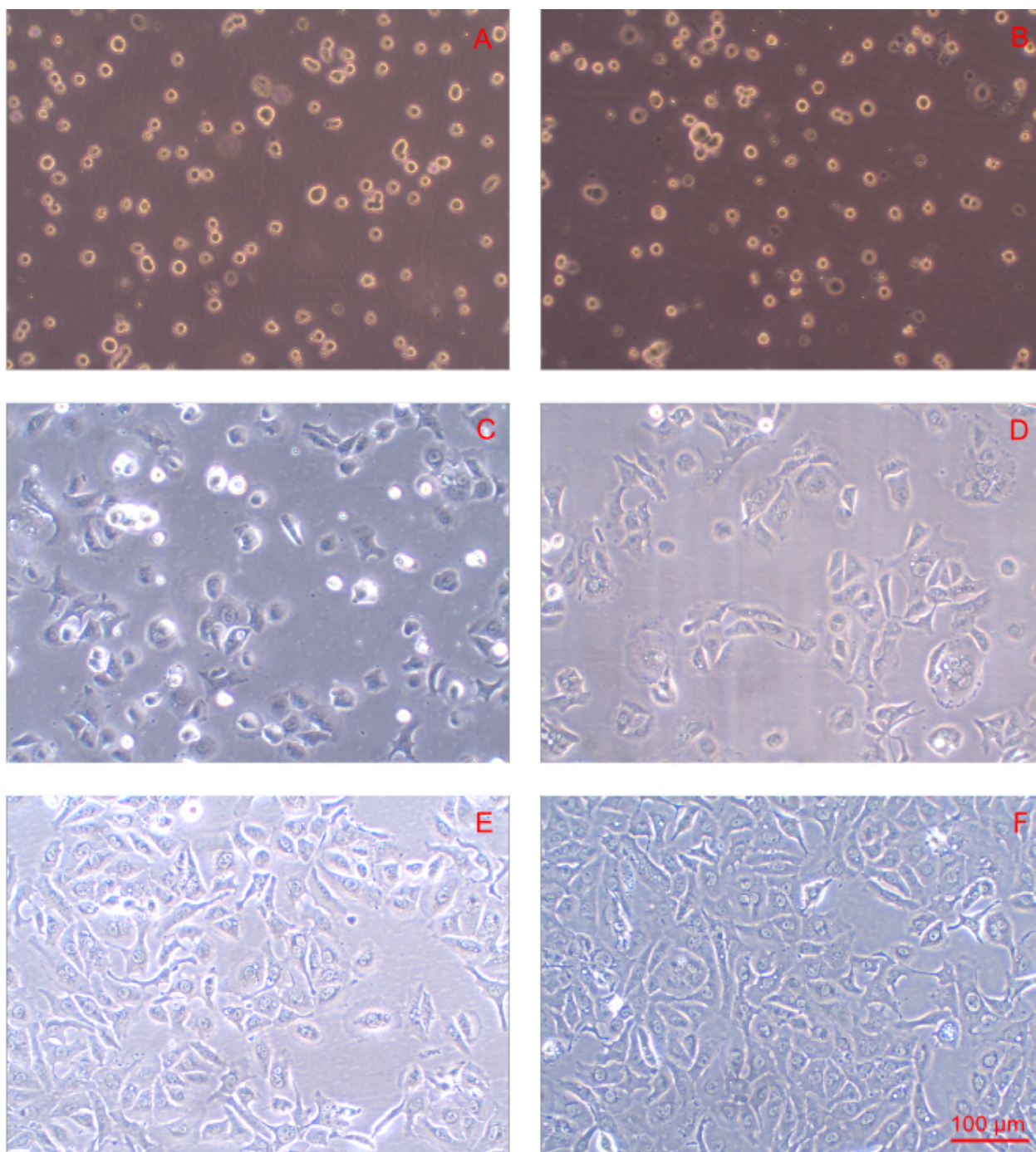


**Figure 2.2:** Images showing the progress of HL-1 cells when  $\sim$  one million cells are seeded in a T25 flask. [A] Immediately after seeding cells started settling to the base of the flask; [B] after 40 minutes a number of cells had settled on the base of the flask; [C] three hours after cells were seeded they started adhering to the coated surface of the flask; [D] after 6 hours the cells plated and numbers visibly increased; [E] 24 hours after seeding the number of cells had increased greatly; [F] after 48 hours, cells were nearly confluent. A  $10\times/0.25$  objective was used.

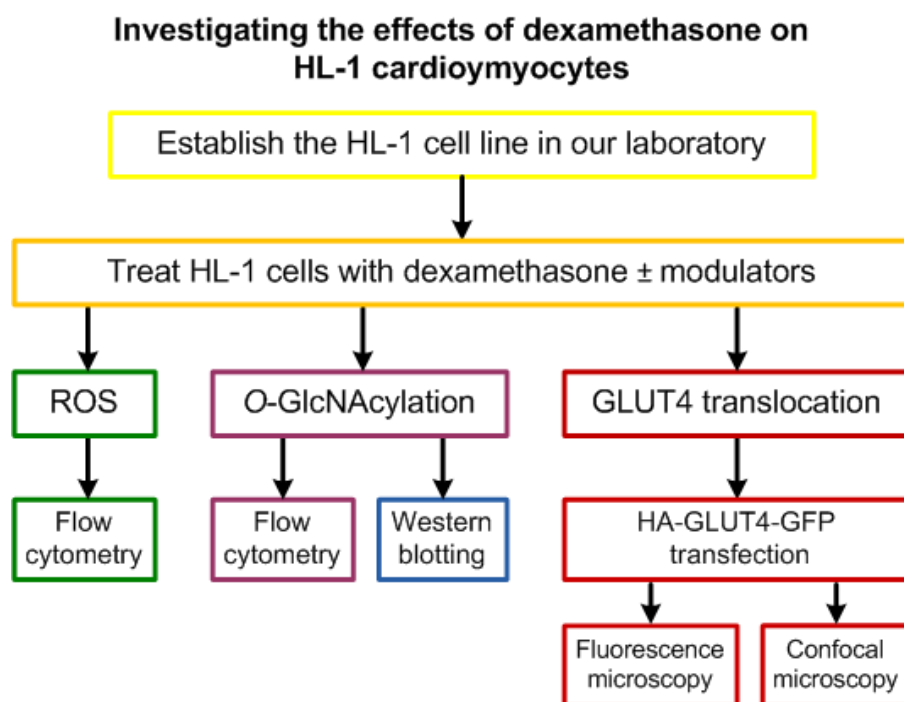


**Figure 2.3:** This diagram provides an overview of the experimental methods carried out and represented in this thesis in order to investigate effects of the synthetic glucocorticoid, dexamethasone, on HL-1 cardiomyocytes.

### 2.2.1 Flow cytometry

Flow cytometry is a quantitative technique used for counting microscopic particles such as cells, and it allows for the multiparametric analysis of the physical and/or chemical characteristics of thousands of particles per second based on their fluorescent properties. The particles are suspended in fluid and pass through lasers at a point of iso-electric focusing. A photomultiplier tube (PMT) detects the emitted light. An optical-to-electronic coupling system records how the cell or particle scatters incident light and emits fluorescence. The characteristics measured include a particle's relative size, granularity or internal complexity, and fluorescence intensity. Molecules of interest can be detected either by staining cells with a fluorescent dye or by the use of appropriately selected antibodies.

A FACS Aria I flow cytometer (Becton-Dickinson Biosciences, San Jose, CA) was used for all flow cytometry analyses. A minimum of 5,000 events per sample were recorded. Excitation of all fluorochromes (FITC and PE-TxRed) at 488 nm was achieved with a solid state sapphire laser. FITC emission was detected by a 502 long pass (LP) and 530/30 band pass (BP) filter.

PE-TxRed fluorescence was detected by a 610 LP and 616/23 BP filter. The geometric mean of the fluorescence intensity signal was measured on the intensity histogram, utilising FACS Diva 6.1 software (Becton-Dickinson Biosciences, San Jose, CA).

## 2.2.2 Flow cytometric measurement of ROS

Dihydrodichlorofluorescein diacetate (H<sub>2</sub>DCFDA), (Invitrogen, Carlsbad, CA) is a dye used for live staining. It is a green fluorescing, fluorescein-based, fluorophore used for the detection of ROS. FITC fluorescence is emitted (upon excitation) and the fluorescence intensity can be used as a measure of the degree of ROS within the system. DCF is used to measure general ROS since it is sensitive to many types of ROS, including superoxide, oxidised glutathione, nitric oxide, and peroxynitrite.

HL-1 cells were subcultured in T25 flasks (Greiner, Kremsünster, Austria), about one million cells per flask, and incubated with 3 ml of supplemented Claycomb media [Appendix A.1] for 48 hours at 37°C under a humidified atmosphere of 95% air and 5% CO<sub>2</sub>. As previously shown in Figure 2.2, cells are nearly confluent after 48 hours. Thereafter, treatment with dexamethasone for 2, 3, and 4 hours was administered as indicated in Figure 2.4.

### 2.2.2.1 Preparing cells for flow cytometry

After treatment with dexamethasone each flask was washed with calcium-free, magnesium-free Dulbecco's Phosphate-Buffered Saline (PBS) (D8537, Sigma-Aldrich, Germany) and trypsinised with 0.05% Trypsin-EDTA (T3924, Sigma-Aldrich, Germany). Trypsin was inhibited with a soybean trypsin inhibitor (T6522, Sigma-Aldrich, Germany) in a 1:1 ratio. Each flask was rinsed with wash medium (Claycomb medium supplemented with 5% FBS and 1% penicillin-streptomycin) and the cells from each flask were transferred to 15 ml conical tubes (SPL Life Sciences, Korea) to be centrifuged at  $500\times g$  for 5 minutes in a Digicen 20-R centrifuge (Orto Alresa, Spain).

H<sub>2</sub>DCFDA was dissolved in distilled water to make up a 1 M stock from which 10 mM aliquots were made by diluting 10  $\mu$ l of the stock in 990  $\mu$ l of DMSO. For the working solution, the 10 mM dye was diluted 1:200 in PBS. When working with the ROS dye, great care was taken to handle the cells (that were still viable) very gently at every step so as not to agitate them

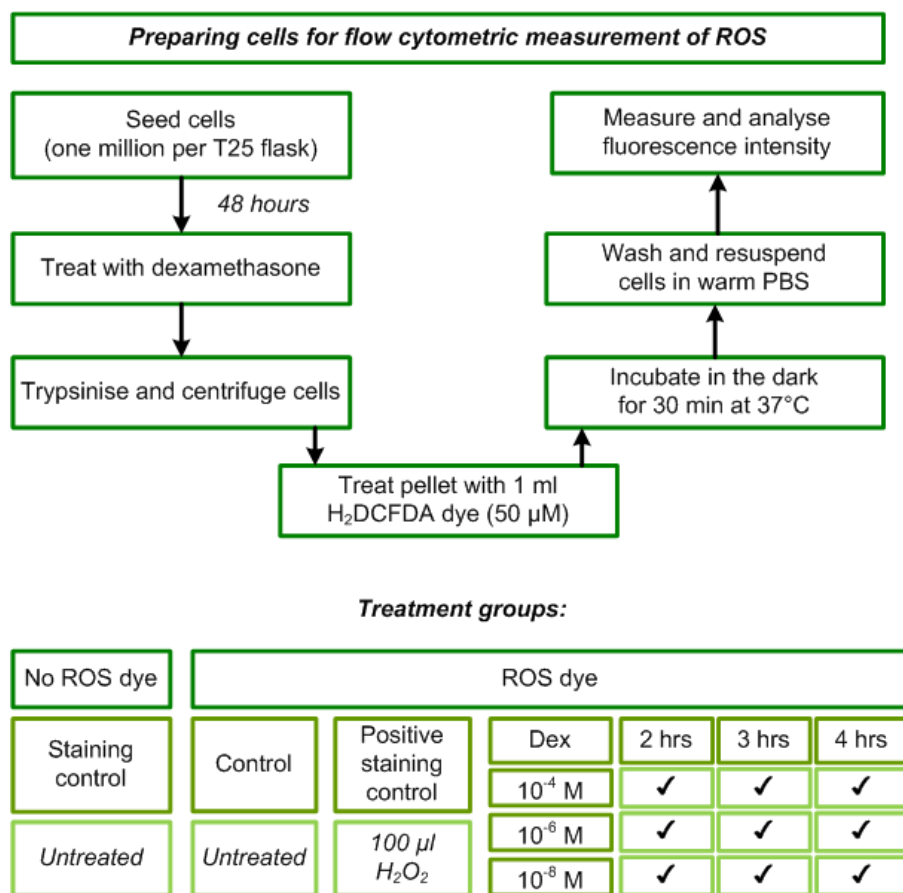


**Figure 2.4:** This diagram provides an overview of experimental protocol and treatment groups used for measurement of ROS. There are nine different dexamethasone treatments which can be compared to the untreated control. Then there is a staining control so that autofluorescence can be subtracted. The positive control is treated with hydrogen peroxide (H<sub>2</sub>O<sub>2</sub>) to confirm the activity of the H<sub>2</sub>DCFDA ROS dye, and give a relative indication of a positive signal. Dex; dexamethasone.

unnecessarily in order to limit the production of false signal.

After cells were trypsinised and centrifuged, the pellet was treated with 1 ml of the H<sub>2</sub>DCFDA ROS dye working solution. The live cell suspension was incubated in the dark for 30 minutes at 37°C. This process needs to be carried out in the dark since the cleaved DCF is a fluorescent substrate and any external light affects the signal. The cells were then washed [refer Appendix C.1] with 2 ml of warm PBS and the dye removed. Subsequently, the pelleted cells were resuspended in warm PBS and transferred to flow cytometry tubes for flow cytometric analysis. The cells were then run through the FACS ARIA 1 flow cytometer and population data obtained. Cells not stained with the ROS dye served as negative control, whilst stained cells incubated

with 100  $\mu\text{l}$  30% w/v  $\text{H}_2\text{O}_2$  for 10 minutes served as the positive control. There was also a staining control (to detect autofluorescence) which contained cells that were neither treated nor stained.

### 2.2.3 Flow cytometric measurement of *O*-GlcNAc

Primary antibodies have a high affinity for unique epitopes, and secondary antibodies bind to primary antibodies or antibody fragments (such as the Fc or Fab regions). Secondary antibodies are usually labelled with probes, and for flow cytometric application these are fluorophores. When *O*-GlcNAc is bound by its primary antibody, and this in turn bound by a fluorescent secondary antibody, such as R-phycoerythrin-conjugated Texas Red (PE-TxRed), (Jackson ImmunoResearch, West Grove, PA). The greater the fluorescence intensity, the more protein present.

HL-1 cells were subcultured and about one million cells were seeded per T25 flask and incubated with 3 ml of supplemented Claycomb media [Appendix A.1] for 48 hours at 37°C under an atmosphere of 95% air and 5%  $\text{CO}_2$ . Cells were then treated with dexamethasone for 2, 3, and 4 hours as indicated [Figure 2.5].

Flasks were washed with warm PBS, and cells were trypsinised and pelleted by centrifugation [refer Section 2.2.2.1]. All samples were permeabilised with 200  $\mu\text{l}$  ice cold methanol-acetone (1:1) to facilitate intracellular probing by antibodies, and then incubated on ice, or at 4°C for 10 minutes before being washed with PBS. This was followed by a 20 minute blocking step at room temperature with 200  $\mu\text{l}$  of 5% donkey serum (D9663, Sigma-Aldrich, St Louis, MO) made up in PBS. After an additional centrifugation step (500 $\times g$  for 5 minutes) the serum was aspirated, and monoclonal primary antibody (anti-*O*-GlcNAc, CTD110.6, Santa Cruz Biotechnology, CA) added to all samples save the staining control, to which only PBS was added. Upon the addition of 200  $\mu\text{l}$  primary antibody per tube (1:200 dilution in PBS), cells were incubated in the dark at room temperature for at least 90 minutes. Cells were washed with PBS before addition of 200  $\mu\text{l}$  of secondary antibody, PE-Texas Red (1:200 in PBS), followed by a 30 minute incubation step at room temperature in the dark, and a final washing step. [Note comment on washing steps under *Flow cytometry* in Appendix C.1.]

Cells were suspended in warm PBS and transferred to flow cytometry tubes for flow cytometric analysis [refer Section 2.2.1]. For each condition investigated, three independent experiments

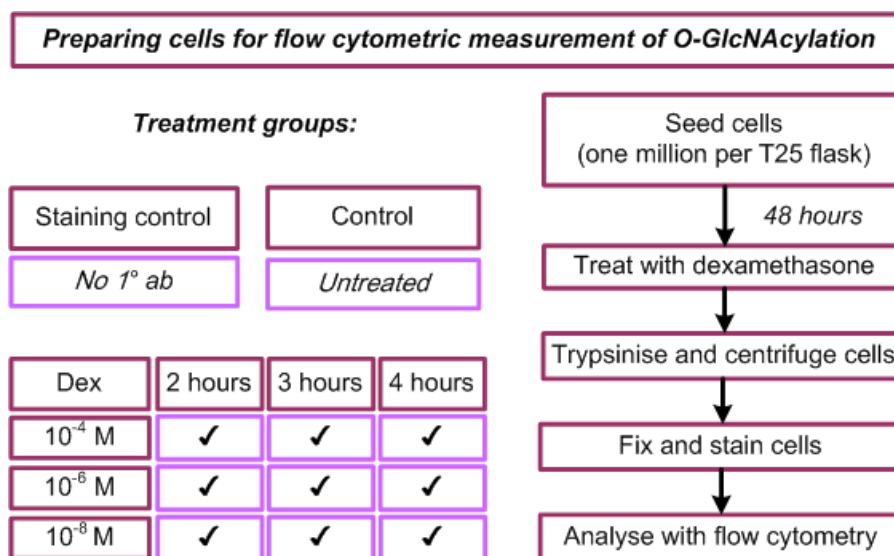


**Figure 2.5:** This diagram provides an overview of experimental protocol and treatment groups used for measurement of *O*-GlcNAc. The staining control is stained with the secondary antibody only (no primary antibody) and serves as a guide for the subtraction of non-specific fluorescence. The untreated control provides a baseline with which to compare the nine dexamethasone-treated samples. 1° ab; primary antibody. Dex; dexamethasone.

were conducted. In order to analyse the data, the geometric mean of the fluorescence intensity of a cell population was used to represent the numerical value of the experiment.

## 2.3 Measurement of *O*-GlcNAcylation by Western blotting analysis

In addition to flow cytometry, Western blotting was used to assess the overall degree of *O*-GlcNAcylation of cells treated with dexamethasone for 2, 3, and 4 hours, respectively.

### 2.3.1 Cell culture, pharmacological treatments, and lysate collection

Cells were cultured in T25 flasks, with a seeding density of  $\sim 10^6$  cells per flask, for 2 days before administering treatments (dexamethasone  $\pm$  OHCA). Following treatment [Figure 2.6], cells were harvested and lysates were prepared [refer Appendices D.1 and D.2].

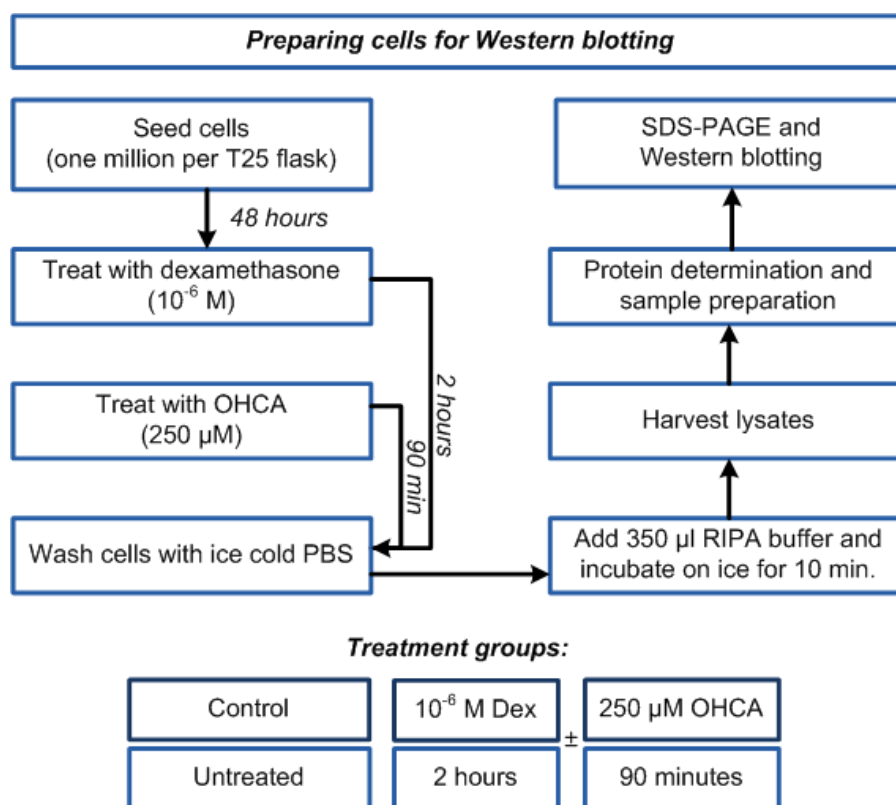


**Figure 2.6:** Overview of treatment protocol prior to Western blotting. The untreated control serves as a reference to which dexamethasone- and OHCA-treated groups can be compared. Dex; dexamethasone. OHCA;  $\alpha$ -cyano 4-hydroxyl cinnamic acid.

### 2.3.2 Preparing samples for Western blotting

The protein content of lysate samples was determined using the Bradford method [Appendix D.3]. To facilitate protein determination a standard curve was prepared with bovine serum albumin (BSA) shown in Table D.2 [Appendix D.3]. Once protein content of the lysates had been established, samples (commonly known as ‘blues’ due to the Coomassie Brilliant Blue stain in the sample buffer) were prepared for sodium dodecyl sulphate-polyacrylamide gel electrophoresis (SDS-PAGE) [refer *Sample preparation for SDS-PAGE* in Appendix D.4].

### 2.3.3 Gels

Polyacrylamide gels were prepared for protein separation by electrophoresis as described in Appendix D.5. 10% resolving gels were used with 5% stacking gels [Table D.3, Appendix D.5].

### 2.3.4 Electrophoresis

The samples (prepared as discussed in Appendix D.4) were loaded onto 10-well gels along with a molecular weight marker (Protein-Marker IV, 27-2110, peqGOLD Biotechnologie GmbH, Erlangen, Germany) and electrophoresis initially carried out at 80 V for 10 minutes, followed by a further  $\sim 80$  minutes at 100 V [refer Appendix D.5].

### 2.3.5 Electrotransfer

The process of electrotransfer [refer Appendix D.6] from gel to membrane was carried out on semi-dry transfer apparatus at 15 V and 0.5 A for  $\sim 80$  minutes. A PVDF membrane (0.45  $\mu\text{m}$  Biotrace PVDF, 66543, PALL Corporation, Life Sciences, Pensacola, FL) was used although nitrocellulose membranes also work well.

### 2.3.6 Probing the membrane

The membrane was washed with TBS-T and non-specific binding blocked with 1% BSA. The length of blocking depends on the protein(s) of interest and the antibodies (and antibody concentrations) being used [Appendix D.7]. When probing for *O*-GlcNAc [Appendix D.7.3], the CTD110.6 primary antibody was used in a 1:1000 dilution in TBS-T. The peroxidase conjugated, goat anti-mouse antibody (31440, Thermo Scientific, Rockford, IL) was used as secondary in a 1:4000 dilution.

The rabbit,  $\beta$ -actin primary antibody (4976S, Cell Signalling Technology, Boston, MA) was used in a 1:1000 dilution when probing for  $\beta$ -actin [Appendix D.7.4], and bound by a 1:4000 dilution of goat anti-rabbit, peroxidase conjugated secondary (611 1302, Rockland Immunochemicals, PA, USA).  $\beta$ -actin is a protein that is widely distributed throughout all eukaryotic cells and is therefore commonly used as a loading control in assays such as Western blotting.<sup>3</sup>

### 2.3.7 Developing the membrane

Membranes were developed as described in Appendix D.8.  $\beta$ -actin blots were usually exposed for about 5 seconds whereas *O*-GlcNAc blots were exposed for approximately 1 minute.

---

<sup>3</sup>It should be noted that arguments have been made against the reliability of  $\beta$ -actin as a loading control, particularly in the case of higher total protein loads as required for detecting proteins of low abundance [112].

### 2.3.8 Densitometry

The developed film was scanned with an HP Scanjet 3500c scanner (Hewlett packard, Palo Alto, CA) and Un-Scan-It Gel 5.1 software (Silk software, Orem, UT) was used to digitise images and perform densitometric analysis. Each lane was analysed separately and normalised to the densitometry value of the corresponding  $\beta$ -actin. Relative differences in protein expression were assessed statistically using the normalised densitometric value.

## 2.4 Experimental protocol for the assessment of GLUT4 translocation

### 2.4.1 Transfections

To explore the potential effect of dexamethasone on the translocation of GLUT4 to the sarcolemma, HL-1 cells were transfected with a haemagglutinin (HA)-tagged GLUT4-GFP construct.<sup>4</sup> The GLUT4 DNA construct contains a sequence coding for green fluorescent protein (GFP) attached at the C-terminal. This allows the translocation of the GLUT4 to be tracked by monitoring the distribution of the GFP within the cell and at the plasma membrane. The fusion protein is tagged with an HA epitope in the first exofacial loop of GLUT4 which enables the exposure of the GLUT4 to the extracellular surroundings of the cell to be determined in a quantitative manner.

The transfected HL-1 cells (after being fixed, but not permeabilised) were stained with an antibody against HA [Figure 2.7]. By measuring the total cellular GFP fluorescence, the expression level of GLUT4 was determined. With this knowledge the surface level of GLUT4 (quantified by the fluorescence of HA antibody) was normalised to the total cellular expression of the protein [113].

HL-1 cells were cultured to confluency under an atmosphere of 95% air and 5% CO<sub>2</sub> at 37°C, trypsinised, counted and seeded in 500  $\mu$ l of supplemented Claycomb medium in 8-well chambered coverslides (Nunc Lab-Tek, SA). Approximately 15, 000 cells were seeded per well one day prior to transfection, to reach 50-80% confluency at the time of transfection.

---

<sup>4</sup>Professors Gavin Welsh and Jeremy Tavaré from the University of Bristol, Bristol, UK, kindly donated the GLUT4 construct. Dr Craig Kinnear (Department of Medical Biochemistry, Stellenbosch University, Tygerberg, South Africa) assisted by amplifying the construct.

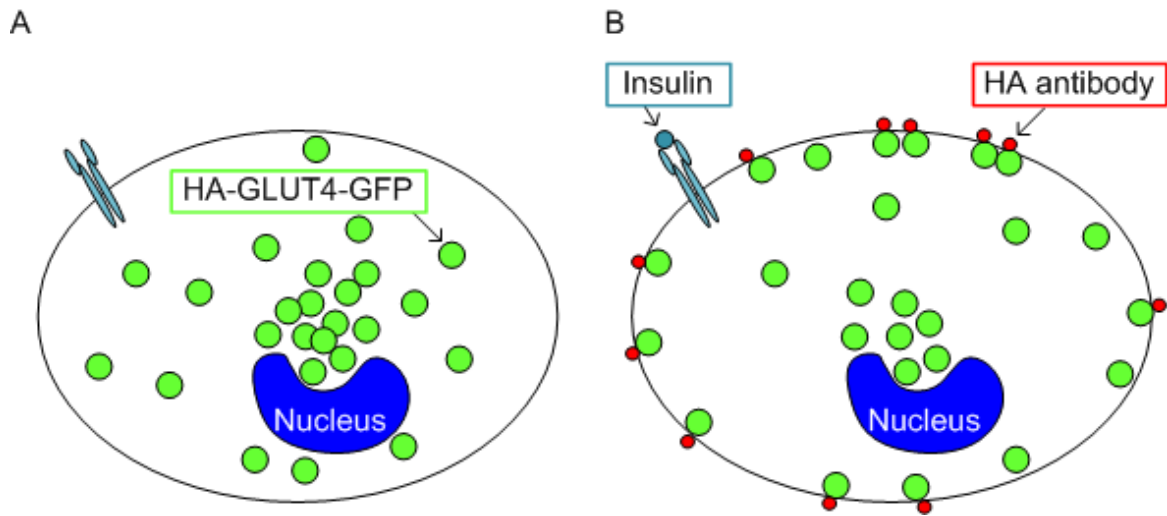


**Figure 2.7:** Simplistic diagrammatic scheme representing the HA-GLUT4-GFP model used to analyse GLUT4 translocation. [A] GFP indicates the presence of GLUT4 in the cell. [B] Insulin stimulation enhances GLUT4 translocation to the cell membrane. Once GLUT4 associates to the membrane, the HA-tag is exposed to the extracellular environment allowing binding of HA-antibody. A ratio of cell surface GLUT4 (HA) to total GLUT4 (GFP) can thus be calculated per cell.

24 hours after seeding, the cells were transfected [Figure 2.8] using the Lipofectamine™ LTX and PLUS™ Reagents (15338-100 Invitrogen, Carlsbad, CA) according to the Standard Protocol [refer *Transfection protocol*, Appendix E.1]. In brief, the medium was replaced with 500  $\mu$ l fresh supplemented medium [Appendix A.1] 24 hours after transfection, although it can be refreshed within 4-6 hours of transfection. 45 hours after transfection, and 3 hours prior to fixing, the cells were serum starved for 3 hours. One hour into serum starving the cells were treated with  $10^{-6}$ M dexamethasone for 2 hours. The cells were treated with 300 nM insulin 15 minutes prior to fixing.

Cells were fixed with 2% paraformaldehyde and probed overnight with a 1:50 dilution HA-tagged primary antibody (2367S Cell Signalling Technology, Boston, MA) in PBS. After a washing step, a 1:200 dilution of anti-mouse TxRed, secondary antibody (Invitrogen, Carlsbad, CA) was added. Hoechst 33342 (B2261, Sigma-Aldrich, Steinheim, Germany) was used as nuclear dye diluted 1:1000 in PBS (0.05 mg/ml). Cells washed three times with PBS and mounted by using a drop of fluorescent mounting medium (S3023, Dako North America Inc., Carpinteria, CA).

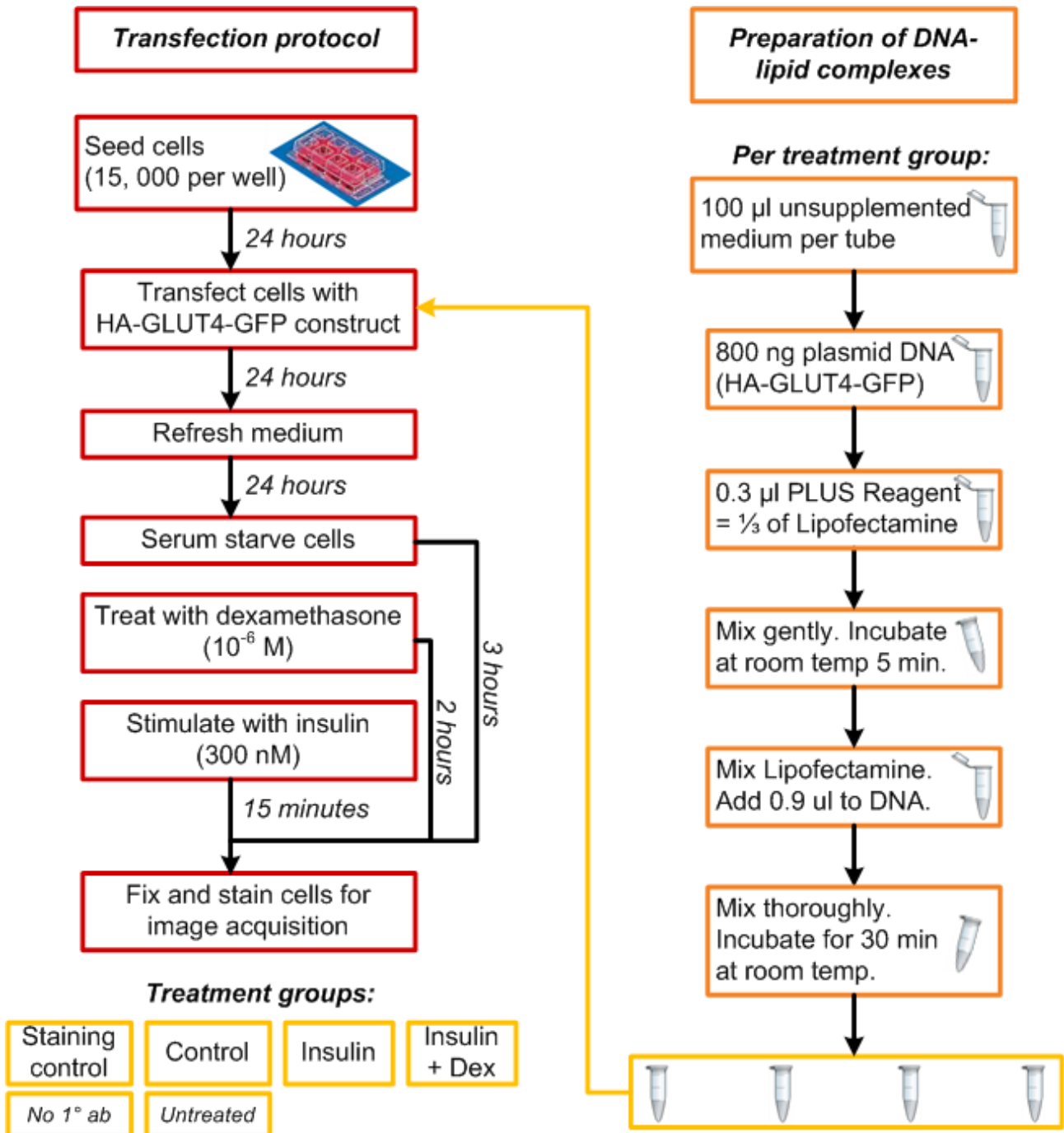


**Figure 2.8:** Overview of the HA-GLUT4-GFP transfection treatment protocol. As a reference for non-specific signal, a staining control was stained without primary antibody, but with secondary antibody only. One group was left untreated to serve as control. The two remaining groups were stimulated with insulin, and one of these were treated with dexamethasone. The preparation of DNA-lipid complexes is described in greater detail in Appendix E.1. 1° ab; primary antibody. Dex; dexamethasone.

### 2.4.2 Assessing HA-GLUT4-GFP transfection by immunofluorescence microscopy

An Olympus Cell<sup>^</sup>R system attached to an IX 81 inverted fluorescence microscope (Olympus Corporation, Tokyo, Japan) was used to perform image acquisition. The microscope was equipped with an F-view-II cooled CCD camera (Soft Imaging Systems, Olympus Biosystems GmbH, Germany). Images were acquired using a Xenon-Arc burner (Olympus Biosystems GmbH, Germany) as light source with 360 nm (for DAPI-based staining), 492 nm (for FITC-based staining), and 572 nm excitation filters (for TxRed-based staining). A UBG triple-bandpass emission filter cube (Chroma Technology Corp., Bellow Falls, VT) was used to collect emission signal. For the z-stack image frame acquisition a step width of 0.4-0.5  $\mu\text{m}$ , an Olympus Plan Apo N 60  $\times$ /1.42 or 100  $\times$ /1.4 oil objective were utilised. The Cell<sup>^</sup>R imaging software was used for image processing, background subtraction, projecting the images in a maximum intensity format and data acquisition.

### 2.4.3 Assessing HA-GLUT4-GFP transfection by confocal microscopy

Confocal microscopy was performed on an inverted Zeiss Axiovert 200M LSM 510 META microscope (Carl Zeiss MicroImaging GmbH, Germany), a pulsed infrared laser (Mai Tai Deepsee from Spectra Physics, Santa Clara, CA, USA) for 2-photon excitation and non-linear optical (NLO) imaging. Argon laser lines were used to excite in the blue range at 458, 477, 488 and 514 nm, a solid state laser was used for excitation at 561 nm in the green range, and a HeNe laser for the red range at 633 nm. The system is equipped with two conventional confocal detectors, as well as a polychromatic, spectral detection channel (META-detector) which allows for simultaneous detection and separation of up to 8 emission spectra, although only three emission spectra were generated. Additionally, the system has a confocal detector for transmitted light, which allows for optical sectioning of samples whether translucent, unlabelled or in combination with fluorescence labelling. An X-Cite 120 unit with a Xenon lamp (Lumen Dynamics Group, Ontario, Canada) was used for epifluorescence viewing of the specimens. Zeiss LSM and Zen 2009 software (Carl Zeiss MicroImaging GmbH, Germany) were used, which automated z-stacking for optimal increments of single image frames.

## 2.5 Statistical analysis

GraphPad Prism 5 (GraphPad Software, La Jolla, CA) was used for statistical analysis. Results were expressed as mean  $\pm$  standard error of the mean (SEM). Data were analysed by one-way analysis of variance (ANOVA) and Bonferroni post-test. Data from flow cytometry experiments were normalised to control values. Values were considered significant when probability (p)-values were less than 0.05 ( $p < 0.05$ ).

# Chapter 3

## Results

### 3.1 Culturing HL-1 cells

Culturing the HL-1 cardiomyocyte cell line requires careful attention, and a great deal of preparation and optimisation of culturing conditions. Appendix A contains detailed protocols and tips for the *Growth and care of HL-1 cardiomyocytes*. Everything from supplementation of the medium for various purposes [Appendix A.1 - A.3], to *Passaging* [A.6], to delicately *Freezing* [A.7] and *Thawing cells* [A.8] is included.

A few key observations were made whilst establishing the HL-1 cells. Firstly, the cells are very sensitive to CO<sub>2</sub> levels. For a while cells presented inexplicable stunted growth, or even death. Once it was discovered that incorrect CO<sub>2</sub> levels were being displayed by the incubator, and these levels were corrected, cells flourished and were growing normally within 24 hours. The second observation made was that crystals start to precipitate out of the medium while culturing cells [Figure 4.1]. It is therefore essential always to use fresh medium to avoid this problem.

One of the unique properties of this cell-line is that the cells have the capacity to be passaged and remain differentiated and contract in culture [110]. For cells to continue beating, they need to be supplemented with viable medium on a daily basis. It is critical that medium be supplemented with norepinephrine (to a final concentration of 0.1 mM) at least every two weeks [refer Appendix A.1, *Supplemented Claycomb Medium*].

For the first couple of weeks after enduring the courier process (live, at ambient temperature)

from North America to South Africa, the cells exhibited very slow growth and no contractile activity, again emphasising their delicate nature.

Lastly, cells were usually passaged 1:3, twice a week. Once seeded, cells do not immediately exhibit any contractile activity. They grow for about three or four days until almost fully confluent, before single cells dispersed throughout the culture start displaying signs of polarization. At this point adjacent cells start to contract until there are clusters of 'beating' cells around days 4-5.

## 3.2 Measuring ROS by flow cytometry

To assess whether oxidative stress was increased by dexamethasone, overall ROS was measured via flow cytometry [refer Section 2.2.2]. Our results indicate no statistically significant differences between the groups, however, a trend of elevated ROS (11%) was observed in cells treated with  $10^{-8}$  M dexamethasone for 4 hours. The experiment was carried out once so no statistical analysis could be performed. The advantage of flow cytometry, however, is that it enables data to be obtained from an entire population, and a minimum of 5, 000 events were recorded per sample [refer Figure 3.1].

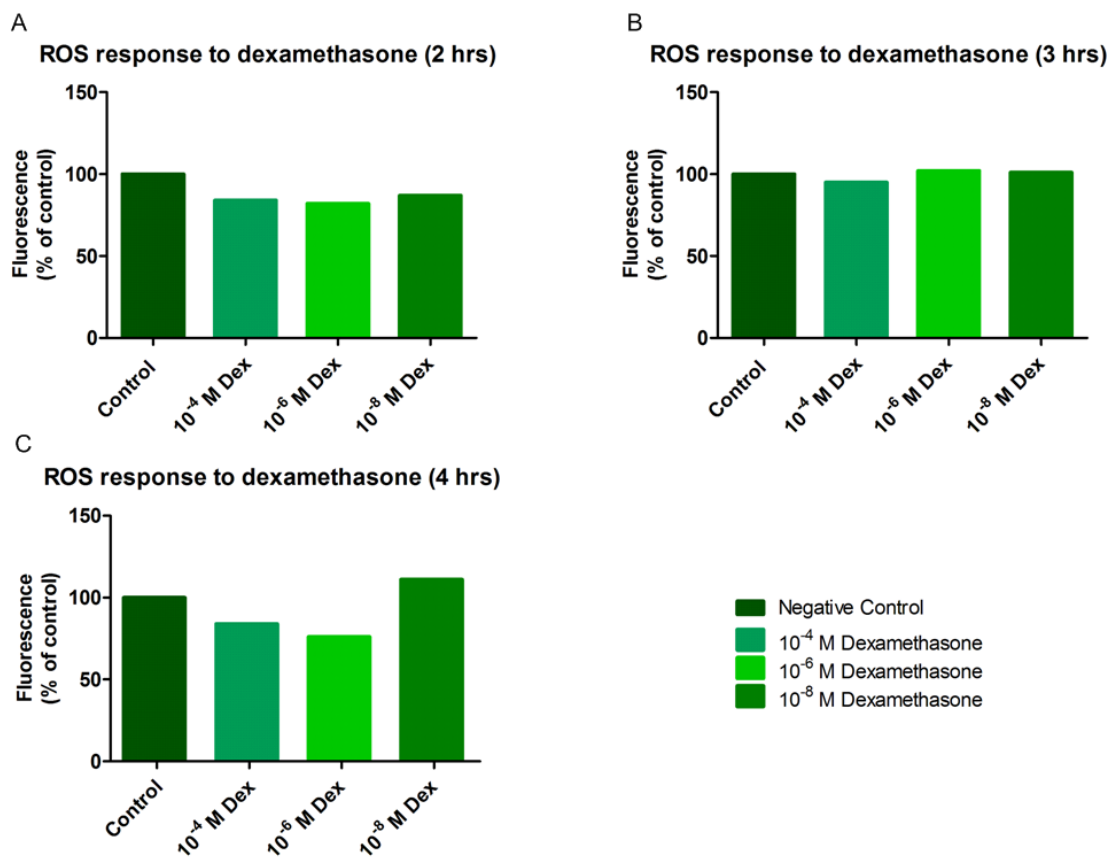


**Figure 3.1:** ROS response to dexamethasone treatments ( $10^{-4}$  M,  $10^{-6}$  M and  $10^{-8}$  M,) after 2, [A]; 3, [B]; and 4 hours, [C], respectively. All treatment groups have been normalised to the control, and are represented as a percentage of control values. These are matched observations where  $n=1$  with at least 5, 000 events recorded per sample. Significance could not be determined, but the greatest increase in ROS (11%) was observed after 4 hours exposure to  $10^{-8}$  M dexamethasone. Dex; dexamethasone.

### 3.3 Measuring the degree of *O*-GlcNAcylation

#### 3.3.1 Flow cytometry measurement of *O*-GlcNAc

After looking into the effects of dexamethasone on ROS, the effects of the synthetic glucocorticoid on HBP flux were assessed. Flow cytometry was employed to measure the degree of *O*-GlcNAcylation [Figure 3.2]. Our results indicate no statistically significant differences, however, a trend of increasing *O*-GlcNAcylation ( $26.4 \pm 12.59\%$ ) was observed in the group exposed to  $10^{-6}$  M dexamethasone for 2 hours.

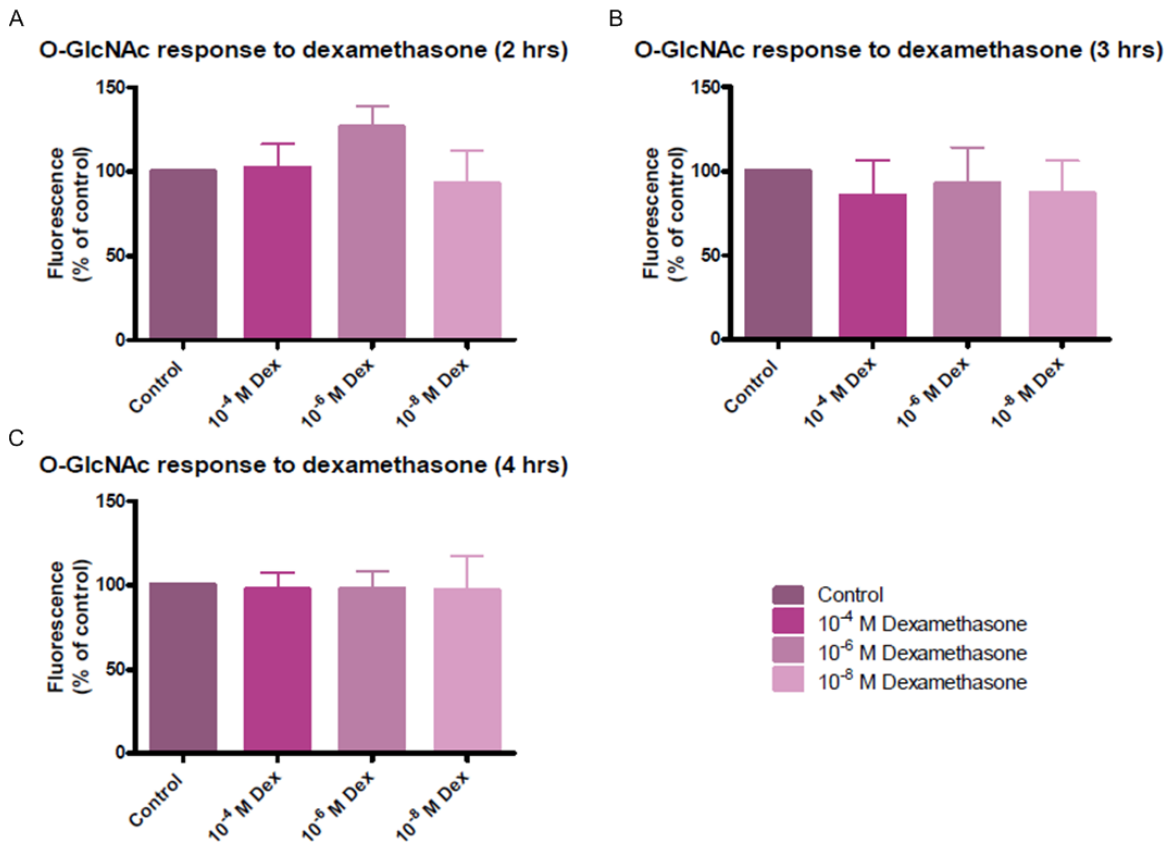


**Figure 3.2:** Flow cytometry measurement of *O*-GlcNAc of cells treated with  $10^{-4}$  M,  $10^{-6}$  M, and  $10^{-8}$  M dexamethasone. Treatments lasted 2, [A]; 3, [B]; and 4 hours, [C], respectively. Results were normalised to controls and represented as a percentage of control values. Matched observations were used to compare data sets, i.e. we employed an  $n=3$  for the 2 and 4 hour groups respectively, whilst we used an  $n=2$  for the 3 hour treatment group. On average  $\sim 10,000$  events were recorded per sample. There were no significant differences. The most noteworthy change was the  $26.4 \pm 12.59\%$  increase of *O*-GlcNAcylation after a 2 hour exposure to dexamethasone at a concentration of  $10^{-6}$  M [A]. Dex; dexamethasone.

Representative scatterplots and intensity histograms of the control and aforementioned dexamethasone group are shown in Figure 3.3. Mean intensity was measured in the gate P2, which is a daughter population of P1, ensuring that only cells (and not debris) are considered for the mean intensity analysis. The intensity histogram indicates an increase in fluorescence intensity of P2 in the dexamethasone-treated group (PE-TxRed peak shifts to right).

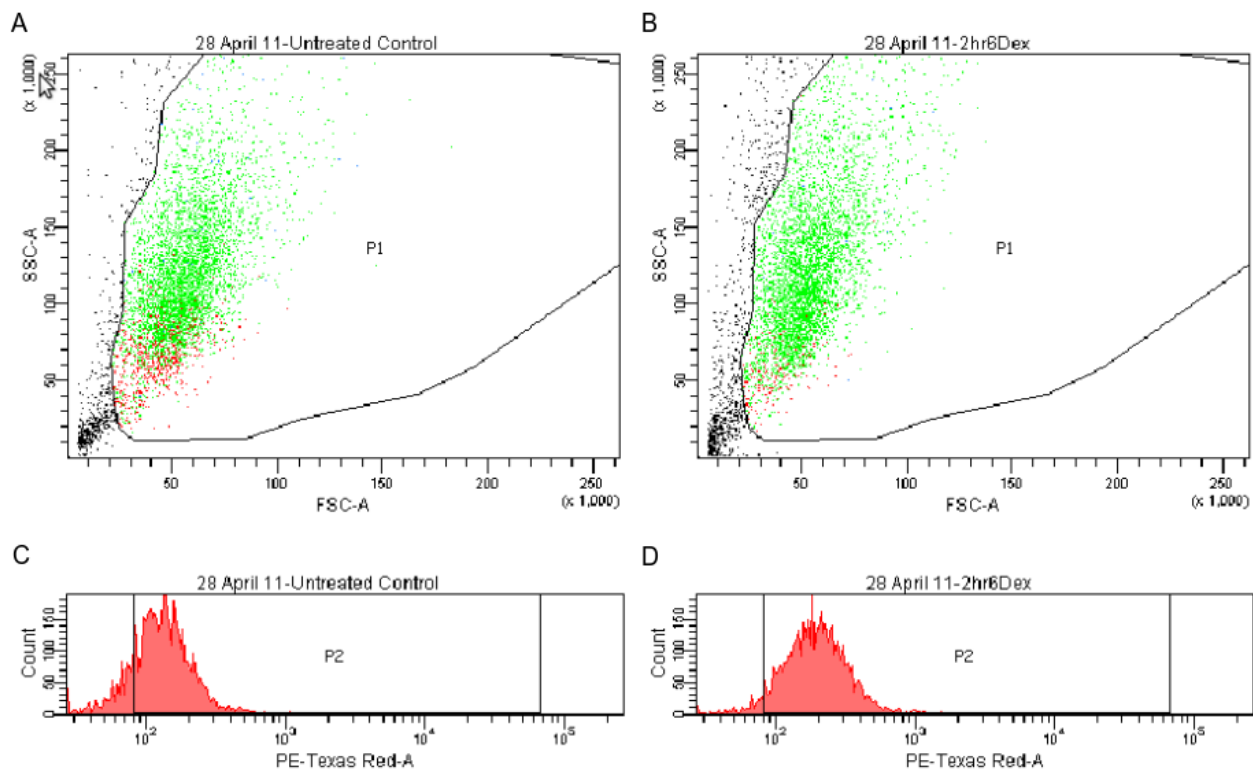


**Figure 3.3:** Flow cytometry measurements of *O*-GlcNAc in dexamethasone-treated cells. The greatest increase of *O*-GlcNAcylation in relation to the control [A and C] occurred after a 2 hour exposure to dexamethasone at a concentration of  $10^{-6}$  M [B and D]. The scatterplots [A and B] provide information about granularity of the cells in the side scatter channel (SSC, y-axis); and can roughly equate particle size allowing for differentiation between intact cells and cellular debris in the forward scatter channel (FSC, x-axis). Intensified fluorescence is indicated by the shift to the right in the PE-TxRed peak of the representative intensity histograms [C and D].

### 3.3.2 Western blotting measurement of *O*-GlcNAc

Next, we determined *O*-GlcNAcylation by Western blotting [refer Figure 3.4]. Dexamethasone-treated cells exhibited a similar amount of *O*-GlcNAc to the control group (Western blotting).

For this set of experiments we also included an antioxidant (OHCA). However, OHCA treatment resulted in no significant changes in the degree of *O*-GlcNAcylation. No statistically significant differences were observed between groups.

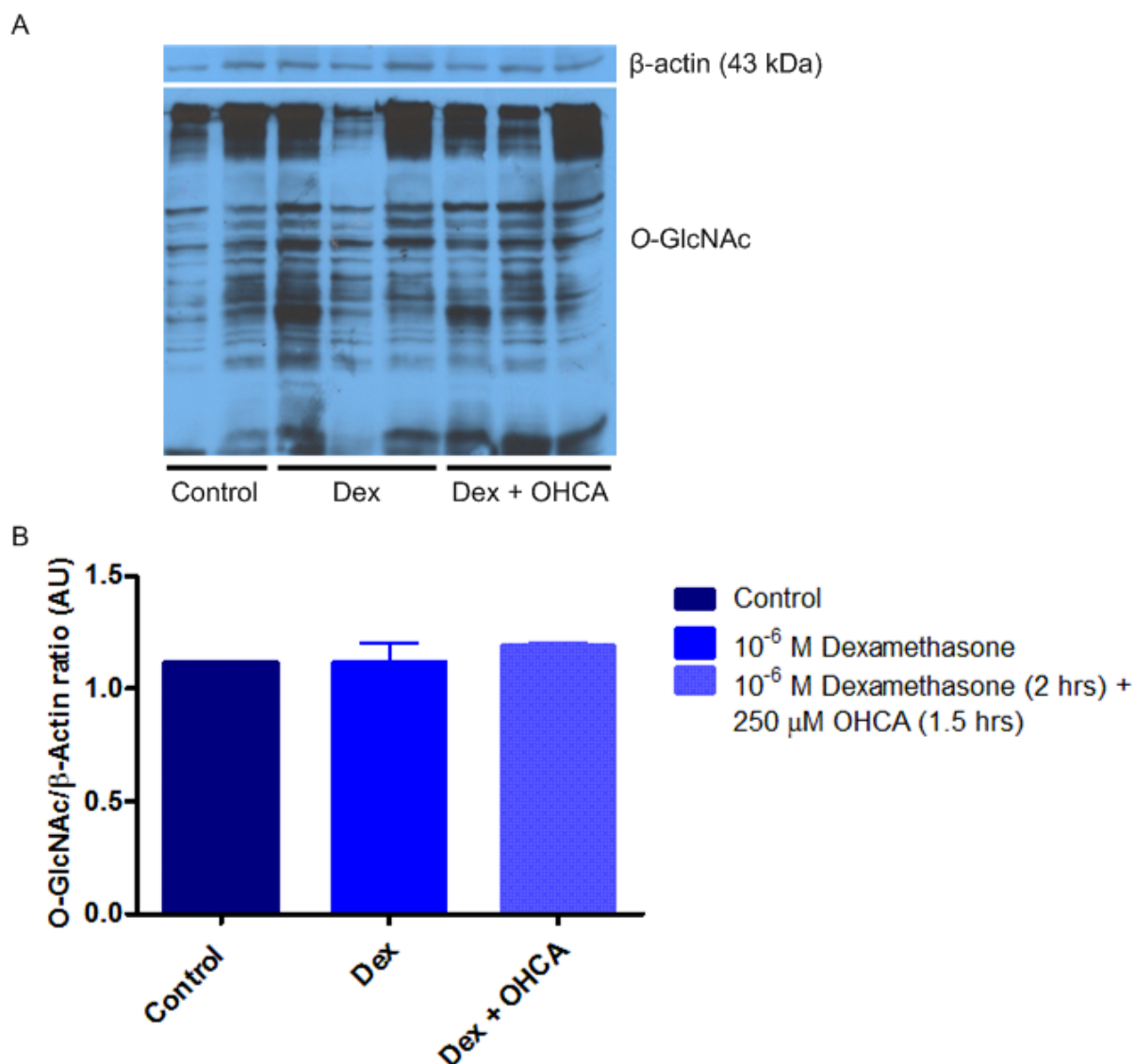


**Figure 3.4:** [A] Western blot of *O*-GlcNAc (bottom), and the corresponding  $\beta$ -actin for loading control (top). [B] Scanned images of the blots were digitised and, per lane, values normalised to  $\beta$ -actin. Results are presented in arbitrary units. No significant differences were observed ( $n=5$ ). AU; arbitrary units. Dex; dexamethasone. OHCA;  $\alpha$ -cyano 4-hydroxyl cinnamic acid.

## 3.4 Determining the degree of GLUT4 translocation

Both fluorescence microscopy as well as confocal microscopy were used to investigate GLUT4 translocation with HA-GLUT4-GFP transfected cells, based on the HA:GFP ratio [refer Chapter 2.4.1].

### 3.4.1 Immunofluorescence microscopy

Dexamethasone significantly reduced the HA:GFP ratio of insulin-stimulated cells. In comparison to the control group [Figure 3.5], the HA:GFP ratio was reduced by  $20.23 \pm 0.993\%$  in insulin-stimulated, dexamethasone-treated cells [Figure 3.7]. In relation to insulin-stimulated cells [Figure 3.6], dexamethasone treatment reduced HA:GFP by  $20.53 \pm 1.202\%$ . No statistically significant difference was observed between control and insulin-stimulated cells [Figure 3.8].

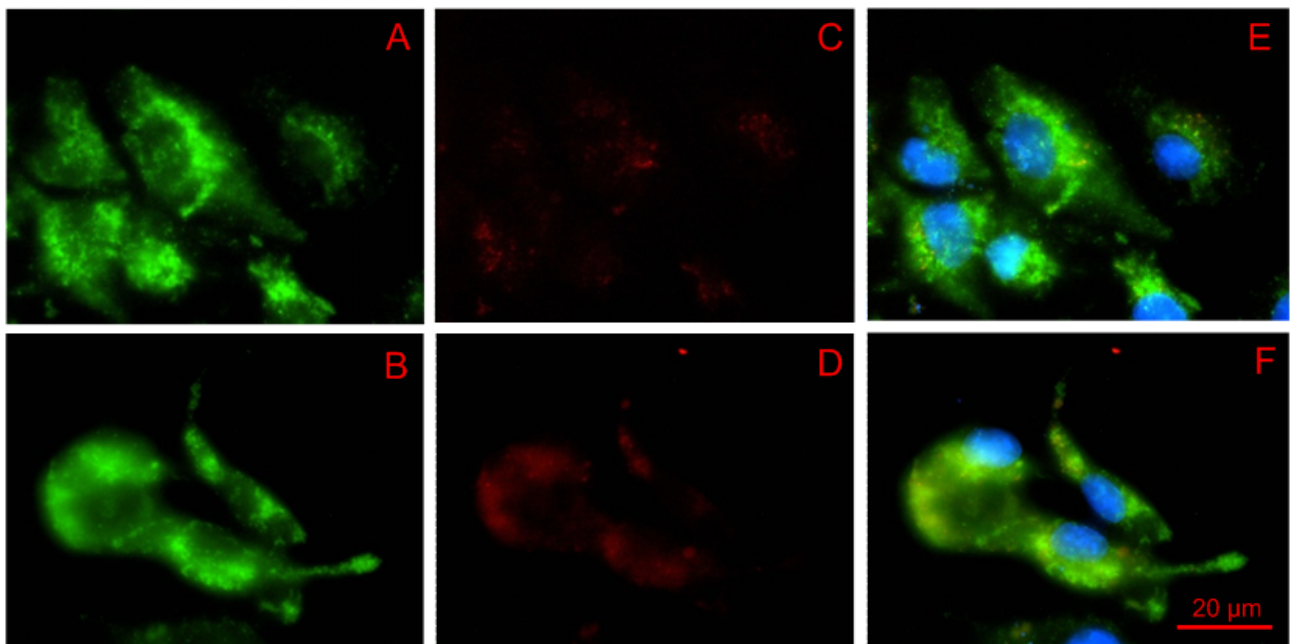


**Figure 3.5:** Maximum intensity projections of the GFP, [A] and [B]; HA, [C] and [D]; and overlay of all colour channels, including the blue nuclear stain, Hoechst, [E] and [F], of control cells. Where green and red signal overlap, it presents as yellow or orange in the overlay. Fluorescence microscopy images of HA-GLUT4-GFP transfected cells captured with a  $60\times$  oil immersion objective.

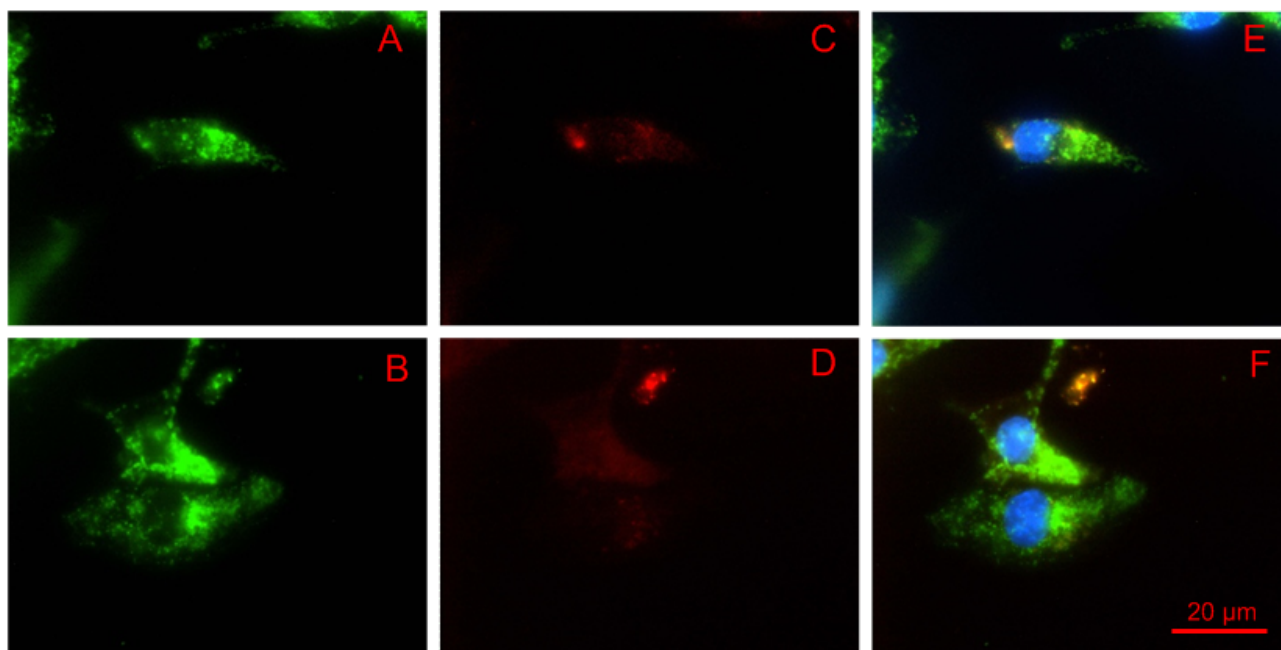


**Figure 3.6:** Maximum intensity projections of the of insulin-stimulated, HA-GLUT4-GFP cells. GFP is displayed in [A] and [B]; HA is represented in the TxRed channel, [C] and [D]; and [E] and [F] provide an overlay of all colour channels, including the blue nuclear stain, Hoechst. Yellow or orange display in the overlay images, [C] and [F], when green and red signal overlaps. Images were captured with a 60 $\times$  oil immersion objective. The HA:GFP ratio was calculated per cell and used to determine mean values for each treatment group.

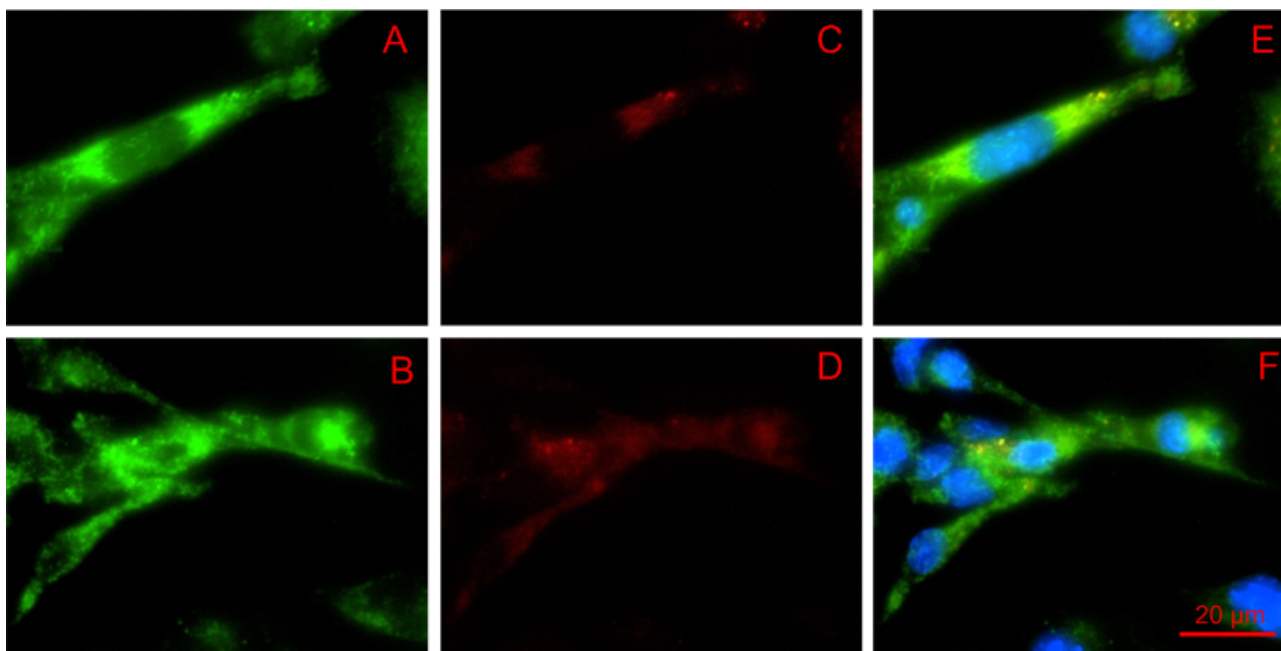


**Figure 3.7:** Images of HA-GLUT4-GFP transfected cells that were insulin-stimulated and treated with dexamethasone were projected at maximum intensity. [A] and [B] show GFP signal; [C] and [D], the HA represented in the TxRed channel; and [E] and [F] display an overlay of all colour channels, including the nuclear stain, Hoechst, in blue. Green and red signal overlapping results in yellow or orange in the overlay. A 60 $\times$  oil immersion objective was used. Per cell calculations of the HA:GFP ratio were made for the group, and the mean value used to compare to other groups.

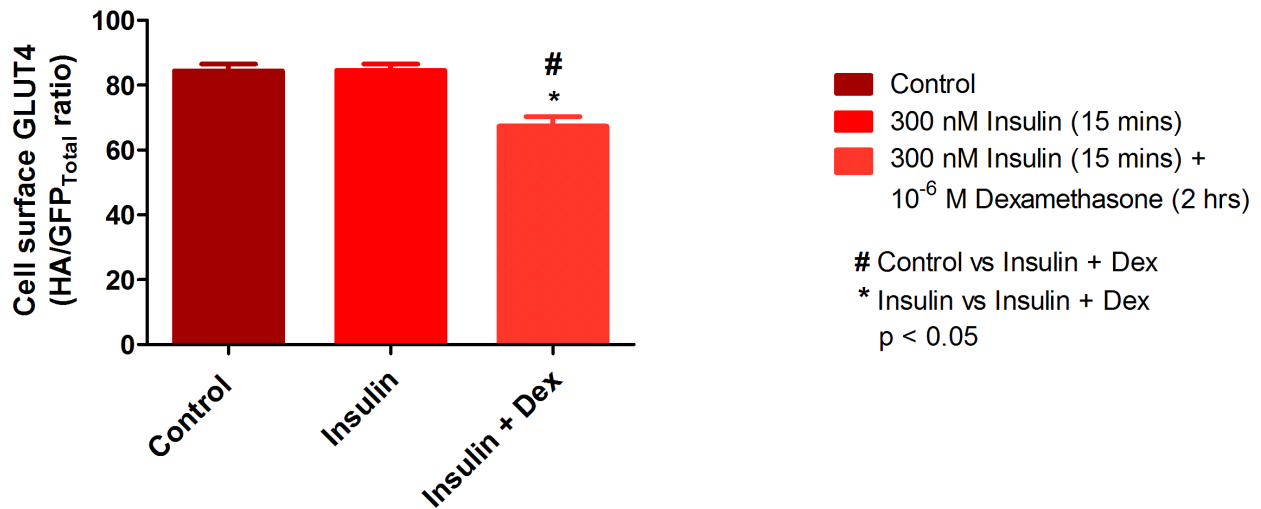


**Figure 3.8:** The HA:GFP ratio represents the measure of GLUT4 present at the sarcolemma. Dexamethasone treatment of insulin-stimulated cells significantly decreased the HA:GFP ratio in with respect to the control ( $20.23 \pm 0.993\%$ ) and insulin-stimulated groups ( $20.53 \pm 1.202\%$ ). (n=7) Dex; dexamethasone.

### 3.4.2 Confocal microscopy

We also made use of confocal microscopy to assess GLUT4 translocation [Figures 3.9, 3.10 and 3.11]. However, due to very low signal in the TxRed channel, no analyses could be performed on these images in order to calculate the ratio of HA (surface GLUT4) to GFP (cytosolic GLUT4). The images acquired do show the specific GFP signal which confirms that the HL-1 cells were transfected with the HA-GLUT4-GFP construct.

Figure 3.12 displays 4 layers from a z-stack taken of a cell stimulated with insulin and treated with dexamethasone and OHCA. Here too, the TxRed signal was too poor to use for analysis and they have been omitted from the figure. As the z-stack moves deeper into the cell e.g. from [A] to [D] to [G] to [J], the diameter increases and more of the nucleus becomes visible as the widest part of its girth is approached.

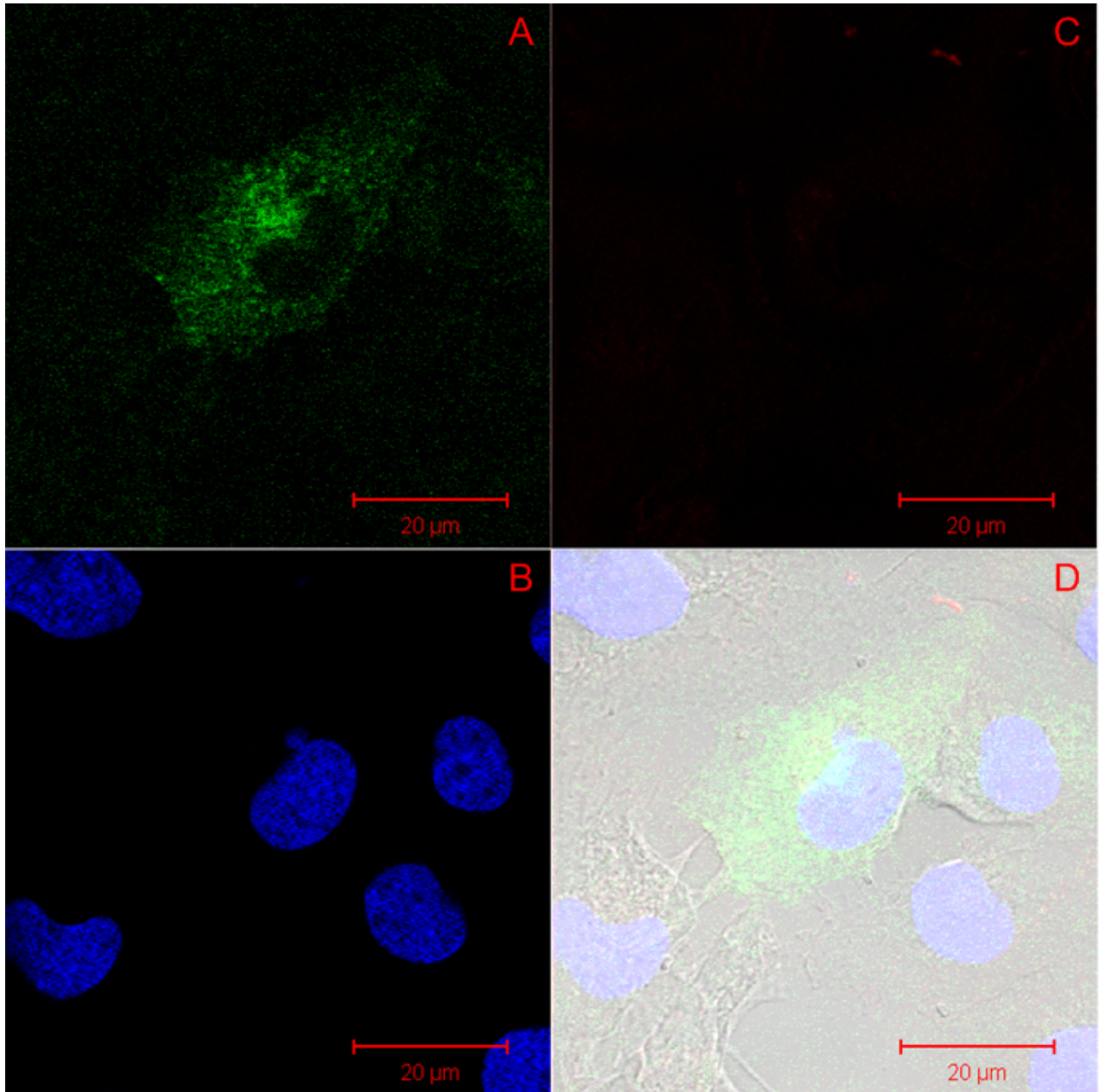


**Figure 3.9:** A control cell transfected with HA-GLUT4-GFP that was neither treated with dexamethasone, nor stimulated with insulin, captured on a confocal microscope. [A] The green represents GFP; [B] with the blue indicating nuclear material; [C] and the red, the HA-tag. [D] Lastly, an overlay of all colour channels including a transmission image (grey) is displayed. The red scalebars represent 20 µm.

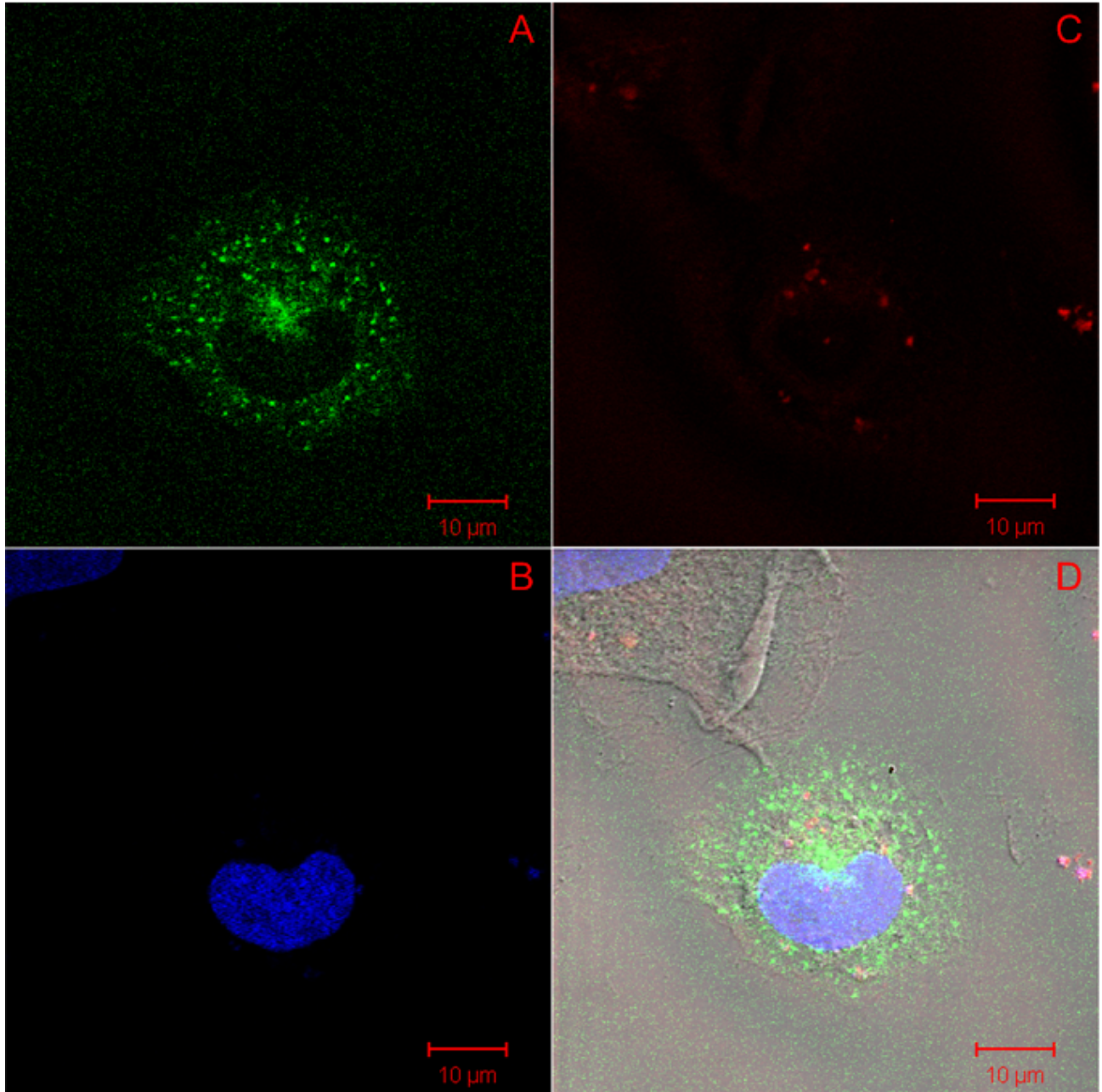


**Figure 3.10:** Image of a cell transfected with HA-GLUT4-GFP and stimulated with insulin. [A] The green represents GFP, [B] the blue indicates nuclear material, [C] and the HA-tag is shown in red, but shows nothing more than a few (intracellular) specks of red, where one would expect a pericytosolic accumulation. [D] An overlay of all colour channels is displayed last, and includes an image of the transmitted light in grey. The red scalebars represent 10 µm.

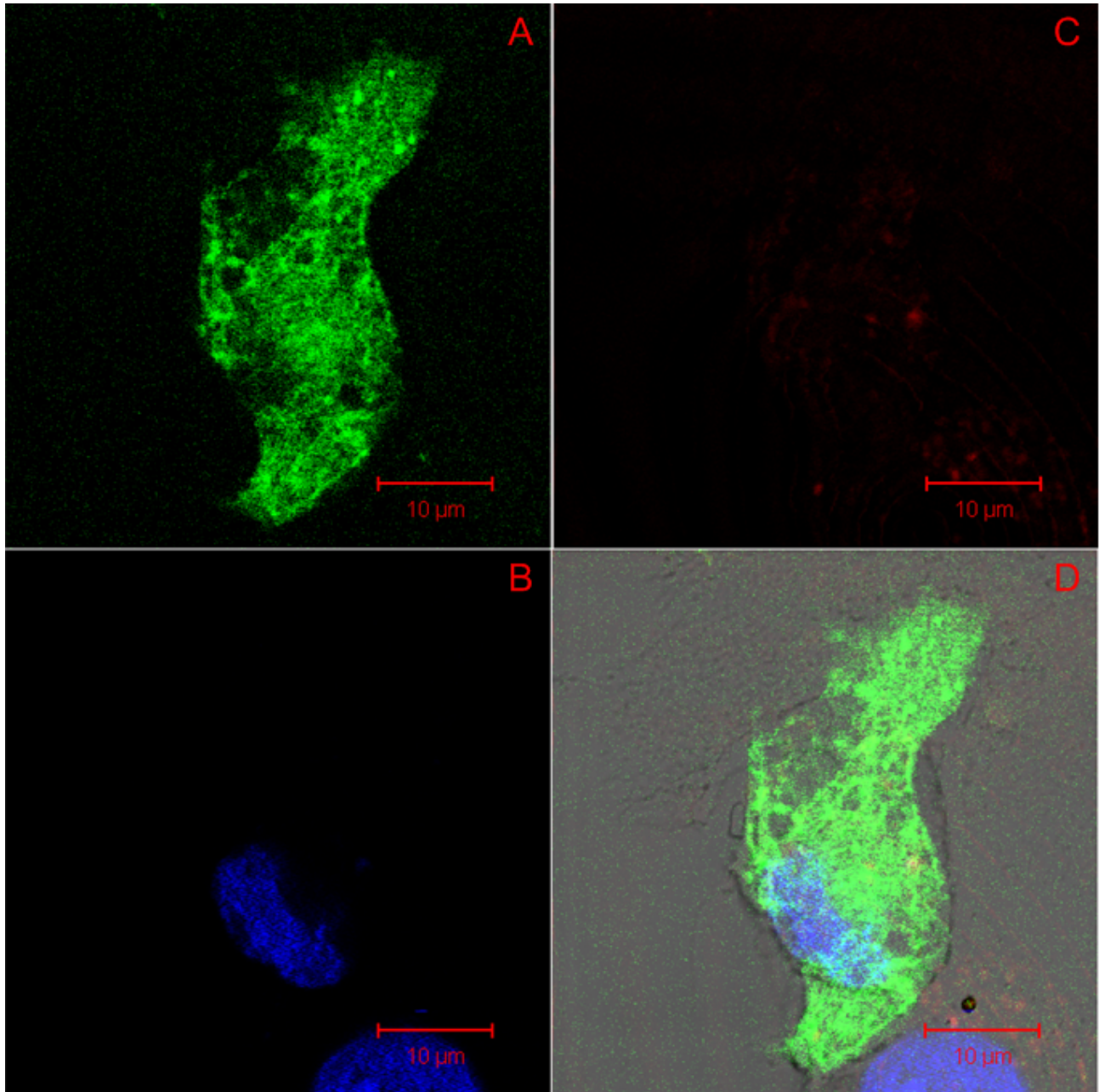


**Figure 3.11:** An HA-GLUT4-GFP transfected cell treated with dexamethasone and insulin-stimulated imaged on a confocal microscope. [A] GFP is represented in green; [B] nuclear material in blue; [C] and the HA-tag in red. [D] Finally all the colours are presented in an overlay which includes the grey transmission image. The red scalebars represent 10 µm.

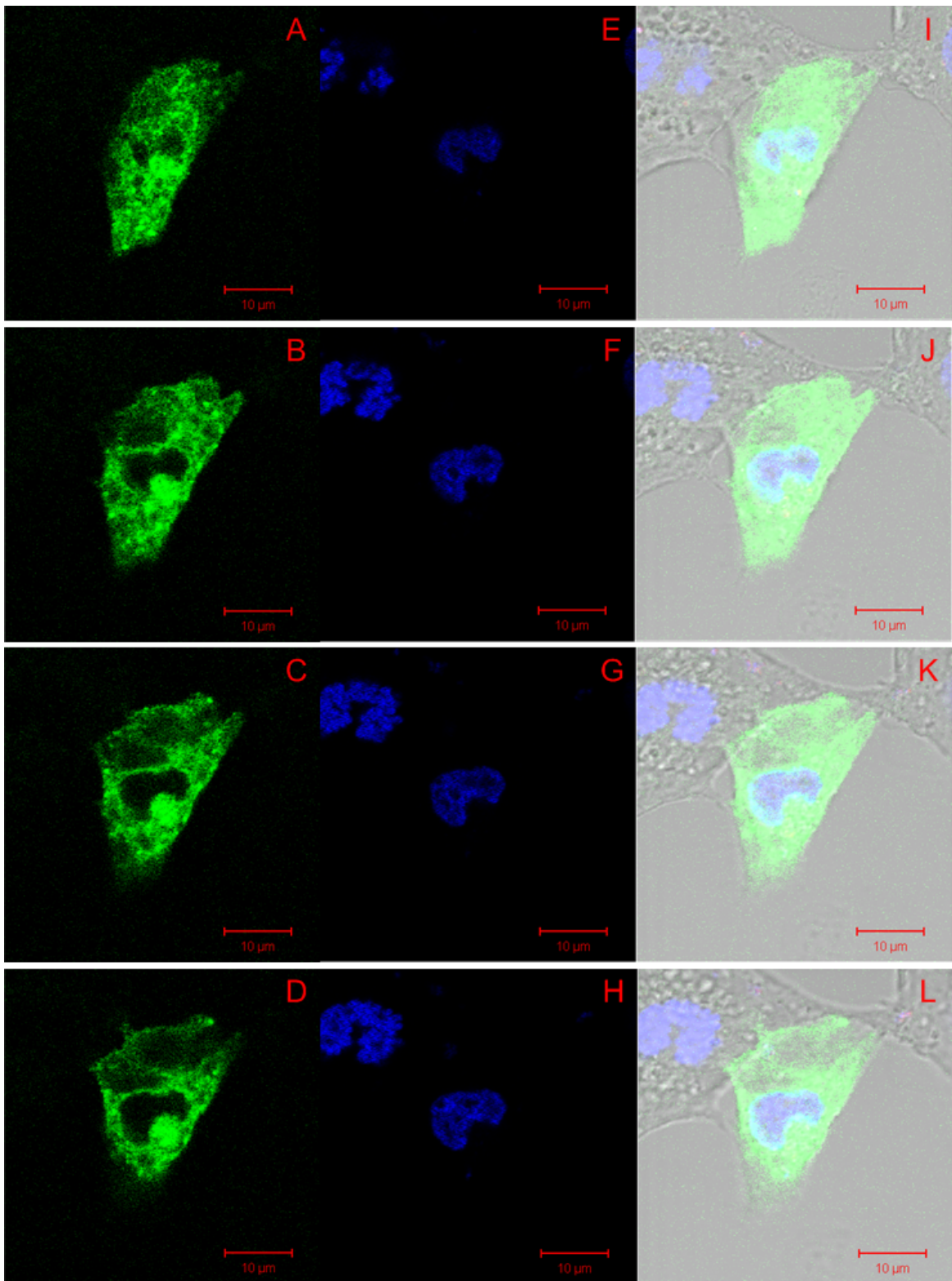


**Figure 3.12:** Z-stack of an HA-GLUT4-GFP transfected cell. The red scalebars represent 10  $\mu\text{m}$ . Images [A] - [D] display the green channel representing the GFP; [E] - [H] display signal of the nuclear dye, Hoechst, in blue; [I] - [L] provide overlay images of all colour channels, including the transmitted light, in grey. This particular cell was stimulated with insulin and treated with dexamethasone and OHCA.

# Chapter 4

## Discussion

### 4.1 Introduction

The metabolic syndrome, and related metabolic perturbations are closely linked to cardiomyopathy and CVD. Insulin resistance is characteristic of metabolic disorders such as diabetes and obesity. Hyperglycaemia significantly induces glucose-utilising pathways [refer Figure 1.6] setting off many adverse effects. Increased flux through the HBP, particularly when chronically activated, plays a causative role in insulin resistance, T2DM, and CVD. More recently, stress has also been implicated as a causative agent for the onset of insulin resistance [15], [114]

With this in mind, a cell model was established to gain insight into the effects of dexamethasone on cardiac (HL-1) cells. We hypothesised that dexamethasone increases oxidative stress, as well as HBP flux increasing *O*-GlcNAc protein modification, resulting in decreased GLUT4 translocation to the sarcolemma, and thus contributing to the onset of insulin resistance.

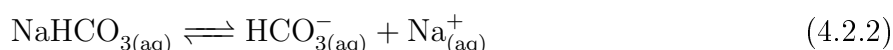
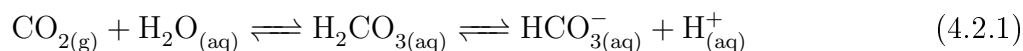
The hypothesis was tested by:

1. measurement of ROS in response to dexamethasone treatment, via flow cytometry;
2. flow cytometric measurement of *O*-GlcNAc in dexamethasone-treated cells;
3. analysis of *O*-GlcNAcylation following dexamethasone administration  $\pm$  OHCA via Western blotting; and
4. determining the degree of GLUT4 translocation.

Our main findings indicated (1) no significant increases in ROS, (2-3) or in *O*-GlcNAc modification, however, a definite trend towards an increase in *O*-GlcNAcylation subsequent to dexamethasone treatment (2 hours,  $10^{-6}$  M) was observed (2), [Chapter 3.3.1]. Furthermore, a significant decrease of GLUT4 translocation was also observed (4), [Chapter 3.4.1].

## 4.2 HL-1 cells

Cell growth is affected by  $\text{CO}_2$  levels since it dissolves easily into water - or in this case the culture medium - and affects the pH. When  $\text{CO}_2$  dissolves into water it produces carbonic acid ( $\text{H}_2\text{CO}_3$ ), which quickly dissociates into bicarbonate ( $\text{HCO}_3^-$ ) and hydrogen ( $\text{H}^+$ ) ions [refer Equation 4.2.1]. Increasing atmospheric  $\text{CO}_2$  will therefore decrease the pH. Similarly, cells produce  $\text{CO}_2$  as they metabolise, which also increases the acidity of the medium. A phenol red indicator (present in Claycomb medium) turns orange when medium becomes acidic, or even yellow in cases of extreme acidity. To buffer this effect, sodium bicarbonate ( $\text{NaHCO}_3$ ) is frequently used in culture media to stabilize pH.  $\text{NaHCO}_3$  dissociates into sodium ( $\text{Na}^+$ ) and bicarbonate ( $\text{HCO}_3^-$ ) ions [refer Equation 4.2.2]. Dissolved  $\text{CO}_2$  is then in equilibrium with bicarbonate ions.



When atmospheric  $\text{CO}_2$  is low, the pH of the medium will increase. We speculate that the HL-1 cells exhibited retarded growth (discussed in Section 2.1.1) as a result of low atmospheric  $\text{CO}_2$  levels (due to an incubator error) which resulted in excessive alkalinity in the medium, indicated by a ‘cool’, deep red appearance. Cells grow best at a relatively neutral pH, when phenol red will give the medium a ‘warm’ red appearance.  $\text{CO}_2$  levels may be maintained more effectively by minimising traffic through the incubator, and monitored with more regular, daily measurements using a fyrite device.

We have also learnt that it is crucial that fresh medium is always used for the culturing of HL-1 cells. If medium gets old, crystals may start to precipitate. Crystals assume what appears to be an octahedron shape, which is typical of sodium chloride ( $\text{NaCl}$ ) crystals [Figure 4.1]. Regardless of their molecular make-up, once the crystal nucleus has formed the crystal

continues to grow, and it has harsh edges that invade the space cells grow in, possibly obstructing cell growth.



**Figure 4.1:** Image of sodium chloride salt crystals similar in structure to those which precipitate out of culture medium. Photograph by the NASA Expedition 6 crew (NASA Image of the Day). The crystals are in a water bubble within a 50 mm metal loop which formed part of an experiment in the Destiny laboratory aboard the International Space Station.

Furthermore, medium should be supplemented with norepinephrine (to a final concentration of 0.1 mM) at least every two weeks [refer Appendix A.1, *Supplemented Claycomb Medium*]. Norepinephrine and retinoic acid are essential to stimulate beating, and maintain a differentiated phenotype [110]. In summary, optimisation of HL-1 cell culturing conditions took a considerable length of time and a significant degree of time spent on this project.

### 4.3 Dexamethasone displays minimal effect on ROS

Flow cytometry data for ROS measurement indicated little or no changes versus controls [refer to Figure 3.1]. However, the  $10^{-8}$  M dose of dexamethasone administered for 4 hours showed a trend of elevated ROS levels compared to other doses.

Oxidative stress has been shown to be involved in cell damage and myocardial cell death. It has recently been found in rat cardiomyocytes that mitochondrial proteins (COX-1 of complex IV of the electron transport chain, and NDUFA9 of complex I in particular) also undergo *O*-GlcNAcylation, and especially when exposed to high glucose conditions [101]. This implicates excessive mitochondrial *O*-GlcNAc modification in adversely altered mitochondrial function. Impaired mitochondrial function is well established in the diabetic cardiomyocyte [115]. Thus a possible link may exist between *O*-GlcNAc-induced malfunctioning of the mitochondria and superfluous superoxide release.

## 4.4 Effect of dexamethasone on degree of *O*-GlcNAcylation

### 4.4.1 Flow cytometry

There were no significant increases in *O*-GlcNAcylation [Figure 3.2], as assessed by flow cytometry [Chapter 3.3.1], which corresponds to ROS data [Chapter 3.2]. The timepoint and concentration that yielded the highest expression of *O*-GlcNAc was 2 hours with  $10^{-6}$  M dexamethasone. We therefore used aforementioned treatment parameters for Western blotting, and microscopy experiments (for GLUT4 translocation investigation) that followed.

### 4.4.2 Western blotting

When cells were treated with dexamethasone ( $10^{-6}$  M for 2 hours) and the antioxidant (OHCA) was administered (250  $\mu$ M for 90 minutes), and analysed by Western blotting for degree of *O*-GlcNAcylation, no significant differences were detected in any of the treatment groups [Figure 3.4]. This corresponds to our ROS data.

These data therefore suggest that dexamethasone did not activate the HBP in our experimental system. It is important to note that *O*-GlcNAcylation is a very dynamic process that cycles rapidly, and it is frequently in competition with phosphorylation for serine/threonine sites. Therefore, with techniques such as flow cytometry and Western blotting which use antibodies that require fixation of cells, only a ‘snapshot’ in time can be assessed. Results gleaned through such a small and warped window should thus be interpreted carefully. To improve sta-

tistical accuracy it is recommended to increase the sample size, and perhaps use a more reliable loading control. No literature was found regarding a direct link between glucocorticoids and HBP activation.

## 4.5 GLUT4 translocation significantly reduced by dexamethasone

### 4.5.1 Immunofluorescence microscopy

Dexamethasone treatment significantly reduced HA:GFP ratio, which implies that GLUT4 translocation was decreased in this model [Figure 3.8]. Treatment with dexamethasone has been associated with decreased glucose uptake in cells [35] and implies that dexamethasone inhibits GLUT4 translocation or its association to the cell membrane [116]. It should be noted that despite the decrease in translocation, GLUT4 protein content is often reported to increase in rat (soleus) skeletal muscle [60], [117], while GLUT4 expression reportedly remains unchanged in adipocytes [118]. In line with this, Vosseler et al. [97] deduced that insulin resistance is induced by increased *O*-GlcNAcylation of GLUT4 rather than decreased expression of the insulin-sensitive glucose transporter. However, further studies are required to confirm these hypotheses, and to elucidate the mechanisms of action. Although the complete mechanism remains unclear, various sources of literature have verified the importance of PI3K and Akt in insulin-stimulated GLUT4 trafficking [119]. Notably, dexamethasone has an attenuating effect on Akt expression [64], possibly explaining, at least in part, the reduction in insulin-stimulated recruitment of the downstream target, GLUT4, to the sarcolemma.

An increase of the HA:GFP ratio is expected in the insulin-stimulated group. Shuralyova et al. [28] (who confirmed the presence of both isoforms of glucose transporters, GLUT1 and GLUT4, in HL-1 cells) documented approximately a threefold increase in glucose uptake by stimulating the cells with insulin (300 nM). No increase is, however, observed in our results. This can possibly be explained by the fact that the culturing medium contains a small amount of insulin (15 µg/l) [111] and that cells were never truly ‘serum starved’ as a result. Consequently, the cells weren’t maximally sensitised to the insulin stimulation, and insulin could not effectively recruit GLUT4 vesicles to the sarcolemma. Thus our experimental system requires further optimisation in terms of our conditions and to make meaningful conclusions. Furthermore, it appears that the TxRed signal (supposed to represent the presence of HA, and thus

surface GLUT4) is relatively non-specific in most of the microscopy images.

### 4.5.2 Confocal microscopy

The TxRed channel in all the confocal microscopy images also contain what appears to be non-specific signal. A cell from the control group is shown in Figure 3.9, while Figure 3.10 shows a cell from the insulin-stimulated treatment group. Figure 3.11 displays a cell from the group stimulated with insulin, and also treated with dexamethasone. In images from the fluorescence microscope it is less visible than those from the confocal microscope (far superior resolution). It is possible, especially with fluorescence microscopy, that HA signal from different layers of the z-stack, or signal from the bright GFP, may have ‘bled’ through (dimensionally and spectrally, respectively) and influenced fluorescence intensity of HA. This would affect the HA:GFP ratio (mean fluorescence intensity of HA divided by mean intensity of GFP). The power of the confocal microscope also clarified the presence of HA signal *within* the cell, when the HA antibody is expected to bind to the cell membrane, extracellularly. Figure 3.10 also displays a staining artefact which looks like red contours arranged concentrically around the nucleus. This may be due to the fluorescent mounting medium used, or more specifically, it spreading unevenly in an open well, as opposed to being covered by a cover slip on a microscope slide.

Interestingly, Figure 3.9 shows a transfected cell with a perinuclear GFP storage pool, typical to GLUT4 distribution in cells [113], nestled in the concave side of the bean-shaped nucleus. Perhaps there is an association between GLUT4 vesicle formation and the endoplasmic reticulum and golgi stacks generally also found in this locale [120].

As with *O*-GlcNAcylation analyses, GLUT4 translocation analysis requires cells to be fixed for the use of HA antibody. This again meant that only a snapshot of the spacio-temporally dynamic process could be captured. Another limiting factor was the very low transfection efficiency, typical of cardiac cells and particularly pronounced in the HL-1 cell line, which meant that very few cells could be analysed by microscopy.

## 4.6 Conclusion

In an attempt to elucidate some of the underlying mechanisms driving the onset of stress-induced cardiomyopathy, we successfully established a cell model for investigating the effects of glucocorticoids on cardiac cells. Firstly, we established the HL-1 cardiomyocyte cell line in

our laboratory [described at length in *Cell culture: Growth and care of HL-1 cardiomyocytes*, Appendix A]. This was followed by various time and dose response analyses for dexamethasone treatment.

We aimed to assess oxidative stress in response to dexamethasone treatment. Here we found that dexamethasone had no noticeable effect on the overall production of ROS, however, this does not rule out the change in production of mitochondrial ROS. Our second aim was to assess the degree of *O*-GlcNAcylation in response to dexamethasone treatment. Here we found no significant changes from the control, but that dexamethasone increased protein modification by *O*-GlcNAc with a maximal effect after a 2 hour treatment with a  $10^{-6}$  M dose. These preliminary data potentially implicate the HBP as a downstream target of glucocorticoids. Further studies are needed to confirm this.

Lastly, insulin-stimulated GLUT4 translocation was significantly decreased subsequent to dexamethasone treatment. Dexamethasone has been linked to changes in GLUT4 translocation in various tissues. Decreases in insulin-stimulated translocation in various tissues including muscle and fat have been reported in literature. However, since insulin stimulation did not increase GLUT4 translocation, further optimisation of the experimental protocol is required to meaningfully investigate this question.

In conclusion, our data suggests a potential novel link between dexamethasone exposure, HBP activation and decreased GLUT4 translocation. Based on our findings we propose that detrimental effects of chronic stress on the heart may be mediated by increased HBP flux. Considering that insulin resistance and thus indirectly, related metabolic derangements and diseases such as diabetes, has been associated with glucocorticoid excess and GLUT4 dysregulation, these results provide new targets for potential therapeutic agents.

Elucidation of these mechanisms and a search for an effective therapeutic agent that may prevent excessive or protracted *O*-GlcNAc modification, and the consequent adverse effects that contribute to cardiovascular complications, remain part of ongoing research in our laboratory.

## 4.7 Future recommendations

The influence of dexamethasone on *O*-GlcNAc modification is poorly documented, especially in the context of cardiovascular or metabolic diseases, making further investigation imperative. Since our flow cytometry results were inconclusive but indicated an upward trend in the extent of *O*-GlcNAcylation in response to certain doses of dexamethasone, significance may be reached with an increase in *n*'s. The differences observed in *O*-GlcNAc were very small, thus flow cytometry may not be sufficiently sensitive for its detection. Other techniques, such as fluorescence or confocal microscopy and Western blotting can be used to supplement the data. Assessing the presence of OGT and OGA, or the availability of UDP-GlcNAc, may also provide information about the extent of *O*-GlcNAcylation under differing conditions.

We also propose that additional experiments be performed to confirm the degree to which dexamethasone plays a role in the production of myocardial ROS. Moreover, a mitochondrial marker, e.g. MitoSOX Red, can be employed to assess mitochondrial changes *per se*, since the DCF dye may not have detected minor changes in this regard. Further studies may also include investigating the effects of various anti-oxidants on ROS production. Additionally, investigating the HL-1 cell line-specific reliance on glycolysis versus glucose oxidation would be of interest with regards to mitochondrial respiratory-related ROS production.

Regarding HA-GLUT4-GFP analysis, optimisation of staining is required. A method by which entry of the HA antibody into the cells could be minimised, thereby preventing non-specific signal, entails incubating the viable cells with primary antibody prior to fixation. If the antibody contains any toxic preservatives such as sodium azide, it should be purified by extensive dialysis [121]. Milder fixative agents may also limit non-specific entry of antibodies into cells. Furthermore, since Claycomb medium contains insulin, the experimental conditions require optimisation in terms of effective insulin-stimulated GLUT4 trafficking. Lastly, a glucose uptake assay spanning a series of time points could assist in defining the optimal time point at which to assess GLUT4 translocation in HL-1 cells.

## Bibliography

- [1] Algazy J, Gipstein S, Riahi F, Tryon K. Why governments must lead the fight against obesity.; 2010. McKinsey & Company. 1
- [2] World Health Organisation. Obesity and overweight, Fact sheet No. 311; 2011. Available from: <http://www.who.int/mediacentre/factsheets/fs311/en/>. 1
- [3] International Diabetes Federation. Diabetes Atlas: Global Burden; 2011. Available from: <http://www.idf.org/diabetesatlas/5e/the-global-burden>. 1
- [4] International Diabetes Federation. Diabetes Atlas: Diabetes; 2011. Available from: <http://www.idf.org/diabetesatlas/5e/diabetes>. 1
- [5] United Nations. Non-communicable diseases deemed development challenge of 'epidemic proportions' in political declaration adopted during landmark General Assembly Summit. United Nations Sixty-sixth General Assembly, GA/11138; 2011. Available from: [www.un.org/News/Press/docs/2011/ga11138.doc.htm](http://www.un.org/News/Press/docs/2011/ga11138.doc.htm). 1
- [6] International Diabetes Federation. Diabetes Atlas: Africa; 2011. Available from: <http://www.idf.org/diabetesatlas/africa>. 1
- [7] Ziraba AK, Fotso JC, Ochako R. Overweight and obesity in urban Africa: A problem of the rich or the poor? BMC Public Health. 2009;9(465). 1
- [8] Caballero B. A nutrition paradox—underweight and obesity in developing countries. N Engl J Med. 2005;352(15):1514–1516. 1
- [9] Petersen KF, Shulman GI. Etiology of insulin resistance. Am J Med. 2006;119(5 Suppl 1):S10–S16. 1
- [10] Rosmond R. Role of stress in the pathogenesis of the metabolic syndrome. Psychoneuroendocrinology. 2005;30(1):1–10. 2, 4, 14, 16

- [11] Reaven GM. Banting lecture 1988. Role of insulin resistance in human disease. *Diabetes*. 1988;37(12):1595–1607. 2
- [12] Alberti KGMM, Eckel RH, Grundy SM, Zimmet PZ, Cleeman JI, Donato KA, et al. Harmonizing the metabolic syndrome: a joint interim statement of the International Diabetes Federation Task Force on Epidemiology and Prevention; National Heart, Lung, and Blood Institute; American Heart Association; World Heart Federation; International Circulation. 2009;120(16):1640–1645. 2, 3
- [13] Beaudoux JL, Nivet-Antoine V, Giral P. Resveratrol: a relevant pharmacological approach for the treatment of metabolic syndrome? *Curr Opin Clin Nutr Metab Care*. 2010;13(6):729–736. 4
- [14] Abraham NG, Brunner EJ, Eriksson JW, Robertson RP. Metabolic syndrome: psychosocial, neuroendocrine, and classical risk factors in type 2 diabetes. *Ann N Y Acad Sci*. 2007;1113:256–75. 4, 16, 17
- [15] Andrews RC, Walker BR. Glucocorticoids and insulin resistance: old hormones, new targets. *Clin Sci*. 1999;96:513–523. 4, 15, 61
- [16] Mottillo S, Filion KB, Genest J, Joseph L, Pilote L, Poirier P, et al. The Metabolic Syndrome and Cardiovascular Risk. *J Am Coll Cardiol*. 2010;56(14):1113–1132. 4
- [17] Meerwaldt R, Links T, Zeebregts C, Tio R, Hillebrands JL, Smit A. The clinical relevance of assessing advanced glycation endproducts accumulation in diabetes. *Cardiovasc Diabetol*. 2008;7(29). 4
- [18] Whaley-Connell A, Johnson MS, Sowers JR. Aldosterone: role in the cardiometabolic syndrome and resistant hypertension. *Prog Cardiovasc Dis*. 2010;52(5):401–409. 4, 21
- [19] Brownlee M. Banting lecture 2004: The Pathobiology of Diabetic Complications: A Unifying Mechanism. *Diabetes*. 2005;54:1615–1625. 4, 19, 20, 23, 24, 26, 27, 30
- [20] Sharma S, Adrogué JV, Golfman L, Uray I, Lemm J, Youker K, et al. Intramyocardial lipid accumulation in the failing human heart resembles the lipotoxic rat heart. *FASEB J*. 2004;18(14):1692–1700. 4, 5, 12
- [21] Randle PJ. The glucose fatty-acid cycle: Its role in insulin sensitivity and the metabolic disturbances of diabetes mellitus. *Lancet*. 1963;1:785–789. 5, 10, 11

- [22] Randle PJ. Regulatory interactions between lipids and carbohydrates: the glucose fatty acid cycle after 35 years. *Diabetes Metab Rev.* 1998;14(4):263–283. 5
- [23] Qi D, Rodrigues B. Glucocorticoids produce whole body insulin resistance with changes in cardiac metabolism. *Am J Physiol Endocrinol Metab.* 2007;292(3):E654–E667. 5, 17, 18
- [24] Taegtmeyer H. *Energy metabolism of the heart: from basic concepts to clinical applications.* Mosby; 1994. 5
- [25] Taegtmeyer H, Stanley WC. Too much or not enough of a good thing? Cardiac glucolipotoxicity versus lipoprotection. *J Mol Cell Cardiol.* 2011;50(1):2–5. 5, 11, 20, 22
- [26] Morino K, Petersen KF, Shulman GI. Molecular Mechanisms of Insulin Resistance in Humans and Their Potential Links With Mitochondrial Dysfunction. *Diabetes.* 2006;55(Supplement 2):S9–S15. 6
- [27] Whiteman EL, Cho H, Birnbaum MJ. Role of Akt/protein kinase B in metabolism. *Trends Endocrinol Metab.* 2002;13(10):444–451. 6, 7
- [28] Shuralyova I, Tajmir P, Bilan PJ, Sweeney G, Coe IR. Inhibition of glucose uptake in murine cardiomyocyte cell line HL-1 by cardioprotective drugs dilazep and dipyridamole. *Am J Physiol Heart Circ Physiol.* 2003;286(2):H627–H632. 6, 34, 65
- [29] Fischer Y, Thomas J, Muñoz P, Sevilla L, Becker C, Holman G, et al. Insulin-induced Recruitment of Glucose Transporter 4 ( GLUT4 ) and GLUT1 in Isolated Rat Cardiac Myocytes. *J Biol Chem.* 1997;272(11):7085–7092. 6, 7
- [30] Becker C, Sevilla L, Tomàs E, Palacin M, Zorzano A, Fischer Y. The endosomal compartment is an insulin-sensitive recruitment site for GLUT4 and GLUT1 glucose transporters in cardiac myocytes. *Endocrinology.* 2001;142(12):5267–5276. 7
- [31] Lund S, Holman GD, Schmitz O, Pedersen O. Contraction stimulates translocation of glucose transporter GLUT4 in skeletal muscle through a mechanism distinct from that of insulin. *Proc Natl Acad Sci USA.* 1995;92:5817–5821. 7
- [32] Puthanveetil P, Wang F, Kewalramani G, Kim MS, Hosseini-beheshti E, Ng N, et al. Cardiac glycogen accumulation after dexamethasone is regulated by AMPK. *Am J Physiol Heart Circ Physiol.* 2008;295:H1753–H1762. 7, 18

- [33] McGarry JD. Banting lecture 2001: Dysregulation of fatty acid metabolism in the etiology of type 2 diabetes. *Diabetes*. 2002;51(1):7–18. 7
- [34] Unger R. Lipid overload and overflow: metabolic trauma and the metabolic syndrome. *Trends Endocrinol Metab*. 2003;14(9):398–403. 7, 8, 9, 12
- [35] Holland WL, Knotts TA, Chavez JA, Wang Lp, Hoehn KL, Summers SA. Lipid Mediators of Insulin Resistance. *Nutr Rev*. 2007;65(6):39–46. 9, 65
- [36] Grundy SM. Obesity, metabolic syndrome, and cardiovascular disease. *J Clin Endocrinol Metab*. 2004;89(6):2595–2600. 10
- [37] Sjöstrand M, Eriksson JW. Neuroendocrine mechanisms in insulin resistance. *Mol Cell Endocrinol*. 2009;297(1-2):104–111. 10, 15, 20, 21
- [38] Shulman GI. Cellular mechanisms of insulin resistance. *J Clin Invest*. 2000;106(2):171–176. 10, 11
- [39] Savage DB, Petersen KF, Shulman GI. Disordered lipid metabolism and the pathogenesis of insulin resistance. *Physiol Rev*. 2007;87(2):507–520. 10
- [40] Lewis GF, Carpentier A, Adeli K, Giacca A. Disordered fat storage and mobilization in the pathogenesis of insulin resistance and type 2 diabetes. *Endocr Rev*. 2002;23(2):201–29. 12
- [41] Veldman RG. Hyperleptinemia in women with Cushing's disease is driven by high-amplitude pulsatile, but orderly and eurhythmic, leptin secretion. *Eur J Endocrinol*. 2001;144:21–27. 12
- [42] Bhattacharya S, Dey D, Roy SS. Molecular mechanism of insulin resistance. *J Biosci*. 2007;32(2):405–413. 12
- [43] Zachara NE, Hart GW. Cell signaling, the essential role of O-GlcNAc! *Biochim Biophys Acta*. 2006;1761(5-6):599–617. 13
- [44] Love DC, Hanover JA. The hexosamine signaling pathway: deciphering the "O-GlcNAc code". *Sci STKE*. 2005;312. 13, 27
- [45] Butkinaree C, Park K, Hart GW. O-linked beta-N-acetylglucosamine (O-GlcNAc): Extensive crosstalk with phosphorylation to regulate signaling and transcription in response to nutrients and stress. *Biochim Biophys Acta*. 2010;1800(2):96–106. 13, 27

- [46] Zachara NE, Hart GW, Cole RN, Gao Y. Detection and analysis of proteins modified by O-linked N-acetylglucosamine. Ausubel FM, editor; 2002. Chapter 17. 13
- [47] Lefebvre T, Dehennaut V, Guinez C, Olivier S, Drougat L, Mir AM, et al. Dysregulation of the nutrient/stress sensor O-GlcNAcylation is involved in the etiology of cardiovascular disorders, type-2 diabetes and Alzheimer's disease. *Biochim Biophys Acta*. 2010;1800(2):67–79. 13
- [48] Sherwood L. *Human Physiology: From Cells to Systems*. 5th ed. Julet M, editor. Belmont, CA: Brooks/Cole; 2004. 14
- [49] Busciglio J, Andersen JK, Schipper HM, Gilad GM, McCarty R, Marzatico F, et al. Stress, aging, and neurodegenerative disorders. Molecular mechanisms. *Ann N Y Acad Sci*. 1998;851:429–443. 15, 21
- [50] Ray JA, Kushnir MM, Rockwood AL, Meikle AW. Analysis of cortisol, cortisone and dexamethasone in human serum using liquid chromatography tandem mass spectrometry and assessment of cortisol: cortisone ratios in patients with impaired kidney function. *Clin Chim Acta*. 2011;412(13-14):1221–1228. 15
- [51] Levine A, Zagoory-Sharon O, Feldman R, Lewis JG, Weller A. Measuring cortisol in human psychobiological studies. *Physiol Behav*. 2007;90:43–53. 15
- [52] Girod JP, Brotman DJ. Does altered glucocorticoid homeostasis increase cardiovascular risk? *Cardiovasc Res*. 2004;64(2):217–226. 16, 18, 21
- [53] Miller GE, Chen E, Zhou ES. If it goes up, must it come down? Chronic stress and the hypothalamic-pituitary-adrenocortical axis in humans. *Psychol Bull*. 2007;133(1):25–45. 16
- [54] Toussaint O, Fuchs SY, Ronai ZA, Isoyama S, Yuko N, Petronilli V, et al. Reciprocal Relationships between the Resistance to Stresses and Cellular Aging. *Ann N Y Acad Sci*. 1998;851:450–465. 16
- [55] Radahmadi M, Shadan F, Karimian SM, Sadr SSED, Nasimi A. Effects of stress on exacerbation of diabetes mellitus, serum glucose and cortisol levels and body weight in rats. *Pathophysiology*. 2006;13(1):51–55. 17
- [56] Szkudelski T. The Mechanism of Alloxan and Streptozotocin Action in B Cells of the Rat Pancreas. *Physiol Res*. 2001;50:536–546. 17

- [57] Whitworth JA, Williamson PM, Mangos G, Kelly JJ. Cardiovascular consequences of cortisol excess. *Vasc Health Risk Manag.* 2005;1(4):291–299. 17
- [58] Lumbers ER, Boyce AC, Joulianos G, Kumarasamy V, Barner E, Segar JL, et al. Effects of cortisol on cardiac myocytes and on expression of cardiac genes in fetal sheep. *Am J Physiol Regul Integr Comp Physiol.* 2005;288(3):R567–R574. 17
- [59] Kewalramani G, Puthanveetil P, Kim MS, Wang F, Lee V, Hau N, et al. Acute dexamethasone-induced increase in cardiac lipoprotein lipase requires activation of both Akt and stress kinases. *Pharmacology.* 2008;3:137–147. 18
- [60] Dimitriadis G, Leighton B, Parry-Billings M, Sasson S, Young M, Krause U, et al. Effects of glucocorticoid excess on the sensitivity of glucose transport and metabolism to insulin in rat skeletal muscle. *Biochem J.* 1997;321:707–712. 18, 65
- [61] Sakoda H, Ogihara T, Anai M, Funaki M. Dexamethasone-induced insulin resistance in 3T3-L1 adipocytes is due to inhibition of glucose transport rather than insulin signal transduction. *Diabetes.* 2000;49(10):1700–1708. 18
- [62] Giorgino F, Almahfouz A, Goodyear LJ, Smith RJ. Glucocorticoid Regulation of Insulin Receptor and Substrate IRS-1 Tyrosine Phosphorylation in Rat Skeletal Muscle In Vivo. *J Clin Invest.* 1993;91:2020–2030. 18
- [63] Bazuine M, Carlotti F, Tafrechi R, Hoeben R, Maassen J. Mitogen-activated protein kinase (MAPK) phosphatase-1 and -4 attenuate p38 MAPK during dexamethasone-induced insulin resistance in 3T3-L1 adipocytes. *Mol Endocrinol.* 2004;18:1697–1707. 18
- [64] Piroli GG, Grillo Ca, Reznikov LR, Adams S, McEwen BS, Charron MJ, et al. Corticosterone impairs insulin-stimulated translocation of GLUT4 in the rat hippocampus. *Neuroendocrinology.* 2007;85(2):71–80. 18, 65
- [65] Henriksen EJ, Diamond-Stanic MK, Marchionne EM. Oxidative stress and the etiology of insulin resistance and type 2 diabetes. *Free Radic Biol Med.* 2011;51(5):993–999. 19, 21, 22, 23
- [66] Simon HU, Haj-Yehia A, Levi-Schaffer A. Role of reactive oxygen species (ROS) in apoptosis induction. *Apoptosis.* 2000;(5):415–418. 19
- [67] Rojas A, Mercadal E, Figueroa H, Morales MA. Advanced Glycation and ROS: A Link between Diabetes and Heart Failure. *Curr Vasc Pharmacol.* 2008;6(1):44–51. 19

- [68] Burton GJ, Jauniaux E. Oxidative stress. *Best Pract Res Clin Obstet Gynaecol.* 2011;25(3):287–299. 19
- [69] Rajamani U. Hyperglycemia-induced activation of the Hexosamine Biosynthetic Pathway causes Myocardial Cell Death. Stellenbosch University; 2009. 21, 22, 28, 34
- [70] Baynes JW, Thorpe SR. Perspectives in Diabetes. *Diabetes.* 1999;48:1–10. 21
- [71] Evans JL, Goldfine ID, Maddux BA, Grodsky GM. Are Oxidative Stress-Activated Signaling Pathways Mediators of Insulin Resistance and  $\beta$ -Cell Dysfunction? *Diabetes.* 2003;52:1–8. 21, 22
- [72] Sugamura K, Keaney JF. Free Radical Biology & Medicine Reactive oxygen species in cardiovascular disease. *Free Radic Biol Med.* 2011;51(5):978–992. 21, 23
- [73] Karnieli E, Armoni M. Transcriptional regulation of the insulin-responsive glucose transporter GLUT4 gene: from physiology to pathology. *Am J Physiol Endocrinol Metab.* 2008;295(1):E38–E45. 21, 29
- [74] Giacco F, Brownlee M. Oxidative stress and diabetic complications. *Circ Res.* 2010;107(9):1058–1070. 22, 24, 26, 27, 30
- [75] Brownlee M. Biochemistry and molecular cell biology of diabetic complications. *Nature.* 2001;414(6865):813–820. 22, 26, 30
- [76] Cai L, Li W, Wang G, Guo L, Jiang Y, Kang YJ. Hyperglycemia-Induced Apoptosis in Mouse Myocardium. *Diabetes.* 2002;51:1938–1948. 22
- [77] Rajamani U, Essop MF. Hyperglycemia-mediated activation of the hexosamine biosynthetic pathway results in myocardial apoptosis. *Am J Physiol Cell Physiol.* 2010;299(1):C139–C147. 22, 27
- [78] Du XL, Edelstein D, Rossetti L, Fantus IG, Goldberg H, Ziyadeh F, et al. Hyperglycemia-induced mitochondrial superoxide overproduction activates the hexosamine pathway and induces plasminogen activator inhibitor-1 expression by increasing Sp1 glycosylation. *Proc Natl Acad Sci USA.* 2000;97(22):12222–12226. 22, 27
- [79] Bravard A, Bonnard C, Durand A, Chauvin MA, Favier R, Vidal H, et al. Inhibition of xanthine oxidase reduces hyperglycemia-induced oxidative stress and improves mitochondrial alterations in skeletal muscle of diabetic mice. *Am J Physiol Endocrinol Metab.* 2011 Mar;300(3):E581–E591. 23

- [80] Du X, Edelstein D, Brownlee M. Oral benfotiamine plus alpha-lipoic acid normalises complication-causing pathways in type 1 diabetes. *Diabetologia*. 2008;51(10):1930–1932. 24
- [81] Rolo AP, Palmeira CM. Diabetes and mitochondrial function: role of hyperglycemia and oxidative stress. *Toxicol Appl Pharmacol*. 2006;212(2):167–178. 24, 25
- [82] King GL, Brownlee M. The cellular and molecular mechanisms of diabetic complications. *Endocrinol Metab Clin North Am*. 1996;25(2):255–270. 24
- [83] Gabbay K, Merola L, Field R. Sorbitol pathway: presence in nerve and cord with substrate accumulation in diabetes. *Science*. 1966;151:209–210. 24
- [84] Du X, Matsumura T, Edelstein D, Rossetti L, Zsengellér Z, Szabó C, et al. Inhibition of GAPDH activity by poly(ADP-ribose) polymerase activates three major pathways of hyperglycemic damage in endothelial cells. *J Clin Invest*. 2003;112(7):1049–1057. 26, 30
- [85] Sugimoto K, Yasujima M, Yagihashi S. Role of advanced glycation end products in diabetic neuropathy. *Curr Pharm Des*. 2008;14(10):953–961. 26
- [86] Coughlan MT, Thorburn DR, Penfold Sa, Laskowski A, Harcourt BE, Sourris KC, et al. RAGE-induced cytosolic ROS promote mitochondrial superoxide generation in diabetes. *J Am Soc Nephrol*. 2009;20(4):742–752. 26
- [87] Rosca MG, Mustata TG, Kinter MT, Ozdemir AM, Kern TS, Szweda LI, et al. Glycation of mitochondrial proteins from diabetic rat kidney is associated with excess superoxide formation. *Am J Physiol Renal Physiol*. 2005;289:420–430. 26
- [88] Winkler G, Kempler P. Pathomechanism of diabetic neuropathy: background of the pathogenesis-oriented therapy. *Orv Hetil*. 2010;151(24):971–981. 26
- [89] Torres CR, Hart GW. Topography and Polypeptide Distribution of Terminal N-Acetylglucosamine Residues on the Surfaces of Intact Lymphocytes. *J Biol Chem*. 1984;259(5):3308–3317. 26
- [90] Marshall S, Bacote V, Traxinger RR. Discovery of a metabolic pathway mediating glucose-induced desensitization of the glucose transport system. Role of hexosamine biosynthesis in the induction of insulin resistance. *J Biol Chem*. 1991;266(8):4706–4712. 26, 27

- [91] Hart GW, Housley MP, Slawson C. Cycling of O-linked beta-N-acetylglucosamine on nucleocytoplasmic proteins. *Nature*. 2007;446(7139):1017–1022. 27, 29, 31
- [92] Hart GW, Slawson C, Ramirez-Correa G, Lagerlof O. Cross talk between O-GlcNAcylation and phosphorylation: roles in signaling, transcription, and chronic disease. *Annu Rev Biochem*. 2011;80:825–858. 27, 29, 30
- [93] Schimpl M, Schüttelkopf AW, Borodkin VS, van Aalten DMF. Human OGA binds substrates in a conserved peptide recognition groove. *Biochem J*. 2010;432:1–7. 27, 28
- [94] Buse MG, Larter NC, Forbes LB, Elkin BT, Allaire DG, Rosenblatt JE, et al. Hexosamines, insulin resistance, and the complications of diabetes: current status. *Am J Physiol Cell Physiol*. 2006;290:E1–E8. 27
- [95] Chatham JC, Marchase RB. The role of protein O-linked  $\beta$ -N-acetylglucosamine in mediating cardiac stress responses. *Biochim Biophys Acta*. 2010;1800(2):57–66. 27, 29, 31
- [96] Du X, Edelstein D, Obici S, Higham N, Zou MH, Brownlee M. Insulin resistance reduces arterial prostacyclin synthase and eNOS activities by increasing endothelial fatty acid oxidation. *J Clin Invest*. 2006;116(4):1071–1080. 27
- [97] Vosseller K, Wells L, Lane MD, Hart GW. Elevated nucleocytoplasmic glycosylation by O-GlcNAc results in insulin resistance associated with defects in Akt activation in 3T3-L1 adipocytes. *Proc Natl Acad Sci USA*. 2002;99(8):5313–5318. 28, 65
- [98] Fülöp N, Marchase RB, Chatham JC. Role of protein O-linked N-acetyl-glucosamine in mediating cell function and survival in the cardiovascular system. *Cardiovasc Res*. 2007;73(2):288–297. 28
- [99] Luo B, Parker GJ, Cooksey RC, Soesanto Y, Evans M, Jones D, et al. Chronic Hexosamine Flux Stimulates Fatty Acid Oxidation by Activating AMP-activated Protein Kinase in Adipocytes. *J Biol Chem*. 2007;282(10):7172–7180. 28
- [100] Love DC, Kochan JP, Cathey RL, Shin SH, Hanover JA. Mitochondrial and nucleocytoplasmic targeting of O-linked GlcNAc transferase. *J Cell Sci*. 2003;116:647–654. 28
- [101] Hu Y, Suarez J, Fricovsky E, Wang H, Scott BT, Trauger SA, et al. Increased Enzymatic O-GlcNAcylation of Mitochondrial Proteins Impairs Mitochondrial Function in Cardiac Myocytes Exposed to High Glucose. *J Biol Chem*. 2009;284(1):547–555. 29, 64

- [102] Williams G. Increased Hexosamine Biosynthetic Pathway Flux Impairs Myocardial GLUT4 Translocation. Stellenbosch University; 2009. 29
- [103] Federici M. Insulin-Dependent Activation of Endothelial Nitric Oxide Synthase Is Impaired by O-Linked Glycosylation Modification of Signaling Proteins in Human Coronary Endothelial Cells. *Circulation*. 2002;106(4):466–472. 29
- [104] Hebert LF, Daniels MC, Zhou J, Crook ED, Turner RL, Simmons ST, et al. Overexpression of glutamine:fructose-6-phosphate amidotransferase in transgenic mice leads to insulin resistance. *J Clin Invest*. 1996;98(4):930–936. 29
- [105] Liu J, Marchase RB, Chatham JC. Increased O-GlcNAc levels during reperfusion lead to improved functional recovery and reduced calpain proteolysis. *Am J Physiol Heart Circ Physiol*. 2007;293(3):H1391–H1399. 29
- [106] Zachara NE. The sweet nature of cardioprotection. *Am J Physiol Heart Circ Physiol*. 2007;293(3):H1324–H1326. 29
- [107] Hu P, Shimoji S, Hart GW. Site-specific interplay between O-GlcNAcylation and phosphorylation in cellular regulation. *FEBS letters*. 2010;584(12):2526–38. 30
- [108] Soriano FG, Virág L, Jagtap P, Szabó E, Mabley JG, Liaudet L, et al. Diabetic endothelial dysfunction: the role of poly(ADP-ribose) polymerase activation. *Nat Med*. 2001;7(1):108–113. 30
- [109] Zachara NE, O'Donnell N, Cheung WD, Mercer JJ, Marth JD, Hart GW. Dynamic O-GlcNAc modification of nucleocytoplasmic proteins in response to stress. A survival response of mammalian cells. *The Journal of biological chemistry*. 2004;279(29):30133–30142. 31
- [110] Claycomb WC, Lanson NA, Stallworth BS, Egeland DB, Delcarpio JB, Bahinski A, et al. HL-1 cells: A cardiac muscle cell line that contracts and retains phenotypic characteristics of the adult cardiomyocyte. *Proc Natl Acad Sci USA*. 1998;95:2979–2984. 32, 48, 63
- [111] White SM, Constantin PE, Claycomb WC. Cardiac physiology at the cellular level: use of cultured HL-1 cardiomyocytes for studies of cardiac muscle cell structure and function. *Am J Physiol Heart Circ Physiol*. 2004;286:H823–H829. 32, 65, 82
- [112] Dittmer A, Dittmer J. Beta-actin is not a reliable loading control in Western blot analysis. *Electrophoresis*. 2006;14(27):2844–2845. 42

- [113] Welsh GI, Leney SE, Lloyd-lewis B, Wherlock M, Lindsay AJ, Mccaffrey MW, et al. Rip11 is a Rab11- and AS160-RabGAP-binding protein required for insulin-stimulated glucose uptake in adipocytes. *J Cell Sci.* 2007;120(3):4197–4208. 43, 66
- [114] Barbera M, Fierabracci V, Novelli M, Bombara M, Masiello P, Bergamini E. Dexamethasone-induced insulin resistance and pancreatic adaptive response in aging rats are not modified by oral vanadyl sulfate treatment. *Eur J Endocrinol.* 2001;145:799–806. 61
- [115] Tanaka Y, Konno N, Kako K. Mitochondrial dysfunction observed in situ in cardiomyocytes of rats in experimental diabetes. *Cardiovasc Res.* 1992;26(4):409–414. 64
- [116] Weinstein SP, Wilson CM, Pritsker A, Cushman SW. Surface in Rat Skeletal Muscle. *J Biol Chem.* 1998;47(1):3–6. 65
- [117] Weinstein SP, Paquin T, Pritsker A, Haber RS. Glucocorticoid-induced insulin resistance: dexamethasone inhibits the activation of glucose transport in rat skeletal muscle by both insulin- and non-insulin-related stimuli. *Diabetes.* 1995;44.4:441. 65
- [118] Lundgren M, Burén J, Ruge T, Myrnäs T, Eriksson JW. Glucocorticoids down-regulate glucose uptake capacity and insulin-signaling proteins in omental but not subcutaneous human adipocytes. *J Clin Endocrinol Metab.* 2004;89(6):2989–97. 65
- [119] Zeigerer A, Mcbrayer MK, Mcgraw TE. Insulin Stimulation of GLUT4 Exocytosis, But Not Its Inhibition of Endocytosis, Is Dependent on RabGAP AS160. *Mol Biol Cell.* 2004;15:4406–4415. 65
- [120] Guilherme A, Emoto M, Buxton JM, Bose S, Sabini R, Theurkauf WE, et al. Perinuclear localization and insulin responsiveness of GLUT4 requires cytoskeletal integrity in 3T3-L1 adipocytes. *J Biol Chem.* 2000;275(49):38151–38159. 66
- [121] Harlow E. Labeling Antibodies with Biotin. *Cold Spring Harbor Protocols.* 2006;18:4286. 68

# Appendices

# Appendix A

## Cell Culture: Growth and care of HL-1 cardiomyocytes

This appendix is adapted from the ‘Growth and care of HL-cardiomyocytes’ document by the Claycomb Lab. Establishing the cell line within the Cardio-Metabolic Research Group is discussed in Section 2.1.1.

### A.1 Supplemented Claycomb Medium

- Claycomb Medium (51800C, Sigma-Aldrich, Steinheim, Germany), [Table A.1] is extremely light sensitive so take care to wrap the containers (bottles and tubes) in foil.
- Make up small volumes of fresh supplemented Claycomb regularly - salt crystals start to precipitate out of solution if the medium gets old.
- L-glutamine should be replenished after two weeks.
- Table A.2 shows what amounts of Claycomb medium, fetal bovine serum (filter-sterilised), penicillin-streptomycin (optional), norepinephrine and L-glutamine are required to make up 100 ml of supplemented Claycomb Medium.

#### A.1.1 Norepinephrine [(±) arterenol], MW 319.3 g mol<sup>-1</sup>

- Norepinephrine (10 mM stock) is made up in 30 mM ascorbic acid.

Product	Final concentration
Total protein	261 mg/l
Bovine albumin	48.85 mg/l
Nonessential amino acids	0.1 mM
Fetuin	165 mg/l
Transferrin	31.8 mg/l
Retinoic acid	300 µg/l
Human insulin (recombinant)	15 µg/l
Long R <sup>3</sup> IGF-1 (recombinant)	0.1 µg/l
Long EGF-1 (recombinant)	0.1 µg/l
Cholestrol	1.96 mg/l
Linoleic acid	0.78 mg/l
γ-Oleyl-β-pal-α-phosphatidylcholine	1.96 mg/l

**Table A.1:** Formulation of Claycomb Medium [111]

Product	Volume	Final concentration
Claycomb medium	87 ml	
Fetal bovine serum	10 ml	10%
Penicillin/Streptomycin	1 ml	100 U/ml:100 µg/ml
Norepinephrine (10 mM stock) made up in Ascorbic acid	1 ml	0.1 mM 0.3 mM
L-Glutamine (200 mM stock)	1 ml	2 mM

**Table A.2:** Supplemented Claycomb medium

- Add 0.59 g ascorbic acid (Sigma-Aldrich, Steinheim, Germany) to 100 ml of cell culture grade distilled water. This makes a 30 mM ascorbic acid solution.
- To 25 ml of the 30 mM ascorbic acid solution, add 80 mg of norepinephrine.
- Filter-sterilise using a 0.2 µm Acrodisc syringe filter (FLAS25AC2050, Lasec, South Africa).
- Aliquot into sterile, screw-cap microtubes in 1 ml volumes and store at -20°C.
- From this 10 mM stock norepinephrine, 1 ml in 100 ml medium will yield a final concentration of 0.1 mM.
- Make up fresh on a monthly basis.

### A.1.2 L-Glutamine

- L-Glutamine comes as a 100× solution (200 mM).
- Aliquot into working volumes and store at -20°C.

## A.2 Wash Medium

Claycomb medium to be used as wash medium during passaging [Appendix A.6] had the following products added:

- 5% fetal bovine serum (12103C, Batch 8A0177, SAFC Biosciences, Lenaxa, KS)
- 1% (or 100 U/ml:100 µg/ml) penicillin-streptomycin (P4333, Sigma-Aldrich)

## A.3 Freezing Medium

The solution cells are frozen in [see Appendix A.7 for *Freezing cells*] contains dimethyl sulphoxide (DMSO) which is a weakly acidic, polar aprotic solvent that serves a cryoprotectant function. It prevents freezing damage that may result due to ice formation. Although DMSO is less toxic than other members of its class, it is best not to expose cells to this solvent at room temperature for prolonged periods of time. [See also Appendix A.8, *Thawing cells*].

- Freezing medium is made up of 95% FBS/5% DMSO.
- This can be stored up to a week at 4°C.

## A.4 Pre-coating flasks: Gelatin/Fibronectin

### A.4.1 Preparing Gelatin/Fibronectin

- Weigh 0.1 g gelatin (G9391, Sigma-Aldrich, Steinheim, Germany) into a 500 ml glass bottle. Note that the gelatin tends to stick to any surface it makes contact with so try getting it directly into the glass beaker/bottle without touching the sides. Avoid using weighing boats or funnels.
- Add distilled water to the 500 ml mark, and autoclave. The gelatin will go into solution while being autoclaved.

- This makes a 0.02% gelatin solution.
- Dilute 1 ml fibronectin (F-1141, Sigma-Aldrich, Steinheim, Germany) in 199 ml of the 0.02% gelatin solution and mix gently.
- Immediately aliquot 6-12 ml volumes into 15 ml conical (centrifuge) tubes.
- Freeze aliquots at -20°C.

#### A.4.2 Coating flasks

- Before culturing cells, coat tissue culture flasks with gelatin/fibronectin (G/F) using 1-2 ml per T25 and 3-4 ml per T75 flask.
- Cap the flasks, and incubate for at least an hour at 37°C.
- Remove the gelatin/fibronectin by aspiration adding cells to the flasks.

### A.5 Culturing cells

- Cultures are fed with supplemented Claycomb Medium [Appendix A.1] every weekday (per T25; 3-5 ml daily)
- More medium can be added on Fridays to avoid feeding cells on weekends. 10 ml of supplemented Claycomb Medium added to a T25 on a Friday afternoon does not need to be changed until the following Monday morning.
- Passaging is the procedure for splitting cells. Depending on the growth rate, cells can either be split 1:2 or 1:3, twice a week, for example, on Mondays and Fridays.
- It is recommended to maintain two sets of cells; a ‘working’ set and one for freezing away cells in order to keep backup stocks [see *Passaging*, Appendix A.6].

### A.6 Passaging

After the cells are first received, it is recommended that they be split when they reach confluency. Keep some cells as a ‘working’ set, and to freeze away four flasks into four cryovials for future use [described in Section 2.1.1]. This can be achieved within a week of receiving the HL-1 cells.

- It is recommended that cultures only be split once full confluence is reached.
- Warm PBS, trypsin/EDTA, wash medium [Appendix A.2], and a small volume of supplemented Claycomb medium [Appendix A.1] to 37°C.
- In the meantime, remove the gelatin/fibronectin solution from the flask(s), and add 2-4 ml supplemented Claycomb medium to each T25. Place in the incubator to warm medium to 37°C.
- Rinse each T25 flask (containing the HL-1 cardiomyocytes) briefly with 2 ml (4 ml per T75) of warm PBS.
- Pipette the PBS, and later the trypsin, onto the bottom of the flask (side opposite the cap) so as not to hit the cells directly.
- Rinse gently and remove by aspiration.
- Add 1 ml of 0.05% trypsin/EDTA per T25 flask (3 ml per T75).
- Incubate for 1 minute at 37°C.
- Aspirate and add fresh 0.05% trypsin/EDTA (same volume).
- Incubate for an additional 2 minutes.
- Examine microscopically to see if cells are still adhered. If so, rap the flask on the benchtop to dislodge the remaining cells.
- Add an equal amount (1 ml per T25) of soybean trypsin inhibitor [Appendix A.6.1] directly onto cells to inactivate the digesting enzyme.
- Transfer cells from the flask into a 15 ml centrifuge tube.
- Use 5 ml wash medium to rinse the flask and add to cells already in the 15 ml tube.
- Centrifuge at  $500 \times g$  for 5 minutes.
- Meanwhile, retrieve the T25 flasks with fresh, supplemented Claycomb Medium from the incubator.
- Remove the tube containing the pelleted cells from the centrifuge and remove the supernatant by aspiration.

- Gently resuspend the pellet in 3 ml of supplemented Claycomb Medium.
- Transfer 1 ml of the cell suspension into each of the three labeled, gelatin/fibronectin-coated T25 flasks.
- Each flask now contains 5 ml of medium.
- If the cells are passaged on a Friday, use twice the volume of supplemented Claycomb Medium per flask.

### A.6.1 Soybean Trypsin Inhibitor

Used to inactivate trypsin during passaging [Appendix A.6].

- In a beaker dissolve 25 mg of soybean trypsin inhibitor in 100 ml Dulbecco's phosphate-buffered saline (PBS; Ca<sup>2+</sup>-free and Mg<sup>2+</sup>-free).
- Filter-sterilise into a 100 ml bottle using a 0.2 µm syringe filter.
- This is good for a month at -20°C.

## A.7 Freezing cells

If new cells are received (or if stocks are low) it is recommended that 4 or more vials are frozen as soon as possible after receipt of the cells [please see note under *Passaging* A.6, and *Cell stocks* 2.1.1]. Freezing away stocks of cells allows you to return to earlier passages, and protects you in case of contamination.

The content of one confluent T75 flask is usually frozen in one cryovial. When cells are needed the cryovial is thawed [see *Thawing cells* A.8] into one T75 flask. Alternatively, the contents of one confluent T75 flask can be split 1:2 (into two vials), and each vial can be thawed into one T25.

- Briefly rinse the T75 flask containing the HL-1 culture with 4 ml PBS warmed to 37°C.
- Remove PBS by aspiration.
- Add 3 ml of 0.05% trypsin/EDTA into the flask and incubate for 1 minutes at 37°C.
- Remove the trypsin/EDTA and replace with 3 ml fresh 0.05% trypsin/EDTA.

- Incubate for 2 minutes at 37°C.
- Examine under a microscope to check that cells are dislodged. If not, rap the flask on the benchtop to loosen adherent cells.
- Inactivate the trypsin enzyme with an equal amount (3 ml) of soybean trypsin inhibitor [see Appendix A.6.1].
- Transfer the 6 ml into a 15 ml centrifuge tube.
- Rinse each empty flask with 5 ml wash medium and transfer this to the 6 ml already in the centrifuge tube.
- Centrifuge tube for 5 minutes at  $500\times g$ .
- Remove the wash medium by aspiration.
- Gently resuspend each pellet in 1.5 ml of freezing medium (95% FBS/5% DMSO) [Appendix A.3].
- Pipette resuspended cells into a cryovial.
- Place the cryovial containing the cells into a freezing jar (5100, Cryo 1°C Freezing Container, “Mr. Frosty”, Nalgene Labware, Thermo Fisher Scientific, Rochester, NY) half-filled with room temperature isopropanol.
- Immediately place the freezing jar into a -80°C freezer. This will allow cells to freeze at a rate of -1°C/minute. Six to twelve hours later, transfer the vial(s) to a liquid nitrogen dewar.

## A.8 Thawing cells

- Gelatin/fibronectin (G/F)-coat [Appendix A.4] a tissue culture flask in an incubator at 37°C.
- After at least an hour, aspirate the G/F from the culture flask and replace with supplemented Claycomb Medium (5 ml per T25, 10 ml per T75).
- Place this flask back into the incubator.

- Transfer 10 ml of wash medium into an empty 15 ml centrifuge tube and warm in a water bath to 37°C.
- Thaw cells quickly (about 2 minutes) by placing the cryovial in the water bath (37°C). Work quickly to prevent damage to cells and reduce toxic effects of DMSO [Appendix A.3].
- Transfer to the 15 ml tube containing the wash medium and centrifuge for 5 minutes at  $500 \times g$ .
- Remove the tube from the centrifuge and aspirate the supernatant.
- Resuspend the pellet gently in 5 ml (3 ml in a T25) supplemented Claycomb Medium and add to the 10 ml medium already in the T75 flask.
- Since the HL-1 cells need to be seeded at a high confluency from the start to grow with ease, and it was observed that cells may have a low viability after thawing, it may be safer to start off in a T25.
- Replace the medium with 10-15 ml (4-8 ml per T25) fresh supplemented Claycomb Medium 4 hours later, once the cells have attached.

# Appendix B

## Staining protocol

Refer to Chapter [2.2].

### B.1 Staining protocol prior to flow cytometry and microscopy

The staining protocol is very similar for a variety of procedures. See flow cytometry [Section 2.2.1], immunofluorescence microscopy [Section 2.4.2], as well as confocal microscopy [Section 2.4.3]. Below is the basic protocol that can be adapted or optimised as needed. Remember to work in the dark, and wrap samples (flow cytometry tubes or microscopy slides) in foil, as the fluorochromes are light sensitive.

- Aspirate medium and rinse with ice cold, sterile PBS.
- Permeabilise cells with 200  $\mu$ l ice cold methanol-acetone (1:1), or fix cells with cold 2% paraformaldehyde.
- Incubate on ice (4°C) for 10 minutes.
- Remove fixative and leave to airdry for 10 minutes.
- In the meantime prepare 5% donkey serum in PBS (100  $\mu$ l per well)
- Rinse cells with cold PBS three times.
- The flow cytometry protocol would require centrifugation for washing steps [Appendix C.1 contains an important note regarding this].

- After washing add 100  $\mu$ l of the 5% donkey serum and incubate for 20 minutes.
- Drain the serum but do not wash the cells.
- Incubate with 100  $\mu$ l primary antibody dilution, e.g. 1:50 or 1:200 in PBS or donkey serum (remembering that the staining control does not get any primary antibody) for at least 90 minutes, or overnight for convenience.
- Remove the primary antibody and wash three times with PBS.
- Add 100  $\mu$ l secondary antibody dilution (1:200 with PBS or donkey serum, but be consistent). Briefly centrifuge the secondary antibody dilution to remove any crystals. Incubate for 30 minutes.
- Add 100  $\mu$ l Hoechst (1:1000) or other nuclear dye, and incubate for 10 minutes.
- Wash three times
- Store wrapped in foil at  $-20^{\circ}\text{C}$  for two weeks.

## Appendix C

# Experimental protocol for analysis after dexamethasone treatment

Refer to Chapter 2.2.

### C.1 Flow Cytometry

Flow cytometry as technique is discussed in Chapter 2.2.1. Preparation of samples for flow cytometry, whether fixing cells for *O*-GlcNAc staining [Section 2.2.3] or using a live stain such as H<sub>2</sub>DCFDA for ROS [Section 2.2.2], requires multiple centrifugation and washing steps. With every step the cells may be agitated and stressed, as well as cells and time being lost. To cut down on the number of washing steps the cells were not centrifuged (to remove supernatant) and washed and centrifuged again every time the protocol called for a washing step. Instead, a large volume (2 ml) of PBS was added to the cells (in suspension with the smaller volume (200  $\mu$ l) of either the methanol-acetone fixative, donkey serum, primary antibody, or secondary antibody) before pelleting. This meant that whatever supernatant could not be aspirated and was left on the pellet was greatly diluted. Cells were also spared the extra rounds of stressful centrifugation.

# Appendix D

## Western blotting

See Chapter 2.3.

### D.1 Cell harvesting

- Cells are washed with ice cold PBS.
- Add PMSF to RIPA buffer to a final concentration of 1 mM [Appendix D.1.1].
- Add ~ 350-500  $\mu$ l RIPA to each T25 flask and leave for 10 minutes.
- Use a cell scraper to lift the adhering cells from the surface of the flask.
- Transfer the cell lysates into microfuge tubes and either proceed with the protocol, or store the lysates at  $-20^{\circ}\text{C}$  for no longer than 2 weeks, or at  $-80^{\circ}\text{C}$  for longer-term storage.

#### D.1.1 Modified RIPA buffer

100 ml of modified RIPA buffer contains:

- 50 mM Tris-HCl: 790 mg of Tris (648310, Calbiochem, Merck, Darmstadt, Germany) and 900 mg of NaCl (582 23 20EM, Merck, South Africa) in 75 ml distilled water, adjusted to a pH of 7.4;
- 10 ml of 10% Nonidet P40 Substitute (74385, Fluka, Sigma-Aldrich, Steinheim, Germany);
- 2.5 ml of 10% sodium deoxycholate (918250, BDH Laboratory Chemicals, Poole, England);

- 1 ml of 100 mM ethylenediaminetetraacetic acid (EDTA, E9884, Sigma-Aldrich, Steinheim, Germany) pH 7.4;
- **Phosphatase inhibitors**
  - 500  $\mu$ l 200 mM activated sodium orthovanadate ( $\text{Na}_2\text{VO}_3$ ) (S6 508, Sigma-Aldrich, Steinheim, Germany);
  - 500  $\mu$ l 200 mM sodium fluoride (NaF);
- **Protease inhibitors**
  - 500  $\mu$ l of 200 mM phenylmethanesulfonyl fluoride (PMSF) (P 7626, Sigma-Aldrich, Schnellendorf, Germany) to be added immediately before use;
  - 100  $\mu$ l of leupeptin (L2884, Sigma-Aldrich, Schnellendorf, Germany) (from 1 mg/ml water stock);
  - 80  $\mu$ l soybean trypsin inhibitor (SBT1) (T9003, Sigma-Aldrich, Schnellendorf, Germany) (from 5 mg/ml water stock);
  - 100  $\mu$ l benzamidine (B6506, Sigma-Aldrich, Schnellendorf, Germany) (1 M stock); and
- 1 ml Triton X-100.

Since products such as sodium deoxycholate are light sensitive, and protease inhibitors have short half-lives it is preferable to work in a cold room, or keep buffer reagents on ice (except for Triton X-100), and protect from light by covering container in foil. Make up to a final volume of 100 ml with distilled water and store at  $-20^\circ\text{C}$ . The final concentrations of reagents in the buffer should be as reflected in Table D.1.

## D.2 Preparing lysates

- Cell lysates, if frozen, should be defrosted slowly, on ice and kept on ice where possible for the remainder of the protocol.
- More PMSF can be added before cell lysates are sonicated using a Misonix S-4000 minisonicator (Misonix Inc, USA).
- Sonicate lysates at an amplitude of 10, three times 5 seconds per sample interspersed with 5 second intervals (ie. 5 seconds sonication, followed by 5 seconds rest, on ice if possible, repeated twice more).

Product	Volume	Final concentration
Tris	790 mg	50 mM
NaCl	900 mg	
Distilled water	75 ml	
10% Nonidet P40 Substitute	10 ml	1%
10% Sodium deoxycholate	2.5 ml	0.25%
EDTA (100 mM) pH 7.4	1 ml	1 mM
Triton X-100	1 ml	
<b>Phosphatase inhibitors</b>		
Na <sub>2</sub> VO <sub>3</sub> (200 mM)	500 µl	1 mM
NaF (200 mM)	500 µl	1 mM
<b>Protease inhibitors</b>		
PMSF (200 mM)	500 µl	1 mM
Leupeptin (1 mg/ml water)	100 µl	1 µg/ml
SBT1 (5 mg/ml water)	80 µl	4 µg/ml
Benzamidine (1 M)	100 µl	1 mM

**Table D.1:** Modified RIPA buffer to be made up to 100 ml and stored at -20°C.

- The samples may foam due to the detergents and reagents in the RIPA buffer. Allow this to settle (about 1 hour).
- Centrifuge the lysates at  $4000\times g$  at 4°C for 10 minutes, and discard the pellets.

### D.3 Protein quantification: The Bradford method

Chapter 2.3.2 deals with the preparation of samples for Western blotting, starting with protein determination. Firstly, a protein standard with which to compare other proteins is required. This standard reference is prepared with varying, known concentrations of BSA. A 200 µg/ml BSA solution is made using distilled water and is used to prepare the standard curve as shown in Table D.2.

- As each of the prepared standards amounts to 100 µl, it is best for consistency's sake to do the same with the lysates of unknown protein concentration. Use 5 µl of every cell lysate sample, adding 95 µl of distilled water to each.
- Add 900 µl of Bradford reagent, [the working solution, Appendix D.3.1] to each of these standards and unknown (cell lysate) samples.
- Vortex gently and allow to stand for  $\sim 5$  minutes.

BSA ( $\mu\text{l}$ )	BSA concentration ( $\mu\text{g}$ )	Distilled water ( $\mu\text{l}$ )
0	0 (Blank)	100
10	2	90
20	4	80
40	8	60
60	12	40
80	16	20
100	20	0

**Table D.2:** Concentrations for standard curve.

- Read absorbances with a Cecil Aurius CE2021 spectrophotometer (Cecil Instruments Ltd, UK) at 595 nm.
- If the absorbance reading for a cell lysate sample falls outside the range of the standards, it should be diluted with RIPA buffer or water (although the detergents in the RIPA buffer may interfere) and its absorbance measured again.
- Plot the standard curve; absorbancies of the BSA standards (on the y-axis) against their concentration values (x-axis) in a linear fashion.
- The protein concentrations of the unknown samples can then be inferred from the standard curve by obtaining the x-axis values corresponding to their absorbance readings.

### D.3.1 Bradford Reagent

- Dissolve 500 mg Coomassie Brilliant Blue G in 250 ml of 95% ethanol.
- Add 500 ml phosphoric acid and stir.
- Make up to 1 litre with distilled water and mix thoroughly.
- Filter and store this stock solution at 4°C.
- Dilute the Bradford stock in a 1:5 ratio using distilled water, filter until it turns an almost clear, light brown colour and use for protein quantification.

## D.4 Sample preparation for SDS-PAGE

Once protein concentrations of the lysates have been determined, samples need to be prepared for denaturing SDS-PAGE [as mentioned in Section 2.3.2].

- A sample buffer stock solution can be prepared by adding 150  $\mu$ l mercaptoethanol to 850  $\mu$ l sample buffer.
- The appropriate amount of protein (as calculated for each cell lysate sample in the previous step) should be added to a microfuge tube containing sample buffer equivalent to half of the volume of the protein.
- The ratio of protein to sample buffer is thus 2:1.
- Following brief centrifugation in a Spectrafuge 24 D bench top centrifuge (Labnet International Inc, USA), the samples can either be stored at  $-80^{\circ}\text{C}$  for later use, or used for Western blot analysis.
- Before proceeding with Western blotting, the samples should be boiled in boiling water or heated on a heating block at  $95\text{-}100^{\circ}\text{C}$  for 5 minutes.
- Brief centrifugation will ensure that the sample collects at the base of the tube.

## D.5 SDS-PAGE

- The following reagents are necessary for the preparation of polyacrylamide gels: 30% acrylamide-bis, (Merck, Darmstadt, Germany); 1.5 M Tris - pH varies for stacking and resolving gels; 10% SDS (L3771, Sigma-Aldrich, Steinheim, Germany); 10% ammonium persulphate (112 37 50, Saarchem, Merck, South Africa); N,N,N',N'-tetramethylene diamine (TEMED) (10732, Merck, Darmstadt, Germany); and distilled water.
- In order to separate the proteins via SDS-PAGE, prepare the polyacrylamide gel [Table D.3] in advance and cool to  $4^{\circ}\text{C}$ .

	<b>10% Resolving gel</b> Volume per (5 ml) gel (ml)	<b>5% Stacking gel</b> Volume per (1 ml) gel (ml)
Distilled water	1.9	0.68
30% acrylamide	1.7	0.17
1.5 M Tris	1.3 (pH 8.8)	0.13 (pH 6.8)
10% SDS	0.05	0.01
10% ammonium persulphate	0.05	0.01
TEMED	0.002	0.001

**Table D.3:** Constituents of polyacrylamide gels for 10% resolving and 5% stacking gels, respectively

- Remember to pour a layer ( $\sim 1$  ml) of water or isobutanol on top of the resolving gel while setting to prevent it from drying out. Rinse with water and remove as much excess fluid as possible before proceeding to cast the stacking gel.
- Work quickly when casting the gels and inserting the well comb as the gel starts to polymerise as soon as the last ingredient has been added.
- Avoid bubbles as oxygen inhibits polymerisation of the gel. Note that incomplete polymerisation is a bigger problem with stacking gels than resolving gels. Take particular care not to trap bubbles beneath the comb as the poor polymerisation will lead to badly formed wells.
- The cast gel can be stored in the fridge overnight wrapped in moist paper towel and cling wrap to prevent it from drying out.
- Best resolution is achieved when gels and buffers are kept cool.
- Assemble the cassette to hold gel(s), using a buffer dam if only one gel is present.
- Load samples into the wells of the gel, remembering to save at least one lane for  $\sim 4$   $\mu$ l of molecular weight marker.
- Once the assembled cassette had been filled with running buffer [Appendix D.5.1], the electrophoresis can commence.
- SDS-PAGE is recommended at 80 V for an initial 10 minutes, and then 100 V for a further 80 - 120 minutes, or until the protein(s) of interest have separated satisfactorily [Section 2.3.4].

### D.5.1 Running buffer

- 10 g SDS
- 30.3 g Tris
- 144.1 g Glycine (G8898, Sigma-Aldrich, Steinheim, Germany)
- Make up in 800 ml of distilled water
- Adjust to 1 l
- Store at room temperature

## D.6 Electrotransfer

- Once proteins have been separated by electrophoresis they can be transferred from the gel onto a PVDF membrane (0.45  $\mu\text{m}$  Biotrace PVDF, 66543, PALL Corporation, Life Sciences, Pensacola, FL) via electrotransfer [Section 2.3.5].
- Soak two pieces of blotting paper (1703969, Extra thick blot paper, Protean XL size, Bio-Rad Laboratories, CA), a little larger than the size of the gel, in transfer buffer [see D.6.1].
- Soak the membrane, roughly the same size as the gel, briefly in methanol ( $\sim 15$  seconds) allowing a few seconds to air-dry before soaking it in transfer buffer. Never touch the membrane with bare hands - always wear gloves so as not to compromise integrity of the membrane with residual fingertip proteins or oils.
- The stacking gel can be cut off the rest of the gel and discarded. Lift the gel gently off the glass plate to prevent tearing it.
- Onto the centre of the semi-dry transfer apparatus (Bio-Rad® Semi-Dry Transfer Cell, Bio-Rad Laboratories, CA) place, in order from bottom to top; a piece of presoaked blotting paper, the PVDF membrane, the gel, followed by the final piece of blotting paper.
- Be sure not to shift the gel on the membrane as this may cause 'smudges' of protein.
- Use a clean, moistened tube to roll over the stack and roll out any air bubbles.
- Transfer the proteins at 15 V, 0.5 A for 1 hour and 20 minutes.
- Once electrotransfer is complete, remove the blot and dry it on a clean surface. This will help to fix the proteins on the blot.
- Proceed, or block the membrane for an hour (1% BSA made up in TBS-T) to store it at  $-20\text{ }^{\circ}\text{C}$ .

### D.6.1 Transfer buffer

Make up 1 litre of transfer buffer by mixing together the following items:

- 100 ml  $10\times$  Tris/Glycine (TG) buffer (161-0771, Bio-RAD Laboratories, CA),

- 200 ml methanol (603-001-00-X, Merck, Darmstadt, Germany), and
- 700 ml distilled water.

1× TG buffer contains 25mM Tris and 192 mM glycine (pH 8.3).

## D.7 Probing the membrane

- After transfer the membrane can be washed in distilled water or Tris-buffered saline-Tween (TBS-T) for 5 minutes.
- Washing is followed by blocking the non-specific binding sites on the membrane in 1% BSA, made up in 50 ml TBS-T, for as long as the specific probing requires (from 40 minutes for *O*-GlcNAc to overnight for other proteins).
- Wash the membrane with TBS-T again for 5 minutes and repeat twice more.
- Incubate the membrane overnight with primary antibody at 4°C. Consider saving the antibody for future blot procedures.
- The TBS-T washing step is repeated, i.e. 3× 5 minutes.
- Incubate the membrane with the appropriate secondary antibody for an hour at room temperature, or overnight at 4°C.

### D.7.1 TBS

For a 10× TBS:

- Dissolve 6.05 g Tris (50 mM) and 8.76 g NaCl (150 mM) in 800 ml of distilled water.
- Adjust the pH to 7.5 with 1 M HCl (~ 9.5 ml).
- Adjust the volume to 1 l with distilled water.
- TBS is stable at 4°C for three months.
- Note that sodium azide inhibits peroxidase activity therefore it is not recommended as an antimicrobial agent.

### D.7.2 TBS-T

For a 1× TBS-T:

- Dilute the 10× TBS stock 1:9 with distilled water.
- Add 1 ml Tween 20 per liter of TBS for a final concentration of 0.1%.

### D.7.3 Detection of *O*-GlcNAc

- The membrane is washed after electrotransfer is completed and then blocked with 1% BSA to prevent non-specific binding of antibodies.
- *O*-GlcNAc blots [Chapter 2.3.6] can be blocked between 40 to 60 minutes.
- Wash with TBS-T for 5 minutes, three times.
- Incubate the membrane overnight with a 1:1000 dilution of the *O*-GlcNAc primary antibody, CTD110.6 (Santa Cruz Biotechnology, CA), in TBS-T at 4°C.
- Wash with TBS-T again for 5 minutes, three times.
- Dilute the anti-mouse, HRP-conjugated secondary antibody at 1:4000 (1.25 µl in 5 ml TBS-T) and add to the membrane for an hour at room temperature with gentle shaking.
- Wash thoroughly by repeating the TBS-T wash steps before developing the blot.

### D.7.4 Detection of $\beta$ -actin

- Before probing for  $\beta$ -actin the membrane needs to be washed after electrotransfer, and then blocked with 1% BSA to prevent non-specific binding of antibodies.
- Block the membrane for 60 minutes.
- Wash with TBS-T for 5 minutes, three times.
- Incubate the membrane with a 1:1000 dilution of the the  $\beta$ -actin primary antibody in TBS-T at 4°C overnight.
- Wash with TBS-T again for 5 minutes, three times.

- Dilute the anti-rabbit, HRP-conjugated secondary antibody 1:4000 (1.25  $\mu$ l in 5 ml TBS-T) and add to the membrane for an hour at room temperature with gentle shaking.
- Wash thoroughly by repeating the TBS-T wash steps before developing the blot.

## D.8 Developing the membrane

Refer to Chapter 2.3.7.

- Treat the membrane with a detection reagent such as ECL Western Blot Substrate (K820-500, BioVision Incorporated, Mountain view, CA) for a minute (mixing the solutions in a 1:1 ratio, or as instructed). Ensure that the mixture covers the entire membrane evenly.
- Place the membrane between two transparencies in a hypercassette (12643, Amersham, Buckinghamshire, UK), making sure not to trap any bubbles. The blot can then be developed in a dark room.
- On top of this sandwiched membrane place a developing film such as CL-XPosure™ Film (34089, Thermo Scientific, Rockford, IL) and close the hypercassette to expose the film.
- The length of exposure (the time the film remains on, or exposed to the membrane) varies between proteins and protocols, and depends on the strength of the fast-decaying signal emitted by the light-sensitive detection reagent.
- $\beta$ -actin blots develop well if exposed for only a few seconds ( $\sim$  5 seconds) whereas *O*-GlcNAc blots may take a little longer ( $\sim$  1 minute).
- Remove the film and immerse it in developing solution for a while until you start to notice bands developing on the film ( $\sim$  10 - 30 seconds).
- Rinse the film briefly in water before placing it in fixative for  $\sim$  15 seconds.
- Densitometric analysis [refer Chapter 2.3.8] can then be performed on the blot.

## D.9 Stripping membranes to reprobe

One membrane can be probed more than once, allowing for the same set of proteins (from the same cells, treated and harvested under the same conditions) to be probed for more than one

kind of protein. This not only means that the SDS-PAGE procedures can be avoided, but also makes data acquired much more comparable.

- Wash the membrane in distilled water, three times for 5 minutes each.
- Immerse the membrane in 0.2 M sodium hydroxide (NaOH) (582 32 00EM, Merck, South Africa) and shake gently on a belly dancer (The Belly Dancer, Stovall Life Science Incorporated, Greensboro, NC) for 5 minutes.
- Repeat the wash steps with distilled water.
- Block and probe again as desired.

# Appendix E

## HA-GLUT4-GFP Transfection

### E.1 Transfection Protocol

Refer to Chapter 2.4.1, and Figure 2.8.

Using the Lipofectamine™ LTX and PLUS™ Reagents (15338-100 Invitrogen, Carlsbad, CA) DNA-lipid complexes can be prepared for each transfection sample by doing the following:

- Place 100 µl of unsupplemented medium in a microfuge tube - one for each well containing cells. Note that the addition of antibiotics to transfection media may result in cell death.
- Add 800 ng plasmid DNA (HA-GLUT4-GFP construct) followed by thorough mixing.
- Add 0.3 µl PLUS™ Reagent (about a third of the volume of Lipofectamine™ LTX that will be added).
- Mix gently and incubate at room temperature for 5 minutes.
- Mix Lipofectamine™ LTX before use, and add 0.9 µl (or 3× the amount of PLUS™ Reagent) directly to the diluted DNA. Mix thoroughly.
- Incubate for 30 minutes at room temperature. DNA-lipid complexes are stable for 6 hours at room temperature.

Add ~100 µl DNA-lipid complex dropwise to each well containing cells. Rock the plate gently back and forth to mix. The total volume in each well now comes to 600 µl so be careful not to spill. Incubate the cells at 37°C for 18 to 48 hours prior to testing for transgene expression.